

DISSERTATION

MULTI-DECADAL IMPACTS OF HIGH-SEVERITY WILDFIRE ON
ECOSYSTEM NITROGEN CYCLING

Submitted by

Allison Elizabeth Rhea

Department of Ecosystem Science and Sustainability

In partial fulfillment of the requirements

For the Degree of Doctor of Philosophy

Colorado State University

Fort Collins, Colorado

Summer 2022

Doctoral Committee:

Advisor: Tim Covino

Co-Advisor: Charles Rhoades

Stephanie Kampf

Sara Rathburn

Copyright by Allison Elizabeth Rhea 2022

All Rights Reserved

ABSTRACT

MULTI-DECADAL IMPACTS OF HIGH-SEVERITY WILDFIRE ON ECOSYSTEM NITROGEN CYCLING

Wildfires modify the amount, form, and distribution of nitrogen (N) throughout an ecosystem. Though N stocks are lost during the combustion of vegetation and surface organic matter, there is often a subsequent increase in inorganic N delivery to streams that provide drinking water to the Western US. This can make streams and reservoirs more susceptible to eutrophication and algal blooms, threatening the delivery of clean drinking water. While many post-fire studies have documented short-term (<5 years) increases in soil and stream inorganic N, long-term monitoring after the Hayman fire has revealed that increases in stream N can persist for decades. This dissertation investigates the long-term controls of elevated post-fire N across spatial scales.

Chapter 2 describes the stream biotic response to the Hayman and High Park fires that burned along the Colorado Front Range. I evaluated stream water chemistry, algal nutrient limitation, benthic biomass, and stream metabolism along stream reaches within three burned and three unburned watersheds. Although the two high-severity wildfires occurred five and 15 years prior to the study, the streams draining burned watersheds still had 23-times higher nitrate (NO_3^-) concentrations than unburned watersheds, a trend that is consistent across seasons and throughout the 15-year post-fire record. Autotrophic N-limitation was reduced in these nitrate-rich burned streams. Consequently, autotrophic biomass and primary productivity were 2.5 and 20-times greater, respectively, in burned relative to unburned streams which indicates post-fire increases in stream N demand. However, the continued export of N out of these burned streams suggests that

terrestrial N supply exceeds in-stream N demand. This suggests that streams have a limited capacity to attenuate N exports from burned watersheds.

It was unclear if terrestrial N delivery to streams was driven by long-term elevated soil inorganic N supply (i.e., pools and net transformation rates) or depressed post-fire vegetation recovery and plant nutrient demand. I address this knowledge gap in chapter 3, by measuring inorganic N in surface mineral soils (0-15 cm), soil leachate (30 cm), and shallow groundwater (40-100 cm) in unburned watersheds dominated by ponderosa pine (*Pinus ponderosa*) and shrub-dominated watersheds that burned 17 years prior in the 2002 Hayman fire. Wildfire caused large C and N losses from soil O horizon during combustion (~1,500 and 50 g /m² of C and N, respectively). However, total C and N stocks, soil-extractable inorganic N, plant-available inorganic N, and net N transformation rates (i.e., nitrification, and N mineralization) differed little between burned and unburned mineral soils. This indicates that there were no long-term post-fire increases in soil N supply. In contrast to the near surface patterns, NO₃⁻ concentrations were four- and ten-times higher, respectively in shallow groundwater and streams of burned watersheds. Tree regeneration has been slower than expected following the Hayman and other fires in the western US and these biogeochemical patterns suggest that low plant N demand may prolong the impacts of wildfires on stream nutrients where more extreme fire behavior and climatic conditions inhibit vegetation recovery.

Finally, in chapter 4, I investigated the landscape and stream network drivers of persistent elevated stream NO₃⁻ in nine watersheds that were burned to varying degrees by the Hayman fire. I evaluated the ability of multiple linear regression and spatial stream network modeling approaches to predict observed concentrations of the biologically active solute NO₃⁻ compared to the conservative solute sodium (Na⁺). No landscape variables were strong predictors of stream

Na⁺. Rather, stream Na⁺ variability was largely attributed to flow-connected spatial autocorrelation, indicating that downstream hydrologic transport was the primary driver of spatially distributed Na⁺ concentrations. In contrast, vegetation cover, measured as mean normalized differenced water index (NDMI) was the strongest predictor of spatially distributed stream NO₃⁻ concentrations. Furthermore, stream NO₃⁻ had weak flow-connected spatial autocorrelation and exhibited high spatial variability. This pattern is likely the result of spatially heterogeneous wildfire behavior that leaves intact forest patches interspersed with high burn severity patches that are dominated by shrubs and grasses. Post-fire vegetation also interacts with watershed structure to influence stream NO₃⁻ patterns. For example, severely burned convergent hillslopes in headwaters positions were associated with the highest stream NO₃⁻ concentrations due to the high proportional influence of hillslope water in these locations.

My findings help characterize the potential magnitude, duration, and location of water quality concerns following fire. Slow forest recovery in large, high severity burn patches will likely sustain post-fire N export by limiting vegetation N uptake. As regeneration failures become more common with increasing fire severity and climate aridity, ecosystems will be more susceptible to sustained NO₃⁻ losses. If reforestation is desired, targeted plantings in riparian corridors, severely burned convergent hillslopes, and headwater positions will likely have the largest impact on stream NO₃⁻ concentrations.

ACKNOWLEDGEMENTS

I would first like to thank my advisors, Tim Covino and Chuck Rhoades. This dynamic duo provided such a unique graduate school experience that I value tremendously. Tim, thank you for being a steady guiding force, exposing me to new field methods, and for your patience throughout the writing process. Chuck, thanks for sharing your extraordinary ability to organize field campaigns, introducing me to new scientific fields, and for generously integrating me into your scientific network. Also, thanks to my committee, Stephanie Kampf and Sara Rathburn, for being such effective teachers and thoughtful individuals.

This research involved four field seasons and thousands of water and soil samples, none of that would have been possible without Tim Fegel and the amazing RMRS field crews and biogeochemistry lab. Tim, you provided invaluable expertise in the lab, field, and managing personnel. You were like a third advisor as I was getting my field work up and running. Thanks to Kate Bollen, Brian Orth, Val Doebly, Lizzie Hereford, Noah Sievers, and the multitude of RMRS field and lab technicians that worked on this project. We are also grateful for the financial support that made this work possible - the US Forest Service National Fire Plan (2016-2019), the Joint Fire Sciences Program (JFSP# 14-1-06-11), and NASA Headquarters under the NASA Earth and Space Science Fellowship Program.

Next, thank you to the CSU community. To my amazing lab mates - Alex, Tristan, Karin, and Lauren – for keeping me motivated and teaching me so much. To Juli and Johanna for being the best roommates as we navigated grad school and turning into lifelong friends. To the many ESS, GDPHE, & Geoscience grad students who showed me the beauty of inter-disciplinary

science. To my colleagues at CFRI for your patience as I finish my degree and your genuine excitement for my research and skillset.

Last, but certainly not least, I want to thank my family. To my dear husband Isaac, thank you for giving up your time to help me in the field, lab, or making figures, for always knowing how to make me laugh, for getting me into the mountains on the weekends, and for loving me so well. Thanks to my Mom and Dad for fostering my curiosity, being my sounding board, and always cheering me on. To Collin, Christine, Margot, my grandparents, and the Trujillos, thanks for your unwavering encouragement and love throughout. Finally, thanks to Mila for being my companion while working from home. This dissertation truly is a product of this wonderful community.

DEDICATION

I dedicate this dissertation to my grandmother Beverly Rhea. Your thesis from 1975 sat on my desk and served as inspiration throughout graduate school. Thanks for teaching me what hard work looks like.

TABLE OF CONTENTS

ABSTRACT.....	ii
ACKNOWLEDGEMENTS.....	v
DEDICATION.....	vii
LIST OF TABLES.....	x
LIST OF FIGURES	xi
1. Introduction.....	1
1.1 Fire in the Western US.....	1
1.2 Nitrogen as an indicator of ecosystem function.....	2
1.3 Nitrogen response to fire.....	3
1.4 Knowledge gaps and research goals.....	4
2. Reduced N-Limitation and Increased In-Stream Productivity of Autotrophic Biofilms 5 and 15 Years After Severe Wildfire	6
2.1 Introduction.....	6
2.2 Methods.....	8
2.2.1 Study area and sampling approach.....	8
2.2.2. Geospatial data.....	11
2.2.3 Stream water chemistry and discharge.....	12
2.2.4 Nutrient-diffusing substrates.....	13
2.2.5 Benthic biofilm.....	14
2.2.6 Stream metabolism.....	15
2.2.7 Statistical analysis.....	17
2.3 Results.....	17
2.3.1 Geospatial data.....	17
2.3.2 Stream nutrients and DOC.....	18
2.3.3 Nutrient-diffusing substrates.....	21
2.3.4 Benthic biofilm.....	24
2.3.5 Stream metabolism.....	26
2.4 Discussion.....	27
2.4.1 Autotrophic response to nutrient amendments.....	27
2.4.2 Biotic regulation of coupled C and N cycles.....	28
2.4.3 Forest disturbance and watershed response.....	30
2.5 Conclusions.....	32
3. Assessing Soil Supply and Plant Demand to Interpret Long-Term Post-Fire Stream N Export.....	34
3.1 Introduction.....	34
3.2 Methods.....	36
3.2.1 Site description.....	36
3.2.2 Vegetation sampling.....	37
3.2.3 Soil sampling.....	38
3.2.4 Water sampling.....	39
3.2.5 Statistical analysis.....	40

3.3 Results.....	41
3.3.1 Seasonal moisture dynamics.....	41
3.3.2 Vegetation cover.....	42
3.3.2 Soil C and N stocks.....	43
3.3.3 Mineral soil inorganic N.....	45
3.3.4 Net N transformations.....	47
3.3.6 Water N concentrations.....	48
3.4 Discussion.....	49
3.4.1 Post-fire soil N supply.....	50
3.4.2 Evidence of persistent plant-mediated NO ₃ ⁻ losses.....	52
3.5 Conclusions.....	56
4. Use of Geostatistical Models to Evaluate Landscape and Stream Network Controls on Post-Fire Stream Nitrate Concentrations.....	58
4.1 Introduction.....	58
4.2 Methods.....	60
4.2.1 Site description.....	60
4.2.2 Stream sampling.....	63
4.2.3 Geospatial analysis.....	64
4.2.4 Statistical modeling.....	66
4.2.5 Longitudinal patterns across two watersheds with inverse burn patterns.....	69
4.3. Results.....	70
4.3.1 Stream Na ⁺ and NO ₃ ⁻ concentrations.....	70
4.3.2 Landscape controls on Na ⁺ and NO ₃ ⁻	70
4.3.3 Stream network controls on Na ⁺ and NO ₃ ⁻	72
4.3.4 Statistical model performance.....	74
4.3.5 Longitudinal patterns across two watersheds with inverse burn patterns.....	75
4.4 Discussion.....	77
4.4.1 Modeling streamwater chemistry in burned watersheds.....	77
4.4.2 Post-fire vegetation is a dominant driver of stream NO ₃ ⁻ patterns.....	78
4.4.3 Burned headwaters are susceptible to elevated stream NO ₃ ⁻	79
4.5 Conclusions.....	81
5. Conclusions.....	82
5.1 Key findings.....	82
5.2 Opportunities for future research.....	83
REFERENCES.....	85
APPENDIX A: Chapter 2 supplemental material.....	101
APPENDIX B: Chapter 3 supplemental material.....	102
APPENDIX C: Chapter 4 supplemental material.....	107

LIST OF TABLES

Table 2.1 Physical characteristics of study watersheds.....	11
Table 2.2 Vegetation characteristics of study watersheds.....	18
Table 2.3 Summary of field measurements.....	21
Table 3.1 Soil C and N content and stocks.....	44
Table 4.1 Physical and chemical characteristics of study watersheds.....	62
Table 4.2 Burn metrics for each study watershed.....	63
Table 4.3 Watershed predictor variables.....	65
Table 4.4 Summary of statistical modeling results.....	71
Table C1 Linear mixed model selection.....	108

LIST OF FIGURES

Figure 2.1- Study area within Hayman and High Park fires.....	9
Figure 2.2 - Field photo illustrating lack of regeneration 16 years post-fire.....	10
Figure 2.3 - Stream chemistry time series.....	20
Figure 2.4 - Results from nutrient diffusing substrate experiments.....	23
Figure 2.5 - Benthic biomass measurements.....	25
Figure 2.6 - Stream metabolism and N uptake estimates.....	26
Figure 2.7 - Conceptual supply-demand balance.....	31
Figure 3.1 – Sampling locations and study design.....	37
Figure 3.2 - Precipitation and stream flow time series.....	42
Figure 3.3 - Substrate and vegetation cover.....	43
Figure 3.4 - Soil-extractable NO_3^- and NH_4^+ concentrations.....	46
Figure 3.5 - Plant-available NO_3^- and NH_4^+ over the summer and winter.....	47
Figure 3.6 - N transformation rates from aerobic laboratory incubations.....	48
Figure 3.7 - NO_3^- concentration time series in soil, ground, and stream water.....	49
Figure 3.8 - Relationships between stream NO_3^- and stage.....	54
Figure 3.9 – Relationship between NO_3^- and annual NPP.....	55
Figure 4.1 – Map of sampled NO_3^- concentrations.....	61
Figure 4.2 - Pearson correlation matrix between all predictor and response variables.....	68
Figure 4.3 - Empirical semivariograms for NO_3^- and Na^+	73
Figure 4.4 - Leave-one-out cross validation	74
Figure 4.5 - Longitudinal patterns in watersheds with inverse burn patterns.....	76
Figure A1 - Relationship between Chl- <i>a</i> and burn extent.....	101
Figure B1 - Continuous stage records for all streams, wells, and piezometers.....	102
Figure B2 - Time series of soil volumetric moisture content.....	103
Figure B3 - NO_3^- concentrations for soil, ground, and stream water.....	104
Figure B4 - Valley width cumulative distribution functions.....	105
Figure B5 - Longitudinal profiles of valley width.....	106
Figure C1 - Map of sampled stream Na^+ concentrations.....	107
Figure C2 - Pearson correlation matrices of selected predictor variables.....	109
Figure C3 - Map of SSN NO_3^- predictions.....	110
Figure C4 - Relationship between predicted and observed stream NO_3^-	111

1. Introduction

1.1 Fire in the Western US

Wildfire is a natural ecological force that shapes forests across the Western US (Whitlock et al., 2003). However, the size and severity of wildfire have been increasing across the Western US since the mid-1980s and are projected to continue increasing (Parks & Abatzoglou, 2020; Westerling, 2016; Williams & Abatzoglou, 2016). This is due to compounding human stressors (i.e., human ignitions, development, fire suppression, Higuera & Abatzoglou, 2021) and increasing atmospheric and fuel aridity (Abatzoglou & Williams, 2016; Williams et al., 2019).

There have been significant declines in post-fire tree regeneration, particularly in dry conifer forests, due to changing climate and fire activity (Chambers et al., 2016; Rother & Veblen, 2016; Stevens-Rumann et al., 2018). For example, increasing climate water deficits have created unfavorable post-fire growing conditions and reduced seedling recruitment in the 21st century (Coop et al., 2020; Stevens-Rumann et al., 2018). Furthermore, large, severe wildfires can limit post-fire recruitment by extending the distance to seed sources beyond a viable range (>50 m) (Chambers et al., 2016; Rother & Veblen, 2016). This trend is only expected to worsen as the occurrence of high severity fire increases across the Western US (Parks & Abatzoglou, 2020).

Observed declines in post-fire tree regeneration have stimulated conversions to non-forest vegetation types (Coop et al., 2020; Tepley et al., 2017; Walker et al., 2018). These conversions have been spatially extensive and temporally enduring (Coop et al., 2020) and typically favor grassland and weedy, herbaceous vegetation types (Walker et al., 2018). There is already evidence of this in Colorado's dry conifer forests where large high severity patches exhibited no post-fire regeneration 10 or more years post-fire (Chambers et al., 2016; Rother & Veblen, 2016) and instead are now dominated by re-sprouting native forbs, graminoids, and woody plants (Fornwalt

& Kaufmann, 2014). This fundamental change in forest composition will undoubtedly influence ecosystem recovery after fire.

1.2 Nitrogen as an indicator of ecosystem function

Nitrogen (N) is an essential element that frequently limits plant production (Schlesinger & Bernhardt, 2013). In low N systems, most N is stored in organic forms whereas inorganic forms, such as ammonium (NH_4^+) and nitrate (NO_3^-), dominate as N availability increases (Chapin et al., 2011). Inorganic N is bio-available and sources include atmospheric deposition, nitrogen fixation, and organic matter decomposition. However, N generally operates in a closed cycle where internal cycling is 10-20 times greater than external inputs (Schlesinger & Bernhardt, 2013). Inorganic N can be lost through plant and microbial assimilation, denitrification, and leaching.

N is a sensitive indicator of ecosystem function (Chapin et al., 2011; Vitousek et al., 1979; Vitousek & Melillo, 1979). In undisturbed forests, N losses are generally small because N is retained so effectively in internal cycling (Binkley & Fisher, 2013). However, N losses are common following forest disturbances such as clear cutting, insect infestation, ice and wind storms, and wildfire (Bernhardt et al., 2003; Hall, 2003; Vitousek & Reiners, 1975). While post-disturbance N levels are generally not directly harmful to human health (Smith et al., 2011), excess N can increase the risk of eutrophication and harmful algal blooms (Dodds & Smith, 2016; Emelko et al., 2016; Smith et al., 2011) and the formation of potentially toxic disinfection by-products (Emelko et al., 2011).

1.3 Nitrogen response to fire

Fire can have profound impacts on the amount, form, and distribution of N in soils and streams (Certini, 2005; Wan et al., 2001). Initially, organic N stocks are lost from the combustion

of O horizon (i.e., forest floor) (Johnson et al., 2005; Murphy et al., 2006) and sometimes upper mineral soils during high severity fire (Bormann et al., 2008). This pyrolysis of organic material causes an immediate, but temporary (<1 year post-fire) pulse of NH_4^+ which stimulates nitrification and causes a delayed pulse of NO_3^- (Covington & Sackett, 1992). Soil inorganic N concentrations often return to pre-fire levels relatively quickly (i.e., <5 years) (Covington et al., 1991; Covington & Sackett, 1992; Grogan et al., 2000; Turner et al., 2007). However, N recovery depends on post-fire plant and microbial demand (Kaye & Hart, 1997; Rastetter et al., 2021; Smithwick et al., 2009) and high severity fires that trigger vegetation conversion have been shown to increase NO_3^- production for several decades (Kurth et al., 2014).

Mineral N that is not taken up by plants or microbes is typically leached from soils to streams in the mobile, dissolved form, NO_3^- (Turner et al., 2007) or eroded as N-rich soil and ash (Grogan et al., 2000; Lane et al., 2008; Pierson et al., 2019). This often causes stream N concentration to increase after fire (Smith et al., 2011). While particle-associated fractions dominate N exports immediately post-fire, these contributions decline sharply within 2 years post-fire due to reduced sediment delivery (Lane et al., 2008). However dissolved NO_3^- has the slowest recovery, likely due to elevated nitrification and persistent leaching (Lane et al., 2008; Rhoades, Chow, et al., 2019). Elevated post-fire stream NO_3^- has been documented after wildfires across the Western US (Rust et al., 2018; Smith et al., 2011) and can persist for decades following fire (Rhoades, Chow, et al., 2019). Stream NO_3^- concentrations have been shown to increase with burn extent, severity, and riparian vegetation exposure, but decrease with post-fire vegetation cover (Rhoades et al., 2011a; Rhoades, Chow, et al., 2019; Riggan et al., 1994; Rust et al., 2019; Stephan et al., 2012) suggesting that fire-impacts on vegetation may be a dominant control on stream NO_3^- recovery. Because forest recovery is the primary mechanism for terrestrial N retention (Dunnette

et al., 2014; Vitousek et al., 1979), long-term conversion from forest to non-forest can fundamentally alter terrestrial N losses to streams for decades.

1.4 Knowledge gaps and research goals

The increasing size and severity of wildfire necessitates evaluation of fire effects at various temporal and spatial scales (Rhoades, Nunes, et al., 2019). Most scientific investigation has focused on short-term (1-5 years) changes in soil or stream N availability, but relatively little is known about long-term (>10 years post-fire) effects of wildfire and what processes regulate long-term recovery (Rhoades, Nunes, et al., 2019; Smithwick et al., 2005). This knowledge gap is particularly important to address as more frequent severe wildfires (Parks & Abatzoglou, 2020; Westerling, 2016; Williams & Abatzoglou, 2016) push previously forested ecosystems into non-forested states (Coop et al., 2020; Tepley et al., 2017; Walker et al., 2018), potentially influencing the long-term recovery of ecosystem N cycling (Dove et al., 2020; Kurth et al., 2014). Furthermore, there is a need for research that links post-fire nutrient uptake and release across spatial scales through coupled stream-reach, hillslope, and catchment-scale observations (Rhoades, Nunes, et al., 2019; Smith et al., 2011). The identification of post-fire sources and sinks will better characterize the capacity of watersheds to mitigate fire impacts.

I directly address these critical knowledge gaps by conducting multi-scale studies 15 or more years after severe wildfire. This dissertation combines field-based experimentation with statistical modeling and is organized by increasing spatial scale, moving from stream reaches, to hillslope gradients, to watersheds. Chapter 2 investigates the stream biotic response to wildfire and evaluates the potential for stream uptake to attenuate NO_3^- losses. The third chapter characterizes terrestrial N sources by measuring inorganic N in mineral soils, soil water, and shallow groundwater along hillslope gradients. Chapter 4 evaluates topographic, vegetation, and fire

controls on the spatial distribution of stream NO_3^- . The final chapter reviews the major findings and discusses how they can inform future post-fire management and research.

2. Reduced N-Limitation and Increased In-Stream Productivity of Autotrophic Biofilms 5 and 15 Years After Severe Wildfire

2.1 Introduction

Wildfire frequency, severity, and extent have been increasing in the western US since the mid-1980s (Abatzoglou et al., 2017; Abatzoglou & Williams, 2016; Westerling, 2016). More than 65% of water supply in the Western US originates in forested headwaters (Brown et al., 2008) so understanding wildfire impacts on headwater stream ecosystems has broad societal relevance. Wildfires that kill vegetation (Keeley, 2009; Parsons et al., 2010) can increase nitrogen (N) availability by reducing plant nutrient demand and increasing mineralization of organic soil N forms (Smithwick et al., 2009; Turner et al., 2007; Wan et al., 2001b). Mineral N that is not taken up by plants or microbes is typically leached from soils to streams in the mobile, dissolved form, nitrate-N ($\text{NO}_3\text{-N}$) (Turner et al., 2007). This increased terrestrial to aquatic N transfer can elevate stream N, with the highest stream $\text{NO}_3\text{-N}$ concentrations typically occurring in severely burned watersheds (Rhoades et al., 2011a; Rhoades, Chow, et al., 2019; Riggan et al., 1994). Elevated post-fire stream $\text{NO}_3\text{-N}$ concentrations have been documented across the western US (Rust et al., 2018), and can remain elevated for decades (Rhoades, Chow, et al., 2019). For example, stream $\text{NO}_3\text{-N}$ was higher in burned compared to unburned watersheds 14 years after the Hayman fire, regardless of season (Rhoades, Chow, et al., 2019). This increases the risk of eutrophication and harmful algal blooms (Dodds & Smith, 2016; Emelko et al., 2016; Smith et al., 2011) and the formation of potentially toxic disinfection by-products (Emelko et al., 2011). Furthermore, N is a sensitive indicator of ecosystem function (Vitousek et al., 1979). Because N is usually in limited supply and constrains plant growth in most terrestrial systems (Chapin et al., 2011), elevated $\text{NO}_3\text{-N}$ export signals decreased watershed nutrient retention.

In headwater streams, NO₃-N export is controlled by the balance between terrestrial supply (Likens et al., 1970) and in-stream biotic demand (Bernhardt et al., 2003; Bernhardt et al., 2005). Following disturbance, terrestrial and stream biogeochemical responses may diverge (Bernhardt et al., 2003; Hall, 2003). Vegetation mortality reduces terrestrial nutrient demand and can increase nutrient delivery to streams (Stephan et al., 2012; Vitousek & Reiners, 1975). Thus vegetation regrowth is the primary mechanism responsible for mitigating terrestrial NO₃-N losses (Vitousek et al., 1979). If vegetation recovery is slow, as has been seen following severe wildfire (Chambers et al., 2016), terrestrial NO₃-N losses may be long-lasting. Once NO₃-N reaches the stream, biotic uptake has the potential to mitigate NO₃-N export. Higher post-disturbance nutrient and light availability can stimulate in-stream metabolism (Bernot et al., 2010) and nutrient demand (Bernhardt et al., 2005) which may buffer watershed NO₃-N exports. There is evidence that benthic biomass (Klose et al., 2015) and stream productivity (Betts & Jones, 2009) increase immediately after fire though the longer-term effects (>5 years post-fire) of wildfire on stream biotic processing remain unclear. While changes in terrestrial supply and aquatic demand both vary widely among disturbance and ecosystem types, in-stream responses may contribute to post-disturbance nutrient retention (Bernhardt et al., 2003).

In this study, I evaluated the consequences of wildfire on nutrient limitation, benthic biofilm biomass, and stream metabolism 5 and 15 years after two severe wildfires. I hypothesized that elevated stream NO₃-N levels would reduce N-limitations on algal growth and increase benthic autotrophic biomass and in-stream productivity in burned watersheds. I tested these ideas by deploying nutrient diffusing substrate (NDS) experiments, sampling benthic biofilms, and measuring stream metabolism in streams draining three burned and three unburned watersheds. I then considered the data within a supply-demand balance to estimate the capacity for in-stream

uptake to regulate post-fire export. By simultaneously considering in-stream nutrient limitation and demand, terrestrial supply, and watershed export, this study develops a more robust understanding of wildfire impacts on watershed nutrient cycling 5 and 15 years post-fire.

2.2 Methods

2.2.1 Study area and sampling approach

I studied the stream biogeochemical impacts of two wildfires, the Hayman and High Park fires, both of which burned within Colorado's Front Range (Figure 2.1). In 2002, the Hayman Fire burned 559 km² of ponderosa pine (*Pinus ponderosa*) and Douglas-fir (*Pseudotsuga menziesii*) forest (Graham, 2003) and 66% of that area burned at high and moderate severity. Prior to 2020, this was the largest wildfire in Colorado's history, occurring 50 km southwest of Denver and affecting the drinking water supply of 2.7 million people (Graham, 2003). This lower montane ecosystem (1980-2750 m elevation) is characterized by poorly developed, coarse sandy loam soils that are susceptible to erosion (Robichaud et al., 2003). Average annual precipitation, including both rain and snow, is 182 cm in the Hayman fire (WRCC 2016, Chessman Station #051528). The 2012 High Park fire burned 354 km² of a mixed-conifer forest, with 47% of that area burning at high and moderate severity. The High Park fire was only 21 km west of Fort Collins, home to 164,000 people (Larimer County et al., 2012). The burned area is dominated by steep slopes and sandy loam soils with frequent rock outcrops (Larimer County et al., 2012). On average, watersheds in the High Park fire receive 469 cm of annual precipitation (WRCC 2016, Buckhorn Mtn 1E Station #051060). Given the large size and high severity of these fires, forest recovery has been sparse (Chambers et al., 2016) and much of the burned area is now dominated by grasses, shrubs, and bare ground (Fornwalt & Kaufmann, 2014) (Figure 2.2).

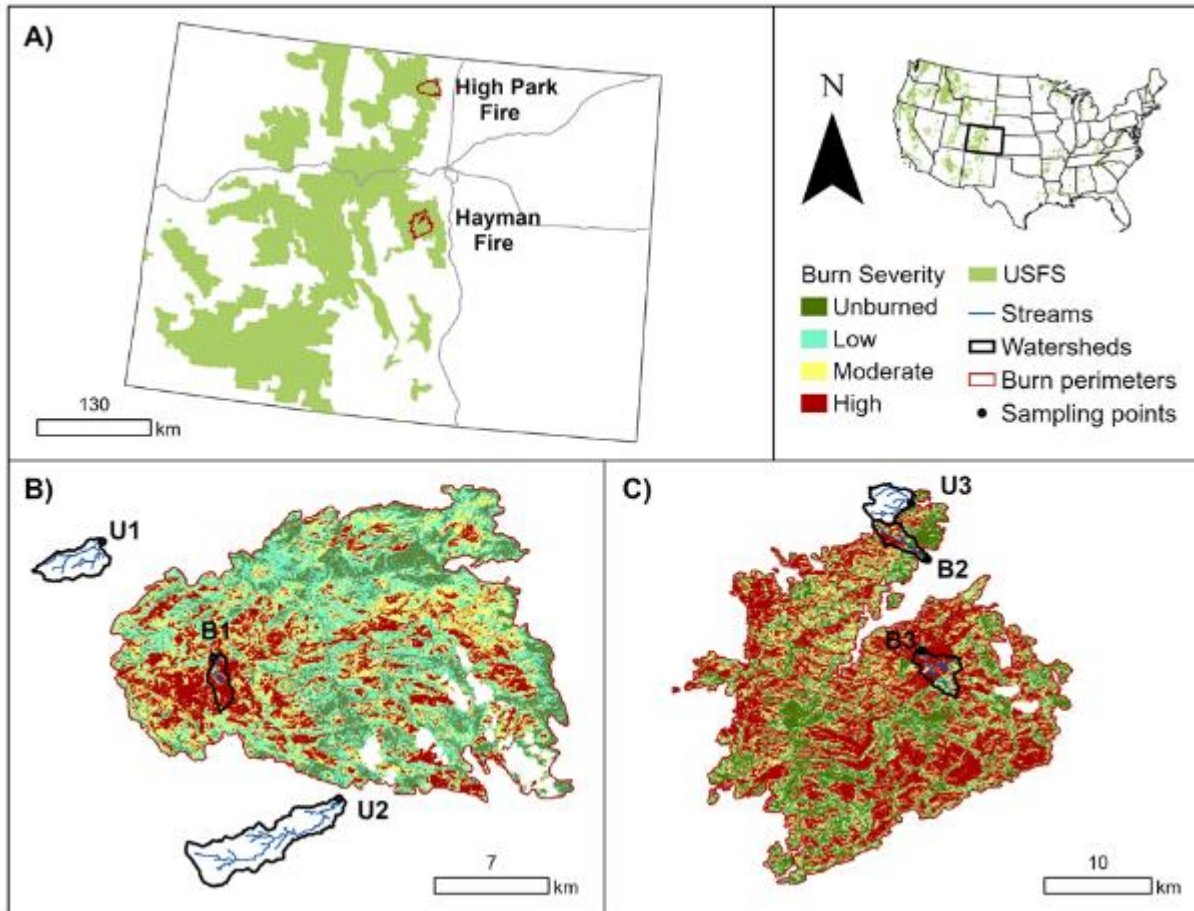


Figure 2.1: A) The 2002 Hayman and 2012 High Park fire perimeters (red) overlain on US Forest Service land (green) and primary highways (grey) in Colorado, USA. B-C) Burn severity maps (mtbs.com) for each fire with 3 unburned (U1-U3) and 3 burned watersheds (B1-B3) outlined in black and stream lines shown in blue.

Sampling occurred in streams draining 3 burned and 3 unburned watersheds (Figure 2.1). Fieldwork was conducted during a 20-day period spanning from July 28, 2017 - August 16, 2017 at Hayman and July 26, 2017 - August 14, 2017 at High Park. Late summer sampling avoided large storms and scouring events that disturb benthic biofilms. Thus, the comparison of burned and unburned watersheds was conducted during a period of relatively stable stream discharge and high in-stream production. Additionally, I analyzed stream nutrients before, during, and after the 20-day experimental period as a part of a larger program in which water chemistry has been

monitored for 19 years following the Hayman fire (Rhoades et al., 2011a; Rhoades, Chow, et al., 2019). All 6 watersheds are steep headwaters and have contributing areas between 3.25-19.38 km² (Table 2.1). I selected experimental stream reaches that had relatively uniform elevation, slope, and aspect (Table 2.1). These small, headwater streams had average stream velocities from 6-27 cm/sec, stream depths from 9-20 cm, and wetted widths from 50-318 cm during the experimental sampling period (Table 2.1).



Figure 2.2: Forests burned by high severity wildfires along the Colorado Front Range have been slow to recover. 16 years after the Hayman fire, tree regeneration is sparse and the post-fire landscape is dominated by shrubs, grasses, and bare ground (Photo taken: May 2018, Location: west of B2 in Fig 1).

Table 2.1: Physical characteristics of unburned watersheds (U1-U3) and watersheds that burned in Colorado wildfires 5 and 15 years prior to this study (B1-B3). Average stream characteristics were based on weekly observations during the 20-day experimental period (July 26 – August 16, 2017).

	Contributing Area (km²)	Elevation Range (m)	Mean Slope (°)	Dominant Aspect	Mean Velocity (cm/sec)	Mean Depth (cm)	Mean Wetted Width (cm)
U1	7.04	2193-2715	17.23	NE	3.51	19.70	88.0
U2	19.38	2059-3263	15.59	NE	6.93	18.19	318.0
U3	8.60	2161-2791	14.78	E	7.85	11.31	100.0
Unburn Mean					6.10	16.40	157.1
B1	3.25	2402-3087	15.43	NW	11.51	9.16	193.3
B2	6.02	1972-2480	15.80	E	6.25	10.31	49.9
B3	8.33	2354-2993	11.62	W	26.75	12.22	55.7
Burn Mean					14.83	10.56	94.7

2.2.2. Geospatial data

I obtained publicly available burn severity maps from the Monitoring Trends in Burn Severity (MTBS) database which classifies severity based on the degree of vegetation combustion (Eidenshink et al., 2009). Normalized Differenced Vegetation Index (NDVI) is a proxy for vegetation cover that is generated from Landsat imagery every 16-days at a 30 x 30 m resolution. I used Climate Engine to derive the mean summer NDVI across the June to August 2017 time period for each study watershed (Huntington et al., 2017). NDVI values range from -1 to 1. Low NDVI (<0.1) is characteristic of bare ground and water, moderate values (0.2-0.3) represent grass or shrub land, and high values (0.6-0.8) represent dense forests (Weier & Herring, 2000). I estimated riparian canopy density from the outlet sampling point to the headwaters of all study watersheds using publicly available 1-m resolution aerial imagery collected in August of 2017 (FSA 2015). I delineated 50-m longitudinal reaches that extended 10-m on each side of the stream. I then classified riparian canopy density of each 50 x 20 m reach as percent of riparian area

occupied by woody vegetation (sparse <30% canopy cover, moderate 30-70% canopy cover, or dense >70% canopy cover).

2.2.3 Stream water chemistry and discharge

I collected stream grab samples to measure total dissolved N (TDN), nitrate-N ($\text{NO}_3\text{-N}$), ammonium-N ($\text{NH}_4\text{-N}$), orthophosphate-phosphorous ($\text{PO}_4\text{-P}$), and dissolved organic carbon (DOC). Samples were collected in pre-washed 1 L high-density polyethylene bottles. Sub-samples were filtered through 0.7 μm glass fiber filters (Whatman International, Ltd., Maidstone, UK) and 0.45 μm polyvinyl diethylene filters (MilliporeSigma, Burlington, MA). Filtered sub-samples were analyzed for TDN and DOC on a total organic C analyzer (TOC-V Combustion, Shimadzu, Columbia, MD) and for cations and anions using ion chromatography (Dionex ICS-3000, Waltham, MA and Waters 580, Sunnyvale, CA).

I used dilution gauging (Rantz, 1982) to measure stream discharge at each site 1-3 times during the 20-day experimental period. I injected sodium chloride as an instantaneous injection and recorded tracer breakthrough curves (BTCs) using in-situ specific conductivity sensors (Campbell Scientific Inc., CS547A, Logan, UT) recording on a 2 sec time-step. The conductivity sensor was calibrated for temperature and electrical conductivity with salt solutions in the laboratory to calculate the relative NaCl concentrations of tracer breakthrough curves. Discharge, $\text{NO}_3\text{-N}$ concentration, and watershed area were used to calculate area-normalized instantaneous $\text{NO}_3\text{-N}$ flux, referred to as watershed $\text{NO}_3\text{-N}$ export, at each site.

2.2.4 Nutrient-diffusing substrates

I deployed in-situ nutrient-diffusing substrate (NDS) experiments to quantify the degree of biofilm nutrient limitation in streams draining burned and unburned watersheds. The nutrient diffusing substrates release nutrients into the water column to evaluate benthic biofilm response relative to an unamended control. I evaluated primary limitations with individual N, P, and C treatments and co-limitation with N+P, C+N, C+P, and C+N+P treatments. The following resource treatments were added to 2% agar biofilm growth medium: N as 0.5 mol N/L of sodium nitrate (NaNO_3), P as 0.2 mol P/L of monopotassium phosphate (KH_2PO_4), and C as 0.5 mol C/L of glucose ($\text{C}_2\text{H}_3\text{O}_2$) and 0.5 mol C/L acetate (CH_3COO^-). Unamended agar was included as a control. The agar solutions were poured into opaque, plastic crucibles (US Plastics, Lima, OH) and capped with fritted glass discs (EA Consumables, Pennsauken, NJ) to form nutrient-diffusers.

NDS experiments were deployed from July 28, 2017 - August 16, 2017 at Hayman and July 26, 2017 - August 14, 2017 at High Park and there were no large storms or scouring events during this period in any of the study streams. The 8 treatments (Control, N, P, C, N+P, C+N, C+P, and C+N+P) were randomly stratified on 6 replicate nutrient-diffuser racks per stream. These diffuser racks were placed beside one another, parallel to flow and anchored to the stream bed. After 20 days, each fritted glass disc was removed, placed in a pre-washed polyphenylene ether container, and kept in a dark freezer (-18°C) until processing. I used chlorophyll *a* (Chl *a*), a photosynthetic pigment common in all autotrophs, as a proxy for autotrophic biomass (Hambrook Berkman & Canova, 2007). I measured biofilm Chl *a* concentrations by extracting each fritted glass disc with 15 mL of 90% HPLC-grade buffered acetone. After 24-hours in a dark refrigerator (4°C), the discs were removed and extracts were analyzed on a fluorometer using a non-

acidification module (Turner Designs, San Jose, CA). The Chl *a* concentration of the extract was calculated using equation 1 (Arar & Collins, 1997):

$$Chl_a = \frac{(R_b - blank) \times F_s \times V}{a} \quad (1)$$

Where R_b is the fluorometer reading of the sample extract (raw fluorescence unit, RFU), $blank$ is the average fluorometer reading of buffered acetone without any sample extract (RFU), F_s is the response factor ($= 0.1724 \mu\text{g/L} * \text{RFU}^{-1}$), V is extract volume (L), and a is the surface area of the fritted glass disc (cm^2).

I calculated response ratios (i.e., $\ln(\text{treatment mean}/\text{control mean})$) to classify biofilm responses and identify nutrient limitations. Positive response ratios indicate that a given amendment enhanced biofilm growth relative to the unamended control, and negative response ratios indicate that the amendment suppressed biofilm growth. Biomass responses are often inversely proportional to ambient stream nutrient concentrations (Klose et al., 2015; Marcarelli et al., 2009; Reisinger et al., 2016). Primary limitation is inferred when an individual addition (N or P or C) elicits a significant, positive response (Tank & Dodds, 2003). Secondary limitation occurs when the combination of two additions has a significant, positive effect, but only one of the additions alone has a significant effect (i.e., N and N+P have a significant response, but P does not) (Tank & Dodds, 2003). Co-limitation is inferred when just the combination of two additions causes a significant effect (i.e., N+P has a significant response) (Tank & Dodds, 2003).

2.2.5 Benthic biofilm

Benthic biofilms are complexes of autotrophic (algae and cyanobacteria) and heterotrophic (bacteria and fungi) microorganisms that attach to stream bed substrate and comprise a large

portion of total biomass in headwater streams (Battin et al., 2008). Hereafter, I use the term “biomass” in reference to stream biofilms. The unamended NDS controls provided a uniform surface area and substrate type to compare ambient autotrophic, heterotrophic, and total benthic biomass between burned and unburned streams. The Chl *a* acetone extraction fluid from each unamended control was filtered through a pre-combusted, pre-weighed GF/F filter to calculate ash-free dry mass (AFDM) (APHA, 1995). Samples were dried (105°C for 27 hours), weighed (W_a), combusted in a muffle furnace (500 °C for 1 hour), and reweighed (W_{ash}). Dried filters were kept in a desiccator throughout the procedure and weights were measured on an analytical balance to the nearest 0.1 mg. AFDM (mg/cm²) was calculated from the dry (W_a , mg) and ashed (W_{ash} , mg) sample weights and the surface area of the fritted glass discs (A_f , cm²) (Equation 2) (Steinman et al., 2006).

$$AFDM = \frac{W_a - W_{ash}}{A_f} \quad (2)$$

This measure of organic material loss upon combustion represents total biofilm biomass (i.e., the sum of autotrophic and heterotrophic biomass). Finally, I calculated the autotrophic index (AI) as AFDM divided by Chl *a* (Steinman et al., 2006). Throughout, I use Chl *a* concentration as a measure of autotrophic biomass, AFDM as a measure of total biofilm biomass, and AI as a relative measure of heterotrophic biomass (Bechtold et al., 2012; Hambrook Berkman & Canova, 2007).

2.2.6 Stream metabolism

The combined activity of benthic, planktonic, and hyporheic biota can be estimated from measured diel changes in stream dissolved oxygen (DO) (Hall & Hotchkiss, 2017; Odum, 1956). I used optical sensors to measure stream DO concentrations (mg/L) and temperature (°C) on 15-

minute intervals throughout the experimental period in all 6 streams (MiniDOT, Precision Measurement Engineering Inc., Vista, CA). Light intensity (lum/m^2) was also measured on 15-minute intervals to determine light and dark hours (HOBO, Onset Computer Co., Bourne, MA). Dissolved oxygen saturation (O_{sat}) was calculated with site-specific atmospheric and temperature corrections. Median stream velocity was measured using NaCl injections and stream depth was recorded with field surveys (Table 2.1). Average stream velocity and depth measured during the experimental period were used to estimate site-specific O_2 gas exchange rates, K_o (Owens et al., 1964, Elmore and West, 1961). I calculated stream metabolism for each site-day using the open-system, single-station diurnal DO change approach (Odum, 1956)(Equation 3). Here, dO/dt is the rate of change in O_2 concentration (mg/L) for each time step, GPP is gross primary productivity ($\text{g } O_2/\text{m}^2/\text{d}$), ER is ecosystem respiration ($\text{g } O_2/\text{m}^2/\text{d}$), K_o is the O_2 gas exchange rate ($1/\text{d}$), O_{sat} is O_2 at saturation for a given temperature and barometric pressure (%), O is the O_2 concentration (mg/L), and z is the mean river depth (m).

$$\frac{dO}{dt} = \frac{GPP}{z} + \frac{ER}{z} + K_o(O_{sat} - O) \quad (3)$$

Production to respiration ratios (P:R) were calculated as GPP divided by the absolute value of ER. Net primary production ($\text{g } O_2/\text{m}^2/\text{d}$) was estimated assuming half of GPP is consumed by autotrophic respiration (Hall & Tank, 2003). Then I used a photosynthetic quotient of 1 to convert NPP from units of O_2 to C and converted from C to N using a median molar ratio of biofilm C:N equal to 12 (sensu King et al., 2014).

2.2.7 Statistical analysis

I analyzed NDS results with a linear mixed-effects model, using the Kenward-Roger method (lme4 package in RStudio Version 1.2.5). The fixed effects were amendment (presence or absence of C, N, and P) and burn condition, the random effect was site, and the response factor was Chl *a* concentration. Data were log-transformed before the analysis to meet assumptions of normal distribution and equal variance. I used Dunnett's test to evaluate the statistical significance of each treatment response relative to the control. I analyzed stream temperature, stream nutrient and DOC concentrations, benthic biofilm, and metabolism data using linear mixed-effects models with burn condition (i.e., burned or unburned watershed) as the fixed effect and site as the random effect. Burned and unburned comparisons that differed at the $\alpha < 0.05$ level were considered statistically significant unless stated otherwise.

2.3 Results

2.3.1 Geospatial data

Even 5 and 15 years following wildfire, burned watersheds had lower riparian cover and stream shading relative to unburned watersheds based on aerial imagery (Table 2.2). All unburned watersheds had dense pine forests and average June-August 2017 NDVI ranged from 0.52-0.59 (Table 2.2). The majority of stream length in unburned watersheds had dense riparian canopy cover (>70% woody vegetation cover within 10 m of the stream, see Table 2.2). In contrast, 73-99% of the 3 burned watersheds was altered by wildfire, resulting in shrub and grass-dominated vegetation with average NDVI (June-August 2017) ranging from 0.34-0.40 (Table 2.2). Riparian canopy cover was lower in the burned watersheds, especially within patches of moderate to high fire

severity; 46-71% of stream length was classified as bare (<30% woody vegetation cover within 10 m of the stream, see Table 2.2).

Table 2.2: Vegetation characteristics of the 6 study watersheds. Burn extent is the proportion of each watershed that was burned by wildfire (mtbs.com). Mean normalized differenced vegetation index (NDVI) is a metric of average vegetation cover throughout each watershed from June to August of 2017. The proportion of stream length with bare (<30%), moderate (30-70%), or dense (>70%) riparian canopy cover corresponds to woody vegetation within 20-m wide riparian zones.

	Burn Extent (%)	Mean June-August NDVI	Proportion of stream length with		
			bare	moderate	dense
			riparian cover (%)		
U1	0	0.52	4	15	81
U2	0	0.59	1	8	91
U3	<1	0.53	6	15	79
Unburn Mean	0	0.55	4	13	84
B1	99.6	0.39	71	15	15
B2	72.3	0.34	61	11	28
B3	89.6	0.40	46	17	37
Burn Mean	87.2	0.37	59	14	26

2.3.2. Stream nutrients and DOC

Stream NO₃-N concentrations were 23-times higher in burned (0.23 mg/L) compared to unburned (0.01 mg/L) watersheds (Figure 2.3a-b). This is consistent with previous studies of the Hayman fire that document elevated stream NO₃-N concentrations in burned watersheds, across all flow conditions for 14 years after the fire (Rhoades et al., 2011a; Rhoades, Chow, et al., 2019). While area-normalized stream discharge was not significantly different with burn condition, area-normalized watershed NO₃-N export was significantly higher in streams draining burned relative to unburned watersheds (Table 2.3) (Rhoades, Chow, et al., 2019). Stream dissolved inorganic N (DIN) was marginally higher and dissolved organic N (DON) marginally lower in burned relative to unburned watersheds (Table 2.3). Stream TDN did not differ (Table 2.3), though most samples in both burned and unburned watersheds exceeded a recommended threshold (0.12 mg/L TN) for

least disturbed, reference streams in the western forested mountains region (EPA, 2000). There was also no difference in $\text{NH}_4\text{-N}$ concentrations in burned and unburned watersheds (Figure 2.3c-d, Table 2.3). $\text{NO}_3\text{-N}$ comprised 75% of TDN in burned watersheds compared to 7% of TDN in unburned watersheds. Stream $\text{PO}_4\text{-P}$ concentrations were below the 0.01 mg/L detection limit in all samples in both burned and unburned watersheds. I observed a marginal decline in median DOC in the burned watersheds during the experimental period (Figure 2.3e-f) that agreed with earlier work showing lower DOC in severely burned Hayman watersheds (Rhoades, Chow, et al., 2019). However, mean DOC concentrations were not significantly different in burned and unburned watersheds as assessed by linear mixed-effects models (Table 2.3).

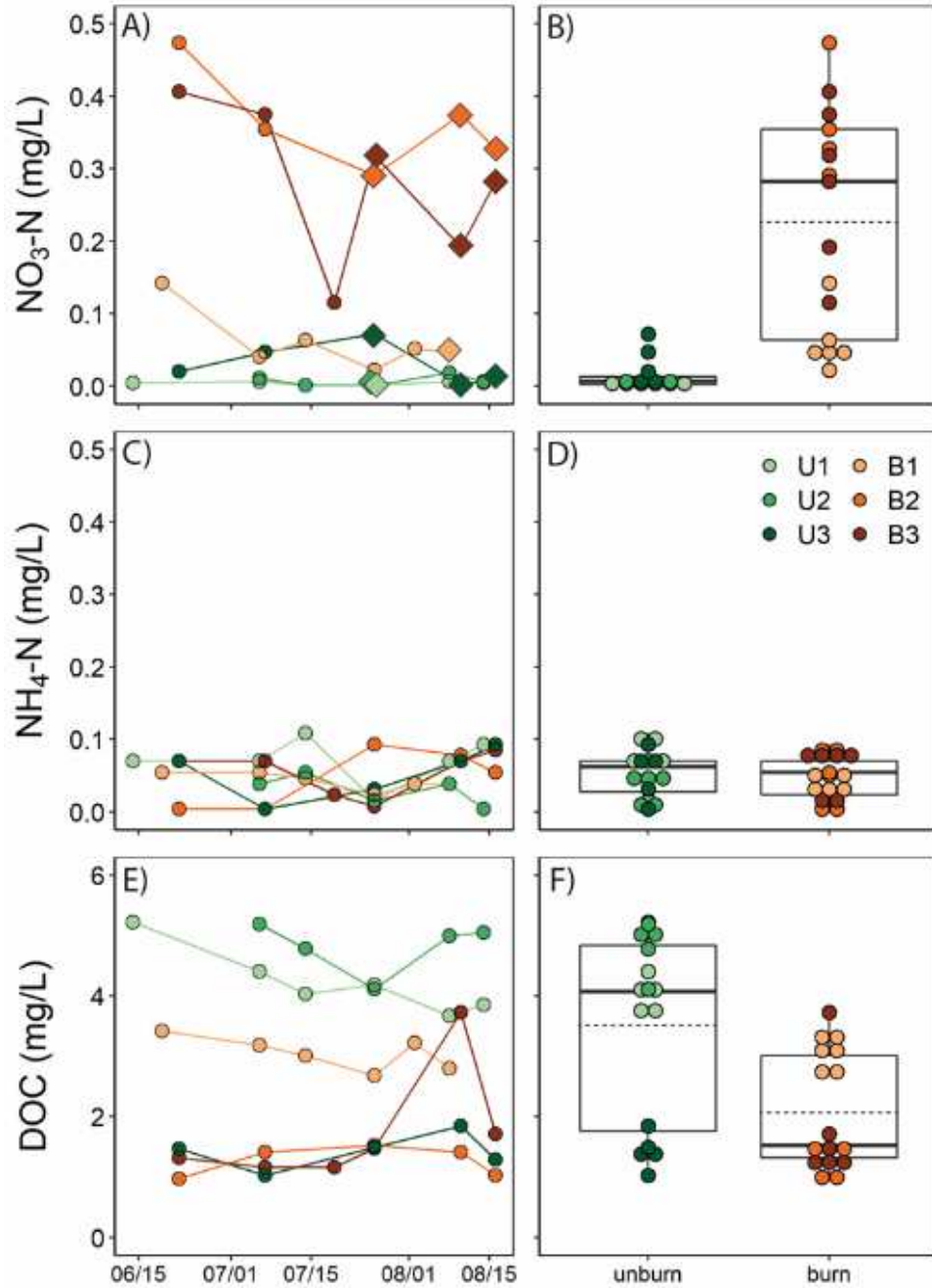


Figure 2.3: A-B) Stream nitrate-nitrogen ($\text{NO}_3\text{-N}$), C-D) ammonium-nitrogen ($\text{NH}_4\text{-N}$), and E-F) dissolved organic carbon (DOC) concentrations from stream grab samples collected between June and August of 2017. Each point represents an observation, color-coded by site; green and orange tones denote unburned and burned watersheds, respectively. Specific site-days with $\text{NO}_3\text{-N}$ export measurements are denoted as diamonds as opposed to circles in panel A (i.e., discharge was measured on that day). The solid horizontal lines in the boxplots (B, D, and F) denote medians, the dashed lines represent means, the upper and lower limits of the box span the interquartile range, the whiskers span 1.5-times the interquartile range, and dots beyond the whiskers are outliers. Only $\text{NO}_3\text{-N}$ was significantly different between burned and unburned streams as assessed by linear mixed effects models (Table 2.3).

Table 2.3: Stream chemistry and discharge, benthic biofilm, and metabolism metrics for the 3 unburned and 3 burned watersheds. Linear mixed-effects p-values indicate whether unburned sites (U1-U3) and burned sites (B1-B3) were significantly different at the $\alpha < 0.05$ level (bolded). Stream water chemistry data were collected 5-6 times at each site throughout the summer of 2017. Benthic biomass was measured on the control NDS disks at the end of the 20-day experimental period at all 6 sites. Metabolism was measured daily during the 20-day experimental period at all 6 sites.

		Unburn	Burn	p-value
Stream Chemistry & Discharge		(Mean / Median)		
Q/area	(mm/hr)	0.004 / 0.004	0.006 / 0.005	0.33
NO ₃ -N*Q/area	(mg N/hr/km ²)	62 / 17	1222 / 1212	0.01
NO ₃ -N	(mg/L)	0.01 / 0.01	0.23 / 0.28	0.01
NH ₄ -N	(mg/L)	0.05 / 0.06	0.05 / 0.05	0.85
DIN	(mg/L)	0.09 / 0.08	0.26 / 0.26	0.10
DON	(mg/L)	0.12 / 0.12	0.05 / 0.05	0.08
TDN	(mg/L)	0.21 / 0.18	0.30 / 0.36	0.19
PO ₄ -P	(mg/L)	<0.01 / <0.01	<0.01 / <0.01	n/a
DOC	(mg/L)	3.54 / 4.07	2.07 / 1.52	0.34
DOC:TDN		20.56 / 23.88	9.92 / 8.92	0.23
Benthic Biofilm				
Chl <i>a</i>	(µg/cm ²)	1.34 / 1.34	3.35 / 3.27	0.007
AI		1367 / 724	1419 / 309	0.81
AFDM	(µg/cm ²)	1074 / 672	4181 / 1082	0.36
Metabolism				
GPP	(g O ₂ /m ² /d)	0.02 / 0.0001	0.45 / 0.22	0.03
ER	(g O ₂ /m ² /d)	-1.43 / -1.30	-1.99 / -1.82	0.37
P:R		0.01 / 0.0001	0.20 / 0.15	0.03
N demand	(g N/m ² /d)	<0.01 / <0.01	0.02 / 0.009	0.03

2.3.3 Nutrient-diffusing substrates

In unburned watersheds, the N amendment had a significant positive effect on Chl *a* (Figure 2.4). There was a 132% increase in Chl *a* concentrations from 1.34 µg/cm² in unamended substrates to 3.12 µg/cm² in amended substrates (Figure 2.4a). The N+P amendment had a similar positive effect (Figure 2.4b), causing a 91% increase in Chl *a* from 1.34 µg/cm² in unamended substrates to 2.57 µg/cm² in amended substrates (Figure 2.4a). The P treatment however, had no significant effect on Chl *a* (Figure 2.4b). The C, C+P, and C+N+P treatments all significantly

suppressed Chl *a* whereas the C+N treatment had no significant effect on Chl *a* in unburned watersheds (Figure 2.4b).

In burned watersheds, both the N ($4.86 \mu\text{g}/\text{cm}^2$, $p=0.07$) and P amendments ($4.94 \mu\text{g}/\text{cm}^2$, $p=0.11$) caused slight increases in Chl *a* compared to the unamended control ($3.35 \mu\text{g}/\text{cm}^2$) (Figure 2.4c-d). However, the N+P treatment caused the only significant, positive response in burned streams (Figure 2.4d) with a 102% increase in Chl *a* concentration from $3.35 \mu\text{g}/\text{cm}^2$ in unamended substrates to $6.77 \mu\text{g}/\text{cm}^2$ in N+P amended substrates (Figure 2.4c). C significantly suppressed and C+P marginally suppressed ($p=0.08$) Chl *a* while the C+N and C+N+P treatments had no significant effect on Chl *a* in burned watersheds (Figure 2.4d).

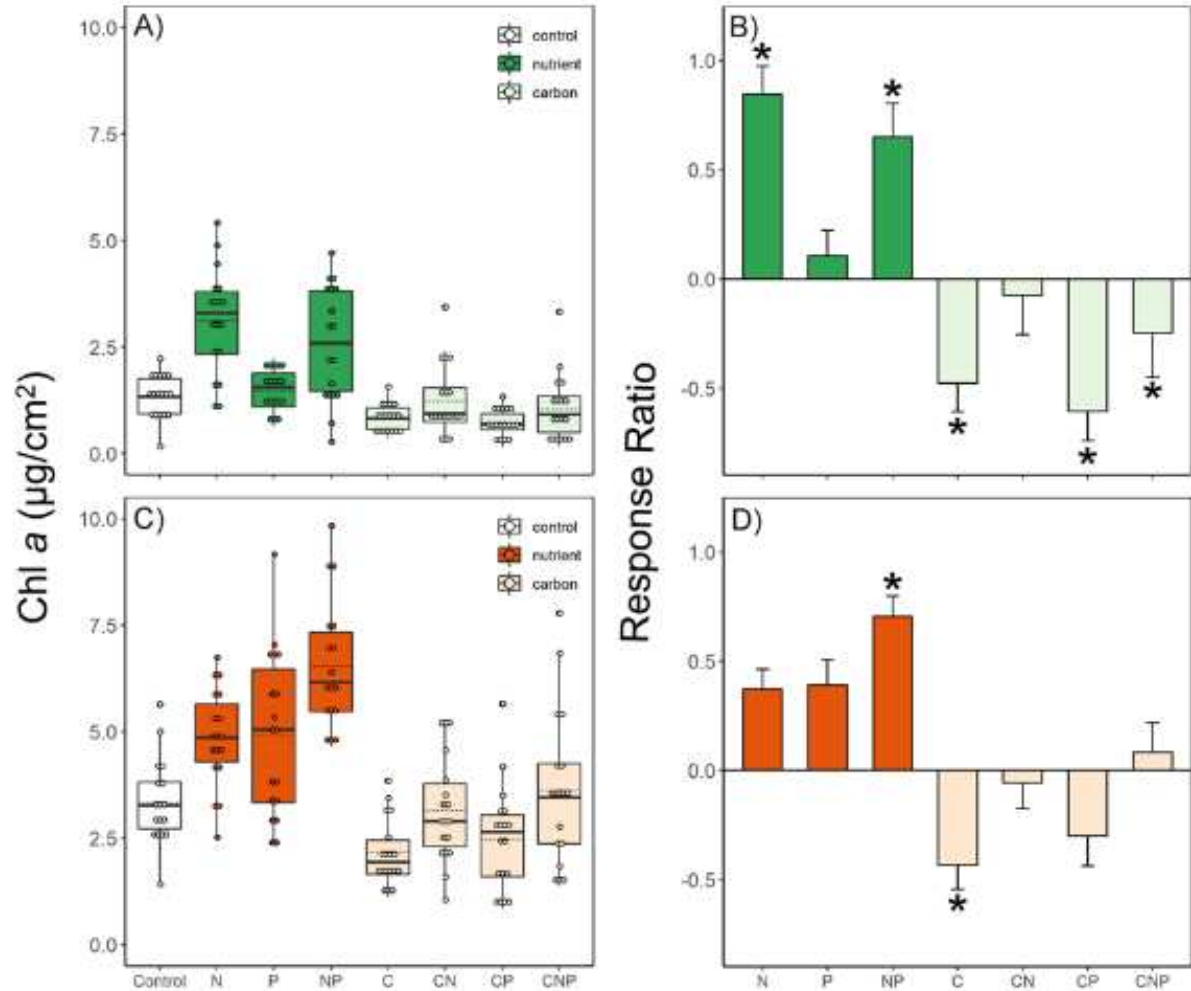


Figure 2.4: Autotrophic response to nutrient diffusing substrate (NDS) experiments for unburned (A-B, green) and burned (C-D, orange) watersheds. The left panels represent raw Chl *a* concentration in A) unburned and C) burned watersheds for each NDS treatment. The horizontal solid line of each boxplot denotes medians, the dashed lines denote means, the upper and lower limits of the box span the interquartile range, the whiskers span 1.5-times the interquartile range, and dots beyond the whiskers are outliers. The right panels display response ratios (i.e., $\ln(\text{treatment mean}/\text{control mean})$) of each treatment for B) unburned and D) burned watersheds representing changes relative to the control. Positive and negative response ratios indicate that amendments enhanced or suppressed Chl *a*, respectively. The dark shaded colors correspond to nutrient treatments (N, P, and NP), the light shades are carbon treatments (C, CN, CP, and CNP), and the unshaded boxes are controls. “*” indicates statistically significant treatment responses ($p < 0.05$).

2.3.4 Benthic biofilm

Autotrophic algal biomass was 2.5-times greater in burned watersheds with Chl *a* concentrations averaging $3.35 \mu\text{g}/\text{cm}^2$ compared to $1.34 \mu\text{g}/\text{cm}^2$ in unburned watersheds (Figure 2.5a). Furthermore, Chl *a* concentration increased with the extent of watershed burned ($p=0.015$, $R^2=0.80$, Figure A1). Heterotrophic bacterial biomass did not differ in burned and unburned watersheds (Figure 2.5b, Table 2.3), but the uniformly high AI values reflect the abundance of heterotrophic biofilms in these headwater streams (Steinman et al., 2006). Total biomass, measured as AFDM, was not significantly different between burned and unburned watersheds (Figure 2.5c, Table 2.3).

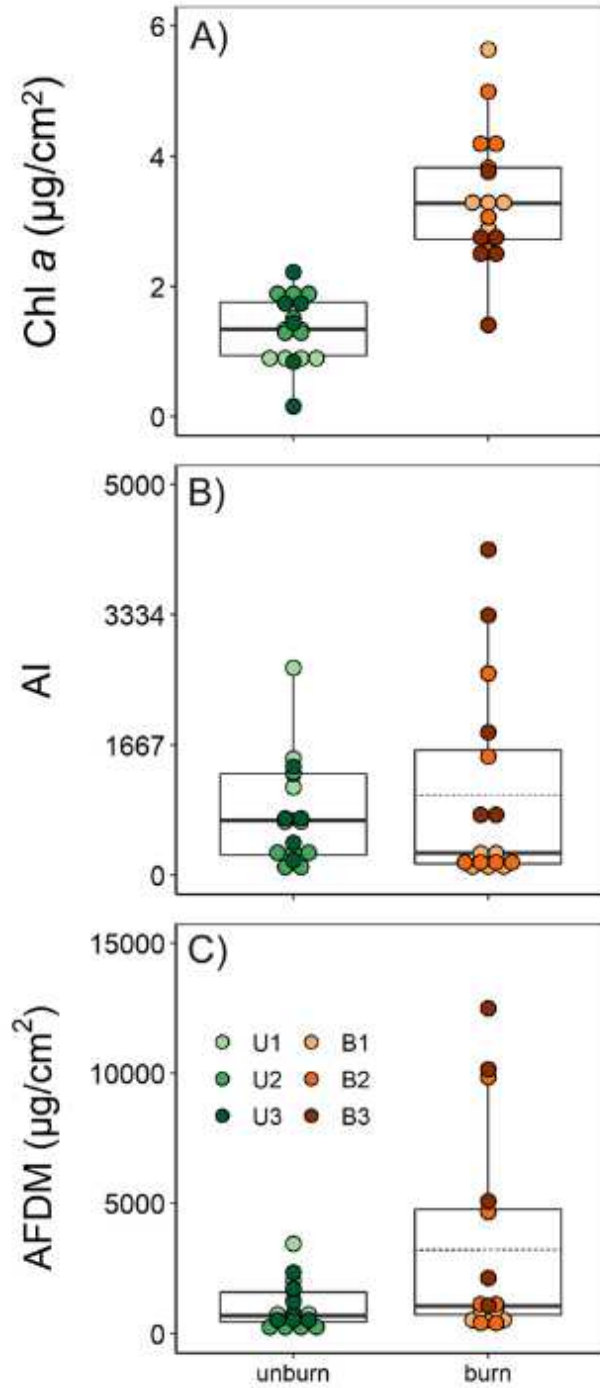


Figure 2.5: A) Autotrophic biofilm biomass based on chlorophyll *a* (Chl *a*) B) heterotrophic biofilm biomass based on the autotrophic index (AI) and C) total biofilm biomass based on ash-free dry mass (AFDM). Each point represents a 20-day in-stream deployment, with 6 replicates per site (color-coded). The solid horizontal line in each boxplot denotes medians, the dashed lines are means, the upper and lower limits of the box span the interquartile range, the whiskers span 1.5-times the interquartile range, and dots beyond the whiskers are outliers. Only Chl *a* differed significantly between burned and unburned watersheds as assessed by linear mixed-effects models (Table 2.3).

2.3.5 Stream metabolism

Mean daily rates of GPP were 20-times higher in streams draining burned (0.45 g O₂/m²/d) compared to unburned watersheds (0.02 g O₂/m²/d, Figure 2.6a, Table 2.3). Daily rates of ER were not significantly different between burned and unburned watersheds (Figure 2.6a, Table 2.3). All study streams had P:R ratios <1 (Figure 2.6b, Table 2.3), indicating that respiration exceeded production, and suggesting that stream biotic production relies on external organic matter inputs. However, the burned streams had significantly higher P:R ratios indicating higher relative primary production compared to unburned streams (Figure 2.6b, Table 2.3). Based on stoichiometric relationships with GPP, I estimated that autotrophic N uptake was 20-times higher in the burned compared to unburned watersheds (Figure 2.6c, Table 2.3).

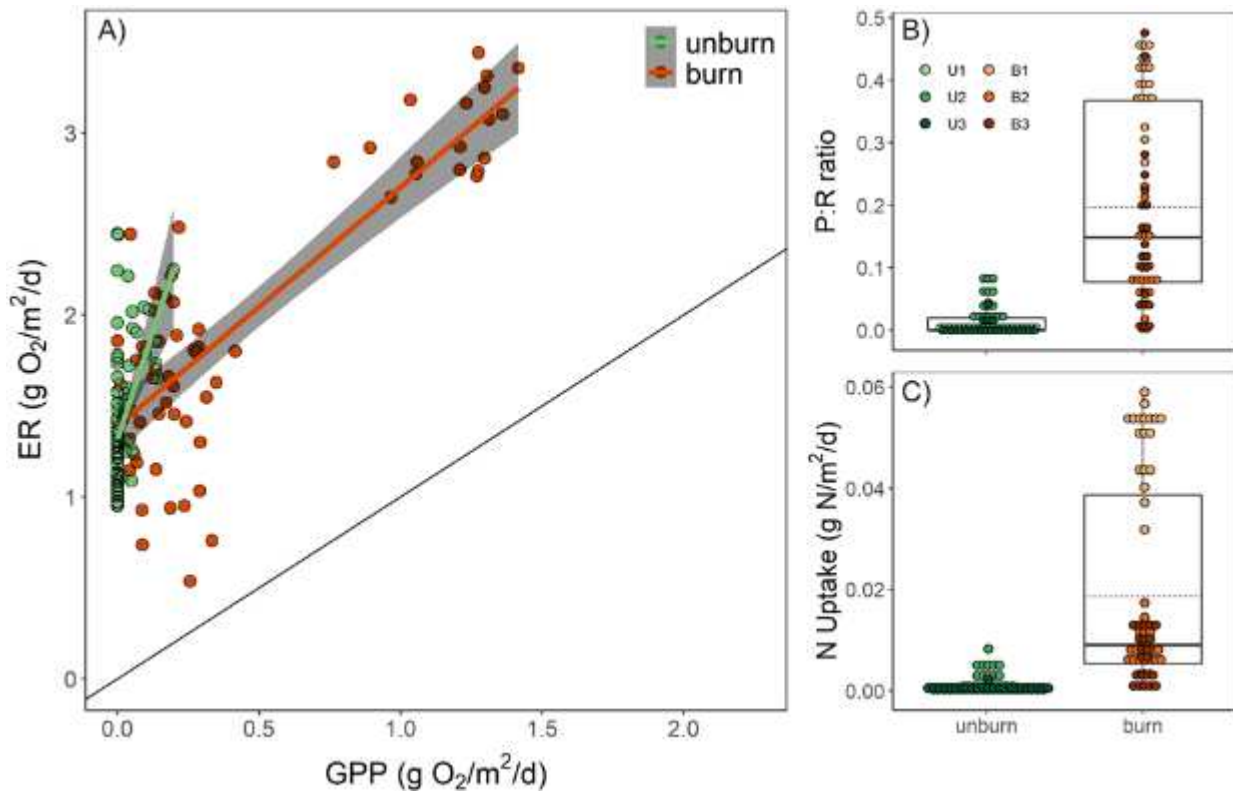


Figure 2.6: A) Stream metabolism for the 3 streams draining unburned watersheds (green) and the 3 draining burned watersheds (orange). Data above the 1:1 line in panel A indicate that ecosystem respiration (ER) exceeded gross primary production (GPP). Each point represents a

site-day metabolism estimate and linear regressions depict the general relations between GPP and ER separately for unburned (green) and burned (orange) watersheds. B) Productivity to respiration (P:R) ratios and C) daily autotrophic N uptake rates derived from daily GPP estimates for each site-day, color-coded by site. The solid horizontal lines in the boxplots denote medians, the dashed lines represents means, the upper and lower limits of the box span the interquartile range, the whiskers include data within 1.5-times the interquartile range, and dots beyond the whiskers are outliers. Statistical significance is denoted in Table 2.3.

2.4 Discussion

2.4.1 Autotrophic response to nutrient amendments

Our NDS experiments demonstrated differences in autotrophic nutrient responses that were related to variability in stream $\text{NO}_3\text{-N}$ concentrations, which were 23-times higher in streams draining burned relative to unburned watersheds. I observed a significant, positive Chl *a* response to N addition in NDS experiments in unburned watersheds (Figure 2.4b). This result indicates that N was a primary nutrient limiting autotrophic biofilms in these unburned systems. In contrast, there was no significant Chl *a* response to N addition in burned watersheds (Figure 2.4d) demonstrating that N was not a primary limiting nutrient in these nitrate-rich burned streams. While the NDS experiments were conducted during a short experimental period, the pattern of elevated $\text{NO}_3\text{-N}$ in these burned streams is consistent and long-lasting (Rhoades et al., 2011a; Rhoades, Chow, et al., 2019).

In contrast to stark differences in $\text{NO}_3\text{-N}$ concentrations, stream $\text{PO}_4\text{-P}$ concentrations were below the analytical detection limit of 0.01 mg/L in streams draining both the burned and unburned watersheds. Despite the low $\text{PO}_4\text{-P}$ concentrations, individual P amendments had no significant effect on Chl *a* in any of the study streams (Figure 2.4). This finding is consistent with experimental studies demonstrating that primary P limitation of autotrophic biofilms is rare, even under low ambient concentrations (Tank & Dodds, 2003). While $\text{PO}_4\text{-P}$ is the dominant

bioavailable form of inorganic P in streams, it is only one component of the total P pool that cycles within forested watersheds (Schlesinger and Bernhardt 2013). Thus, unmeasured organic and inorganic P sources may alleviate autotrophic P-limitation, particularly in burned watersheds as multiple forms of P (soluble reactive, total dissolved, particulate, and total P) have been shown to increase after wildfire (Silins et al., 2014).

While there was no autotrophic biomass response to P addition alone, I did observe positive responses to N+P addition across all study sites. In unburned watersheds, I observed a significant, positive Chl *a* response to both individual N and N+P treatments (Figure 2.4b) indicating that N was primary and P was secondary in limiting autotrophic growth (sensu Tank and Dodds 2003). In burned watersheds, I only observed a significant, positive Chl *a* response to the combined N+P treatment, with non-significant responses when N or P were added individually. This indicates N+P co-limitation and an overall reduction of primary N limitation in burned watersheds. Together, these alterations in autotrophic nutrient limitation 5 and 15 years post-fire represent the lasting influence that upland land cover change can have on stream ecosystems (Johnson et al., 2009). Furthermore, the N+P co-limitation that I observed in burned streams suggests that increases in P loading to nitrate-rich burned streams may stimulate in-stream productivity and enhance the potential for eutrophication of aquatic ecosystems after fire (Emelko et al., 2016; Santos et al., 2015; Smith et al., 2011).

2.4.2 Biotic regulation of coupled C and N cycles

When the supply of labile C is adequate, heterotrophs can outcompete autotrophs for N and P (Bechtold et al., 2012; Weaver, 2019). I did not directly measure the response of heterotrophs to NDS treatments, but were able to infer changes in their behavior based on measured stream

autotroph responses (Weaver 2019). I expected heterotrophs to respond strongly to C amendments (i.e., C, CN, CP, CNP) and outcompete autotrophs, resulting in negative Chl *a* response ratios. Indeed, as reported elsewhere (Bechtold et al., 2012; Weaver, 2019), Chl *a* responded negatively to C amendments in both burned and unburned watersheds (Figure 2.4), indicating that heterotrophs outcompete autotrophs in C-amended NDS treatments in these streams.

Although I observed negative Chl *a* responses to C amendments in all streams, I observed a weaker Chl *a* suppression (i.e., less heterotrophic competition) in burned watersheds (Figure 2.4). This result may indicate reduced in-stream heterotrophic C-limitation following wildfire. In this study, I observed slightly lower DOC concentrations in streams draining burned relative to unburned watersheds (Figure 2.3), which would often be interpreted as more C available for heterotrophic respiration in streams of unburned watersheds. However, because of the broad range of potential reactivities of dissolved organic matter (DOM), inferring bio-available C from DOC concentrations alone can potentially be misleading. For example, other work has demonstrated that although old-growth forests export water with higher DOC concentrations relative to landscapes regenerating from clear-cut harvesting, the DOM exported from the regenerating landscape was five times more reactive as determined from microbial assays (Fegel et al., 2021). Accordingly, it is important to consider not only DOC concentration but also the character and reactivity of the DOM. While I did not analyze DOM character in these study streams, the data demonstrated significantly higher GPP and associated autochthonous production in burned compared to unburned streams. Autochthonous C is generally more reactive than terrestrially-derived C (McKnight et al., 1994; Aiken and Cotner, 1995; Battin et al., 1999). As such, the high levels of in-stream productivity in these burned streams could provide highly reactive C for heterotrophic respiration. This could be partially responsible for the weaker Chl *a* suppression observed in

burned watersheds. Accordingly, wildfire may alter the concentration, character, and reactivity of DOM in streams and the potential for wildfire to alter watershed C cycling warrants further consideration

2.4.3 Forest disturbance and watershed response

Watershed nutrient export is the net balance between terrestrial to aquatic supply (Likens et al., 1970) and in-stream biotic demand (Bernhardt et al., 2003; Bernhardt et al., 2005). Terrestrial to aquatic nutrient transfer in excess of in-stream demand will typically be transported downstream (Earl et al., 2006). In this study, in-stream N demand closely matched N supply in unburned watersheds and resulted in low NO₃-N export (Figure 2.7a). Although both primary productivity and autotrophic N demand increased 20-fold following the studied wildfires (Figure 2.6), NO₃-N export remained higher compared to unburned watersheds (Table 2.3). Results from these study sites suggest that increased N supply from burned uplands exceeded post-fire increases in stream biotic demand (Figure 2.7b). The generalizability of these findings requires additional study across a broader range of wildfires, watersheds, and flow conditions.

In this study, increased in-stream productivity and nutrient demand partially mitigate post-fire nutrient export, but the in-stream response is exceeded by nutrient supply from burned uplands. Given the small spatial extent of streams (<1% of watershed area) relative to the extent of the contributing area that was burned (73-99%), this result seems likely in post-fire watersheds with high burn extent. Additionally, stream productivity can be limited by light, temperature, nutrients, substrate, or streamflow either individually or in combination (Bernot et al., 2010) and when nutrient limitations subside, another factor may constrain productivity. Thus, variation in supply, more so than in-stream demand, can drive stream ecosystem nutrient saturation (Covino et al.,

2018) and partially control watershed nutrient export. In these study watersheds, terrestrial supply exceeded in-stream demand in burned systems, which underlies the persistent nutrient export reported after these (Rhoades, Chow, et al., 2019) and other fires (Rust et al., 2018).

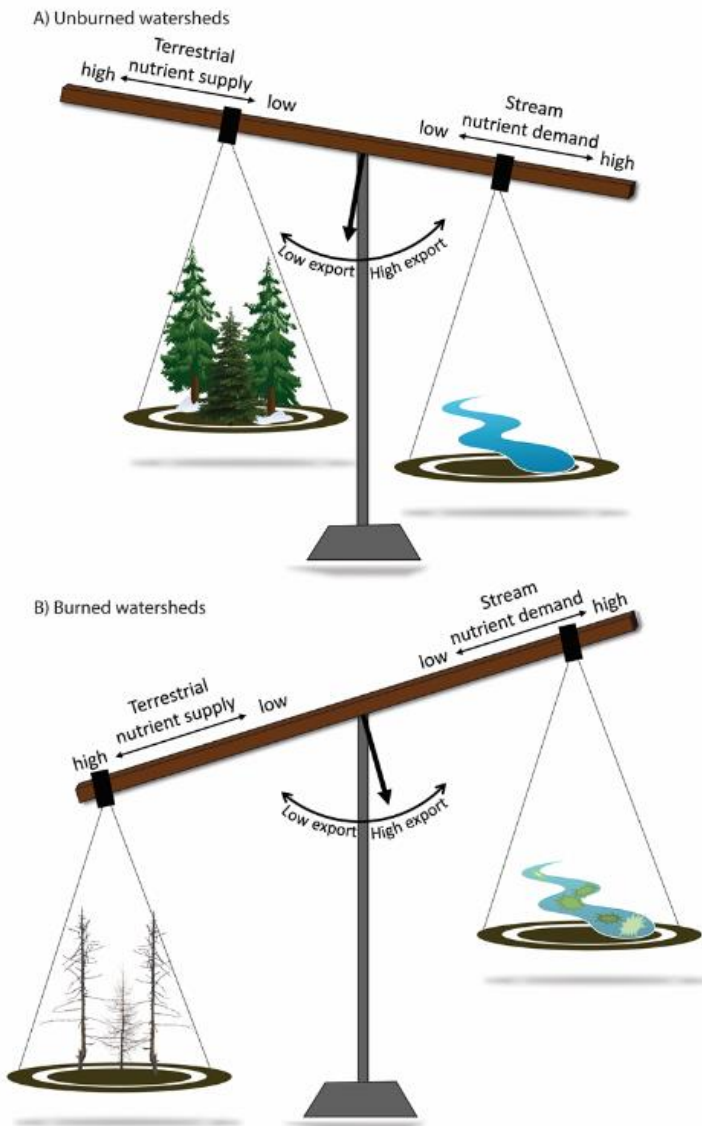


Figure 2.7: Conceptual supply-demand balance where watershed nutrient export is the difference between terrestrial nutrient supply and in-stream nutrient demand. In this study, terrestrial supply was inferred from measured stream demand and watershed export in A) unburned and B) burned watersheds. In the unburned watersheds, low terrestrial supply was balanced by low in-stream demand, causing minimal watershed export. Conversely, the burned watersheds had high terrestrial supply that exceeded high in-stream demand and resulted in elevated watershed $\text{NO}_3\text{-N}$ export. Adapted from Lane (1955).

Previous research has estimated that 97% of N inputs to Hayman watersheds were retained within pre-fire vegetation and soils, but that value declined to <50% in severely burned watersheds (Rhoades et al., 2019). This study and others indicate that reduced terrestrial N retention results in elevated post-fire stream NO₃-N concentrations and watershed export, both of which tend to increase with wildfire severity and extent (Rhoades, Chow, et al., 2019; Riggan et al., 1994; Rust et al., 2018; Stephan et al., 2012). Thus, the increased frequency and severity of projected disturbances (McDowell et al., 2020; Westerling, 2016; Williams et al., 2016) is likely to enhance nutrient loading to aquatic ecosystems and intensify risks of eutrophication and harmful algal blooms both within and downstream of disturbed landscapes (Dodds & Smith, 2016; Emelko et al., 2016; Smith et al., 2011).

2.5 Conclusions

This study evaluated the consequences of wildfire on in-stream nutrient limitation, benthic biomass, and stream metabolism 5 and 15 years after severe wildfire. The comparison of burned and unburned watersheds highlights significant changes in the post-fire watershed nutrient balance. The burned streams in this study had 23-times higher stream NO₃-N concentrations, reduced autotrophic N-limitation, and greater benthic autotrophic biomass and productivity than unburned streams. These data demonstrate that limited post-fire vegetation reestablishment can result in persistent increases in stream nutrient concentrations and change the balance of supply and demand across coupled terrestrial-aquatic ecosystems. These results also demonstrate that increased in-stream N demand does not fully compensate for high terrestrial N loading, even 5 and 15 years after severe wildfire. Accordingly, extensive regeneration will be required to reduce terrestrial to aquatic nutrient supply and minimize watershed NO₃-N export. As severe forest

disturbance increases throughout the western US, it will likely leave lasting effects on biogeochemical cycling within headwater systems.

3. Assessing Soil Supply and Plant Demand to Interpret Long-Term Post-Fire Stream N Export

3.1 Introduction

Fire can have profound impacts on the amount, form, and distribution of nitrogen (N) in soils, groundwater, and streams (Certini, 2005; Wan et al., 2001). Substantial N stocks are lost from the combustion of the O horizon and occasionally upper mineral soils during high severity fire (Bormann et al., 2008; Johnson et al., 2005). The pyrolysis of organic matter initiates an immediate pulse of ammonium (NH_4^+) in soils and streams (Covington & Sackett, 1992; Grogan et al., 2000; Raison, 1979; Wan et al., 2001a). Nitrification is then stimulated by increased NH_4^+ concentrations (Hanan et al., 2016), favorable abiotic conditions (i.e., soil temperature, moisture, and pH) (Bauhus et al., 1993; Hanan et al., 2016), and the presence of alkaline char and ash (Bauhus et al., 1993; DeLuca & Sala, 2006) which causes a delayed, but more prolonged pulse of nitrate (NO_3^-) in soils and streams (Covington & Sackett, 1992; Wan et al., 2001a). Mineral N that is not taken up by plants or microbes is often leached from soils in the mobile, dissolved form, NO_3^- (Gresswell, 1999; Turner et al., 2007) or eroded and deposited downslope as N-rich soil or ash (Grogan et al., 2000; Lane et al., 2008; Pierson et al., 2019).

Post-fire terrestrial N retention is strongly influenced by tree density (Turner et al., 2009). Because dry conifer forests rely on live trees as post-fire seed sources (Bonnet et al., 2005), regeneration into large, high severity patches has been slow (Chambers et al., 2016; Rother & Veblen, 2016). This seed dispersal limitation will likely become more widespread as the annual area burned at high severity increases across the Western US (Parks & Abatzoglou, 2020). When regeneration is slow or absent, burned forests remain in grass- or shrub-dominated states for extended periods (Roccaforte et al., 2012) which is becoming more common as high severity fire

becomes more prevalent and greater annual moisture deficits limit seedling recruitment across the Western US (Coop et al., 2020; Parks & Abatzoglou, 2020; Stevens-Rumann et al., 2018; Tepley et al., 2017; Walker et al., 2018). Slow forest recovery within large, high severity burn patches may sustain post-fire inorganic N export by reducing vegetation N uptake compared to unburned forests (Dove et al., 2020; Kurth et al., 2014).

Recent research documents that wildfires can have persistent impacts on ecosystem N cycling and water quality (Kurth et al., 2014; Rhoades, Chow, et al., 2019; Rust et al., 2018). In Northern Arizona, soil inorganic N pools and soil NO_3^- supplied through nitrification remained elevated for three decades following a stand replacing fire (Kurth et al., 2014). Additionally, stream N remained elevated and post-fire NO_3^- concentrations were lower along streams with greater riparian vegetation cover 14 years after the Hayman Fire in Colorado (Rhoades, Chow, et al., 2019). These studies demonstrate long-term alterations in soil N supply and vegetation N demand that expose a need to investigate which ecosystem component (i.e., soils or vegetation) is driving elevated stream N decades after fire.

This study aims to increase understanding of post-fire N cycling and the processes that contribute to the persistent release of N from burned watersheds. Specifically, the goal was to determine if elevated stream N originated from soil N pools and inorganic N production. I compared inorganic N concentrations, net nitrification, and mineralization in near-surface mineral soils (0-15 cm), N leaching from the surface root layer (30 cm), and N concentrations in shallow groundwater (40-100 cm) in unburned forested watersheds and watersheds burned by severe crown fire during the 2002 Hayman Fire. Because soil, vegetation, fire behavior, and post-fire recovery all vary along topographic gradients (Hinckley et al., 2017; Holyman et al., 2018; Malone et al., 2018; Rother & Veblen, 2016), burn and unburn comparisons were distributed from uplands to

streamside riparian zones. These findings provide insight into an ecosystems capacity to store N in soils and vegetation following severe fire with limited regeneration and therefore could be used to inform where post-fire restoration should be focused to achieve NO_3^- reductions.

3.2 Methods

3.2.1 Site description

The 2002 Hayman Fire burned 550 km² of Colorado's Pike National Forest (Figure 3.1a) which is dominated by ponderosa pine (*Pinus ponderosa*) and Douglas-fir (*Pseudotsuga menziesii*) (Graham, 2003). The understory plant community is dominated by grasses (*Bromus* spp. and *Poa* spp.), wood's rose (*Rosa woodsii*), American red raspberry (*Rubus idaeus*), and *Geranium* sp. The majority of the Hayman Fire and the study area is underlain by the Pike's Peak batholith (Ruleman et al., 2011), which is comprised of medium to coarse-grained biotite and hornblende-biotite granite and weathers to form weakly developed coarse, sandy loam soils (i.e., Ustorthents and Cryorthents) (Moore, 1992; Robichaud et al., 2013). The mineral soil profile ranges from 0-40 cm (Moore, 1992) and coarse fragments comprise 30% of the soil volume. This semi-arid region receives an annual average of 40 cm of precipitation (WRCC, 2021) from both snow and summer monsoons and falls within the intermittent snow zone meaning snow cover does not persist throughout the winter (Richer et al., 2013).

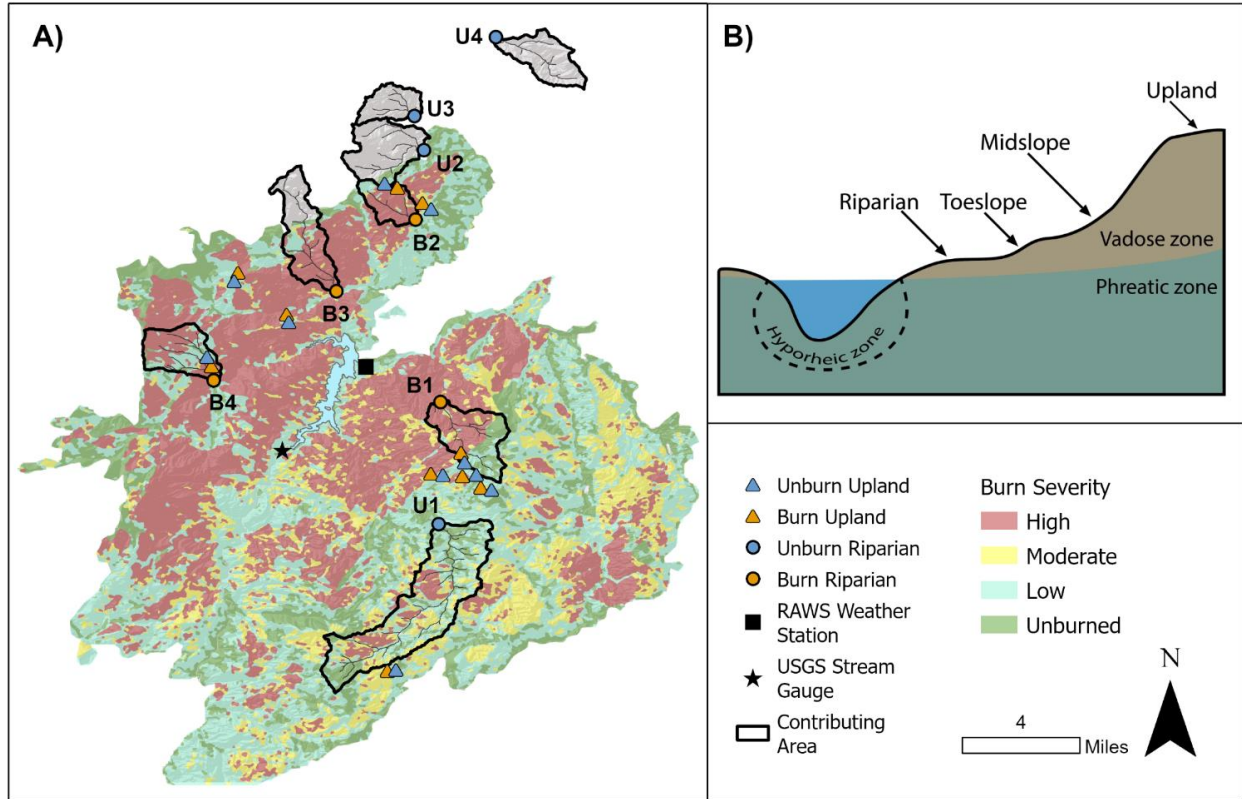


Figure 3.1: A) Sampling locations relative to the 2002 Hayman fire footprint, Colorado, USA. The upland positions are depicted as triangles and lower topographic positions (i.e., riparian, toeslope, and midslope) are grouped together as circles due to their proximity. Note there are two topographic gradients (one on stream left and one on stream right) for each circle displayed on the map. Burned sites are depicted in orange and unburned sites in blue. B) Cross-sectional view of the four topographic positions sampled in this study.

3.2.2 Vegetation sampling

I used the point-intercept method in 1 m² quadrats to characterize surface cover at each plot. Vegetation was differentiated into forb, graminoid, and shrub classes and surface cover was classified as follows: organic horizon, mineral soil, rock, moss/lichen, char, coarse wood (> 7.5 cm), fine wood (< 7.5 cm), coarse roots (> 0.5 cm), fine roots (< 0.5 cm) and other (e.g., scat, bone). Plant N demand scales with foliar N and aboveground net primary productivity (NPP, Turner et al., 2009) so I estimated NPP (kg C/m²) from remote imagery of the study area in 2018

(Robinson et al., 2018). Because this product is constrained to a 30-m resolution, I report one value for each riparian, toeslope, and midslope sequence and one value for each upland plot.

3.2.3 Soil sampling

In the summer of 2018, three mineral soil cores (0-15 cm) were collected from each topographic position and sieved to 2 mm to remove coarse fragments. The entire O horizon (i.e., litter + duff floor) was also sampled in unburned upland positions. A 20 g sub-sample from mineral and O horizons was dried at 105°C for 24 hours, ground in a roller table for 72 hours, and analyzed for total soil C and N content (%) by Dumas dry combustion (LECO CHN 2000; St Joseph, MI). C and N stocks of mineral and O horizons were then calculated by multiplying bulk density by soil depth and % C and N content. While I measured the bulk density of riparian, toeslope, and midslope mineral soils, I assumed O horizon bulk densities of 0.14 g/cm³ based on studies from ponderosa pine forests (Stephens et al., 2004) and upland mineral soil bulk densities of 1.39 g/cm³ (Robichaud et al., 2013). pH was also measured for mineral soils in a 1:1 supernatant of 10 g sub-sample of mineral soil and a slurry of DI.

In June of 2019, three mineral soil cores (0-15 cm) were again collected from each topographic position to measure extractable inorganic N pools and net production rates. All soils were sieved to 2 mm and an initial 20 g subsample was extracted with 100 mL of 2M KCl, shaken for 60 minutes, filtered, and analyzed for NO₃⁻ and NH₄⁺ using spectroscopy (Lachat QuikChem AutoAnalyzer FIA+ 800 Series, Loveland, CO). A second 10 g subsample was oven dried at 105°C for 24 hours to calculate gravimetric moisture content (GMC). A 50 g sub-sample was placed in a loosely capped plastic cup in a 20°C aerobic incubation chamber for 14 days (Binkley & Hart, 1989). Samples were rewetted with DI water periodically to maintain field moisture content. After

14 days, subsamples of the incubated soils were extracted and analyzed as described above. Net mineralization was calculated as the difference in NO_3^- plus NH_4^+ in the initial and incubated soils, net nitrification as the change in NO_3^- , and ammonification as the change in NH_4^+ (Hart et al., 1994).

I used ion exchange resins (IER) as an index of plant-available soil N (i.e., NO_3^- and NH_4^+) (Binkley & Matson, 1983). Six IER bags were buried at 5 cm depth in the mineral soil at each topographic position (i.e., 2 IER bags at each of the 3 plot replicates). I included two deployment periods – May 2019 to October 2019 and October 2019 to May 2020 which were respectively defined as summer and winter deployments. At the end of the incubation period, I extracted resins with 100 mL of 2M KCl, shook samples for 60 minutes, filtered, and analyzed the samples for NO_3^- and NH_4^+ concentrations as described above.

I measured volumetric water content (VWC) monthly from June to September of 2019 using a handheld time domain reflectometry instrument with a 20 cm probe (CD 620, HydroSense Campbell Scientific, Logan UT). Three to four measurements were recorded at each plot replicate and VWC was averaged by plot.

3.2.4 Water sampling

I measured surface water and shallow groundwater chemistry and water level in two burned (B1-2) and two unburned (U1-2) watersheds (Figure 3.1a). I instrumented each of these sites with a stream monitoring station, two riparian groundwater wells, two in-channel nested piezometers, and 14 tension lysimeters. The riparian wells were installed on both sides of the stream to a completion depth of 1 m to sample riparian groundwater. The nested piezometers were installed to depths of 40 cm and 80 cm in the center of the stream bed to sample hyporheic water. Porous cup, tension lysimeters (Soil Moisture Corp, Goleta, CA) were installed to a depth of 30 cm to

sample soil water leachate with 6 in the riparian zone, 6 in toeslope positions, 3 in midslope positions, and none in the uplands given the dry soil conditions.

I sampled stream water 1-2 times per month (5/13, 5/28, 6/12, 6/24, 7/8, 7/22, 8/3, 8/20, 9/14). I sampled shallow groundwater from the riparian wells and nested piezometers on the same dates using a peristaltic pump that was purged with DI water and a sample rinse prior to each sample collection. Soil water leachate was sampled throughout the summer (5/14, 5/29, 6/25, 7/17, 8/7, 9/15) using a hand pump following the same procedures. All water samples were stored on ice in acid-washed HDPE plastic bottles and filtered through 0.45 μm filters (Millipore Durapore PVDF, Billerica, MA). NO_3^- and NH_4^+ concentrations were measured with ion chromatography (Dionex Corp., Sunnyvale, CA). Detection limits were 0.01 mg/L for both NO_3^- and NH_4^+ and concentrations that fell below detection limits were replaced by one half the detection limit concentration (0.005 mg/L). This was only common for lysimeter samples.

TruTrack capacitance rods (Intech Instruments Ltd. New Zealand) were installed in all streams, wells, and piezometers to record stage every 15 minutes from May to October of 2019. These data were averaged by day to reduce noise and converted to station-specific z scores to allow for comparisons between stations. Manual water level measurements were also recorded biweekly throughout the summer field season to check continuously recorded water levels.

3.2.5 Statistical analysis

All measured variables were screened for outliers and averaged at the plot level. Subsequent analyses were conducted on the plot means. T-tests were used to determine whether measured soil, vegetation, and water properties varied with burn condition while stratifying by topographic position. ANOVA was used to determine if these parameters varied with topographic

position while stratifying by burn condition. All statistical analyses were conducted in R (R Development Core Team) and significance was determined at the $\alpha = 0.05$ level.

3.3 Results

3.3.1 Seasonal moisture dynamics

Over the course of the 2019 water year, the Cheesman weather station recorded 16.7 cm of rainfall (WRCC, 2021). The Glen Cove SNOTEL station recorded 37.4 cm of snow water equivalent (NRCS, 2021), but was located south of Hayman, near Pikes Peak at 3,500 m so the magnitude of snowfall was likely lower at the study sites where mean elevation was 2,500 m. Most snowfall occurred in March though snowfall continued through May and rainfall peaked in July (Figure 3.2). The South Platte stream gauge (USGS, 2021) demonstrated peak flows in late June during snowmelt though there were multiple rainfall-driven peaks throughout the season (Figure 3.2). The study watersheds were much smaller (i.e., first order streams draining into the South Platte) and exhibited similar, but muted seasonal trends in streamflow (Figure B1). The volumetric moisture content in the top 20 cm of mineral soils declined throughout the summer sampling period and moving from riparian to upland positions, but was generally similar in burned and unburned soils (Figure B2).

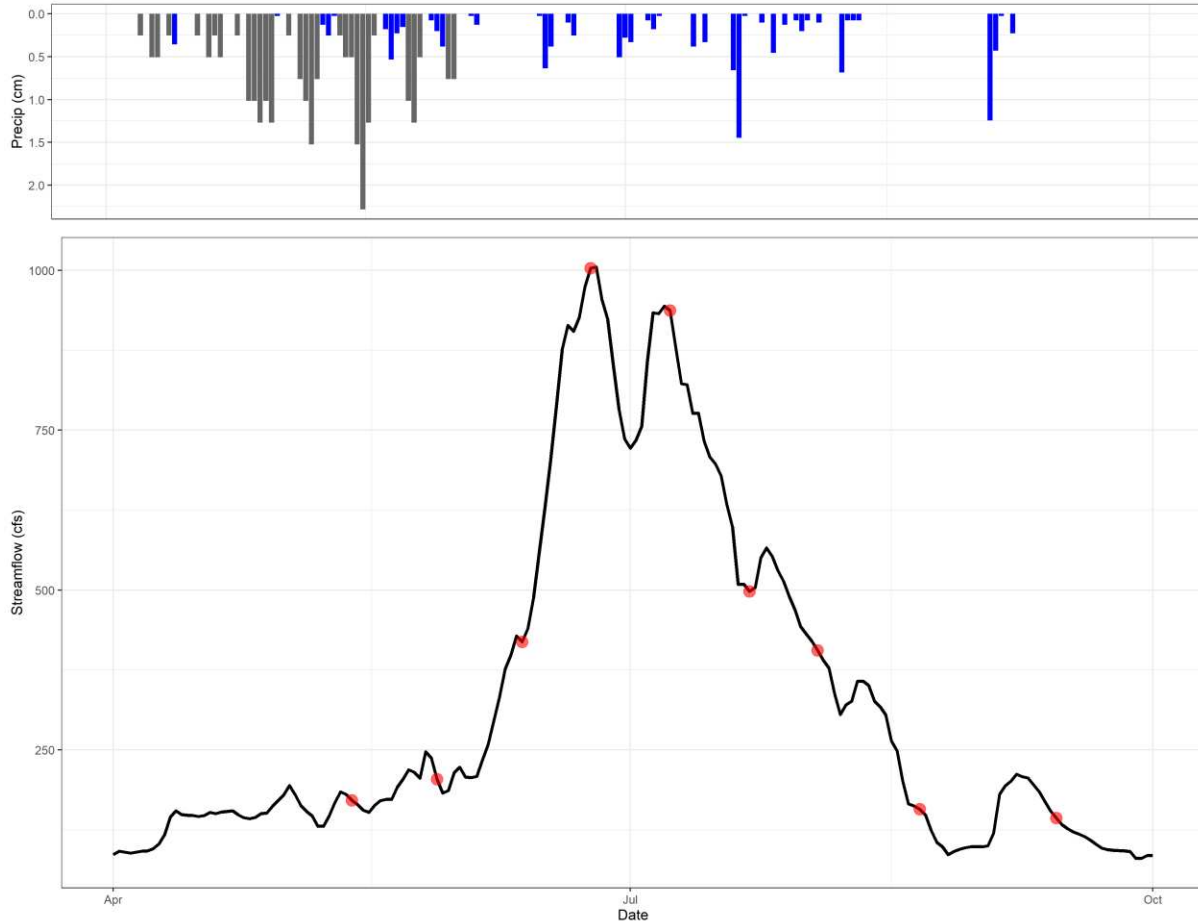


Figure 3.2: Time series of precipitation and discharge from April to October of 2019. Rainfall comes from the Cheesman RAWs station (blue), snow water equivalent from the Glen Cove SNOTEL station (grey), and stream discharge from the USGS South Platte stream gauge above Cheesman Reservoir (black). Water sampling dates are marked by red points.

3.3.2 Vegetation cover

Substrate cover only varied significantly with burn condition in upland positions where O horizon cover was lower and mineral soil and char cover were higher in burned compared to unburned plots (Figure 3.3a). In burned plots, O horizon cover decreased and mineral soil cover increased with distance from stream (Figure 3.3a). Substrate cover did not vary much with landscape position in unburned plots. Forb and graminoid cover were generally higher in burned plots though statistical significance varied with topographic position (Figure 3.3b). Shrub cover was variable, but was significantly higher in burned uplands than unburned uplands (Figure 3.3b).

Mean annual NPP, which is a proxy for vegetation N demand, was 5,666 and 4,669 kg C/m² in unburned riparian corridors and uplands and 1,750 and 1,351 kg C/m² in burned riparian corridors and uplands. Thus, unburned forests had three-times greater NPP, and associated vegetation N demand, compared to shrub-dominated, burned plots (Figure 3.3b). Unburned uplands were dominated by ponderosa pine and Douglas fir though aspen were also found in the toeslopes. There were no live conifers in the burned sites though half of the burned toeslopes had some aspen regeneration.

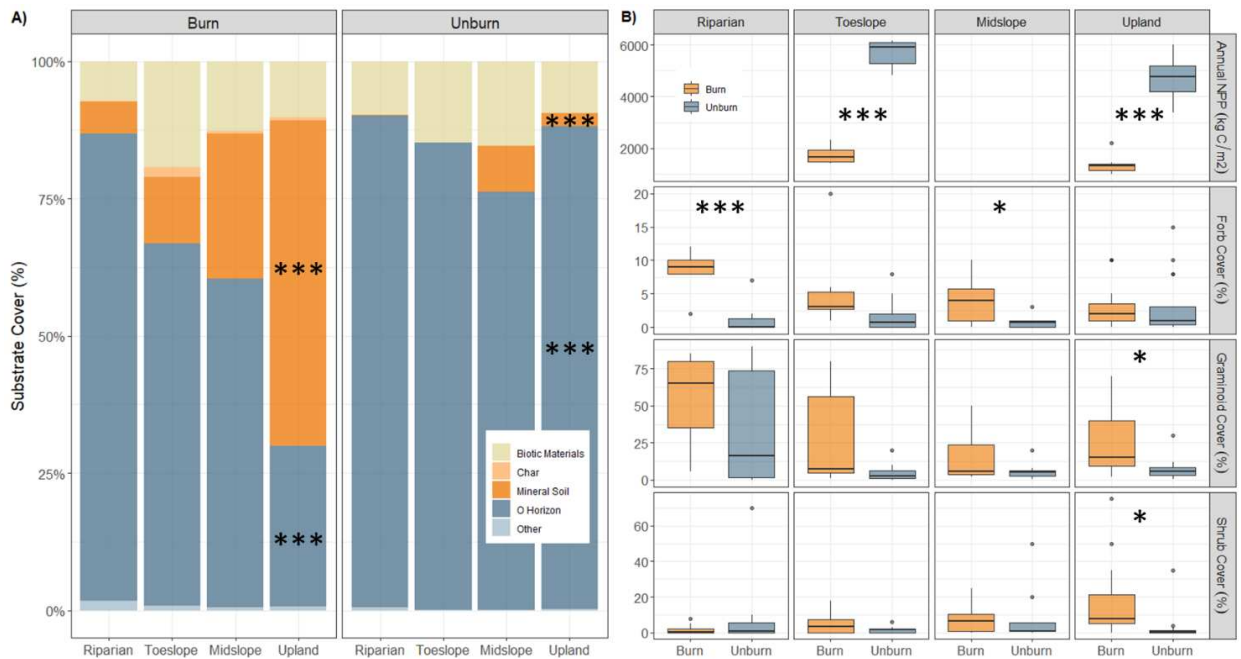


Figure 3.3: Mean A) substrate and B) vegetation cover estimates by burn condition and landscape position. Biotic materials include moss, lichen, coarse and fine wood, and coarse and fine roots and the other category includes rock, scat, and bone. The centerline of the boxplots denote median values, the upper and lower limits span the interquartile range, the whiskers include data within 1.5-times the interquartile range, and the dots beyond the whiskers are outliers. Burn condition significance is denoted by * p<0.05, ** p<0.01, ***p<0.001.

3.3.3 Soil C and N stocks

Mean C content ranged from 1.6% to 16% and was an order of magnitude higher in O horizon samples compared to mineral soils (Table 3.1). Mean C stocks in the top 5 cm of mineral

soils were 2,027 g C/m² in unburned plots and 1,914 g C/m² in burned plots. Mineral soil C stocks were the highest in toeslope positions and lowest in upland positions (Table 3.1). Total C was 1,620 g C/m² lower in burned than unburned uplands when summed across the top 5 cm of mineral soils (108 g C/m² lost) and the O horizon (1,512 g C/m² lost) which is similar to previously reported losses of 1,900 g C/m² (Bormann et al., 2008).

Table 3.1: Total C and N content (%) and C and N stocks (g N/m²) for mineral and O horizons. Mineral soils stocks were calculated for the top 5 cm and the full O horizon was sampled in unburned uplands.

		Mineral Soil		O Horizon		
		Burn	Unburn	Unburn		
C Content (%)	Riparian	2.5	3.2	-		
	Toeslope	3.1	3.7	-		
	Midslope	2.5	3.0	-		
	Upland	1.6	1.7	16		
N Content (%)	Riparian	0.14	0.18	-		
	Toeslope	0.17	0.19	-		
	Midslope	0.14	0.14	-		
	Upland	0.08	0.07	0.57	Burn-Unburn	% Change
C Stock (g C/m ²)	Riparian	1,859	2,028	-	-169	-8
	Toeslope	2,649	2,559	-	91	4
	Midslope	2,104	2,368	-	-264	-11
	Upland	1,044	1,152	1,512	-108	-9
N Stock (g N/m ²)	Riparian	103	119	-	-15	-13
	Toeslope	146	133	-	13	9
	Midslope	115	109	-	6	5
	Upland	55	45	55	9	20

Mean N content ranged from 0.07% to 0.57% and was generally similar in burned and unburned mineral soils (Table 3.1). Mean N stocks were 102 g N/m² in the top 5 cm of unburned mineral soils and 105 g N/m² in burned mineral soils. Mineral soil N stocks were also the highest in toeslope positions and lowest in upland positions (Table 3.1). Mineral soil N stocks were reduced by 45 g N/m² in burned uplands when summed across the top 5 cm of mineral soils (10 g

N/m² increase) and O horizon (55 g N/m² loss) which again is similar to previously reported losses of 55 g N/m² (Bormann et al., 2008).

3.3.4 Mineral soil inorganic N

Mean soil extractable NO₃⁻ concentrations were 1.75 mg/kg in burned mineral soils and 0.64 mg/kg in unburned mineral soils (Figure 3.4a). While NO₃⁻ concentrations did not vary significantly with burn condition (Figure 3.4a). Within burned sites, midslopes had the highest and uplands the lowest NO₃⁻ concentrations whereas NO₃⁻ did not vary consistently with topographic position in unburned sites (Figure 3.4a). Mean soil extractable NH₄⁺ concentration did not vary significantly with burn condition or topographic position (Figure 3.4b). NO₃⁻ comprised 51% of DIN on average in burned mineral soils and 34% in unburned mineral soils.

Plant-available NO₃⁻ was generally similar in burned and unburned mineral soils, though NO₃⁻ was 2.4-times greater in burned midslopes compared to unburned midslopes over the winter deployment period (Figure 3.5a). Plant-available NO₃⁻ was up to 2.8-times greater in the winter compared to the summer and did not vary with burn condition in riparian, toeslope, or upland positions (Figure 3.5a). Plant-available NH₄⁺ was higher in burned than unburned soils, with the exception of uplands (Figure 3.5b).

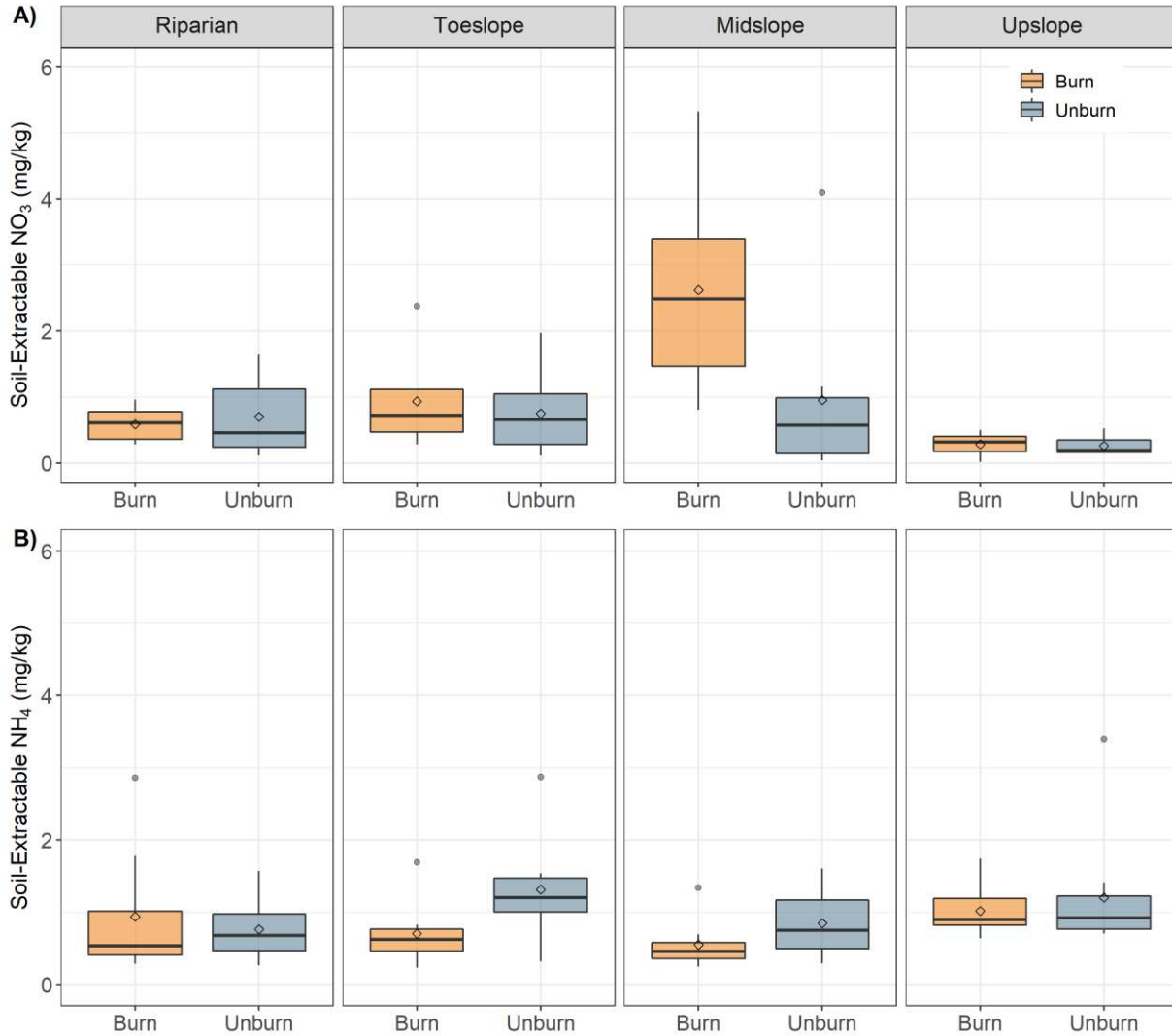


Figure 3.4: Soil-extractable A) NO₃ and B) NH₄ concentrations for the top 15 cm of burned (orange) and unburned (blue) mineral soil. Data were normalized per kg of dry soil. The centerline of the boxplots denote median whereas the open diamond denotes the mean, the upper and lower limits span the interquartile range, the whiskers include data within 1.5-times the interquartile range, and the dots beyond the whiskers are outliers. Burn condition significance is denoted by * p<0.05, ** p<0.01, ***p<0.001.

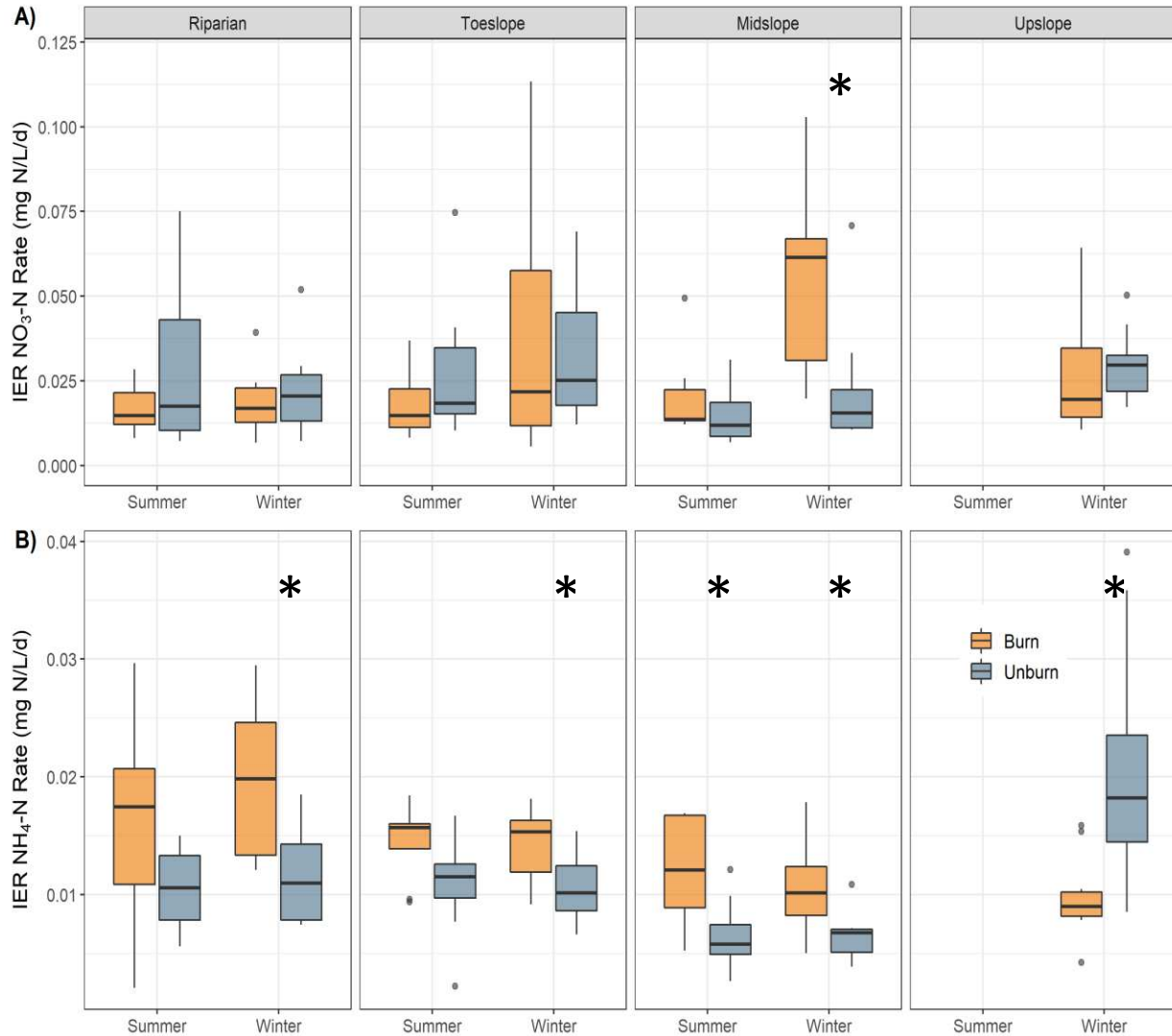


Figure 3.5: Ion exchange resin A) NO₃ and B) NH₄ availability separated by summer and winter deployment periods. This represents inorganic N availability in the top 5 cm of mineral soil and is normalized per kg of dry soil per day. Upslope positions only have winter data. The centerline of the boxplots denote median values, the upper and lower limits span the interquartile range, the whiskers include data within 1.5-times the interquartile range, and the dots beyond the whiskers are outliers. Burn condition significance is denoted by * p<0.05, ** p<0.01, ***p<0.001.

3.3.5 Net N transformations

Net ammonification rates were negative or near zero across all landscape positions and burn conditions (Figure 3.6). In contrast, net nitrification and mineralization rates were positive in all unburned soils and burned uplands (Figure 3.6). Burned soils in lower topographic positions

(i.e., riparian, toeslope, and midslope) exhibited negative or near zero nitrification and mineralization rates (Figure 3.6). Given the high observed variability, neither ammonification, nitrification, nor N mineralization varied significantly with burn condition ($p=0.08$).

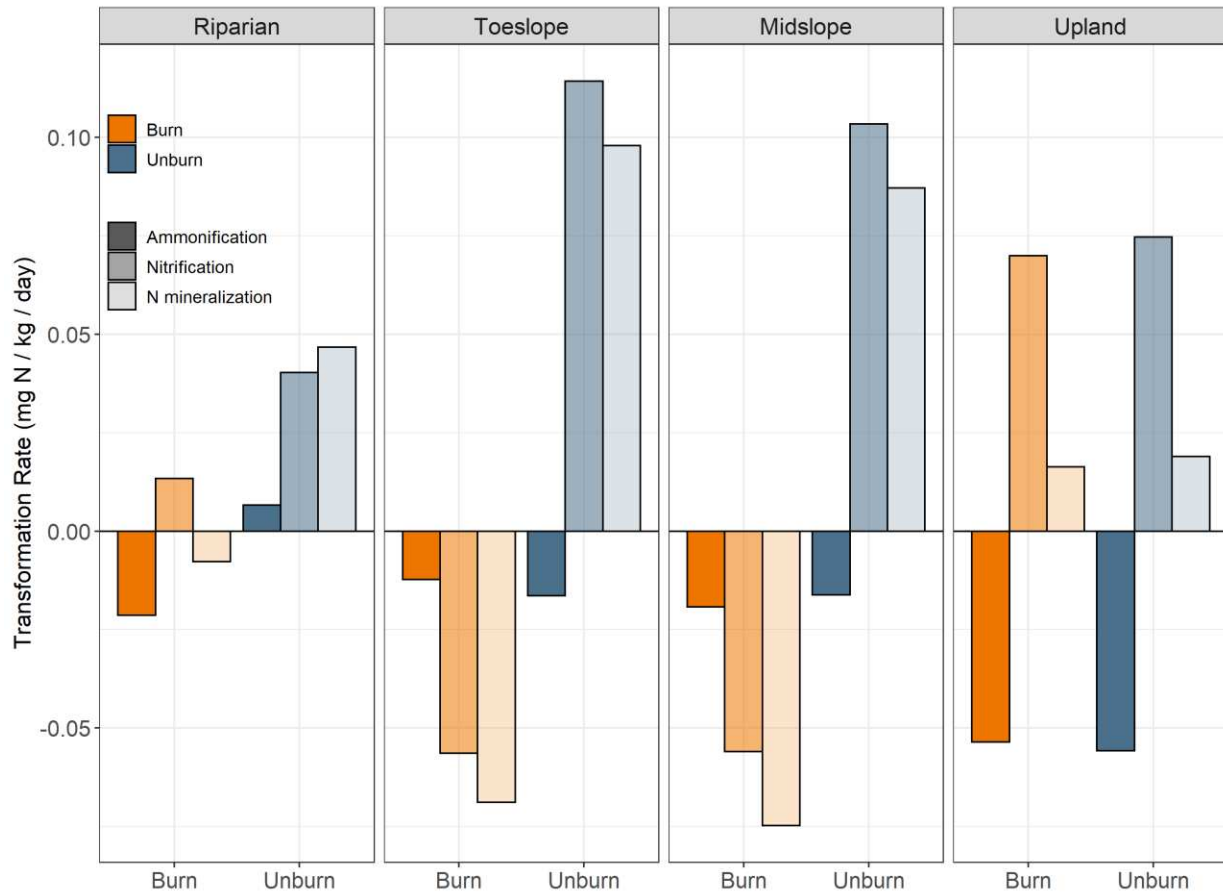


Figure 3.6: Mean net ammonification, nitrification, and N mineralization rates from 14-day aerobic laboratory incubations by burn condition and topographic positions.

3.3.6 Water N concentrations

Mean soil water NO_3^- concentrations were 0.21 mg/L in burned soils and 0.14 mg/L in unburned soils which is much lower than NO_3^- concentrations observed in shallow groundwater and streamwater (Figure 3.7). Shallow groundwater NO_3^- concentrations from the riparian wells and nested piezometers were consistently higher in burned (0.64-4.07 mg/L) compared to unburned watersheds (0.01-3.42 mg/L) (Figure 3.7b-c). Stream NO_3^- concentrations were also

consistently higher in burned (0.67-4.25 mg/L) compared to unburned watersheds (0.01-0.59 mg/L) (Figure 3.7d). Stream, groundwater, and soil water NH_4^+ concentrations were very low, ranging from 0.005 mg/L (i.e. detection limit) to 0.75 mg/L across all sampling locations and dates.

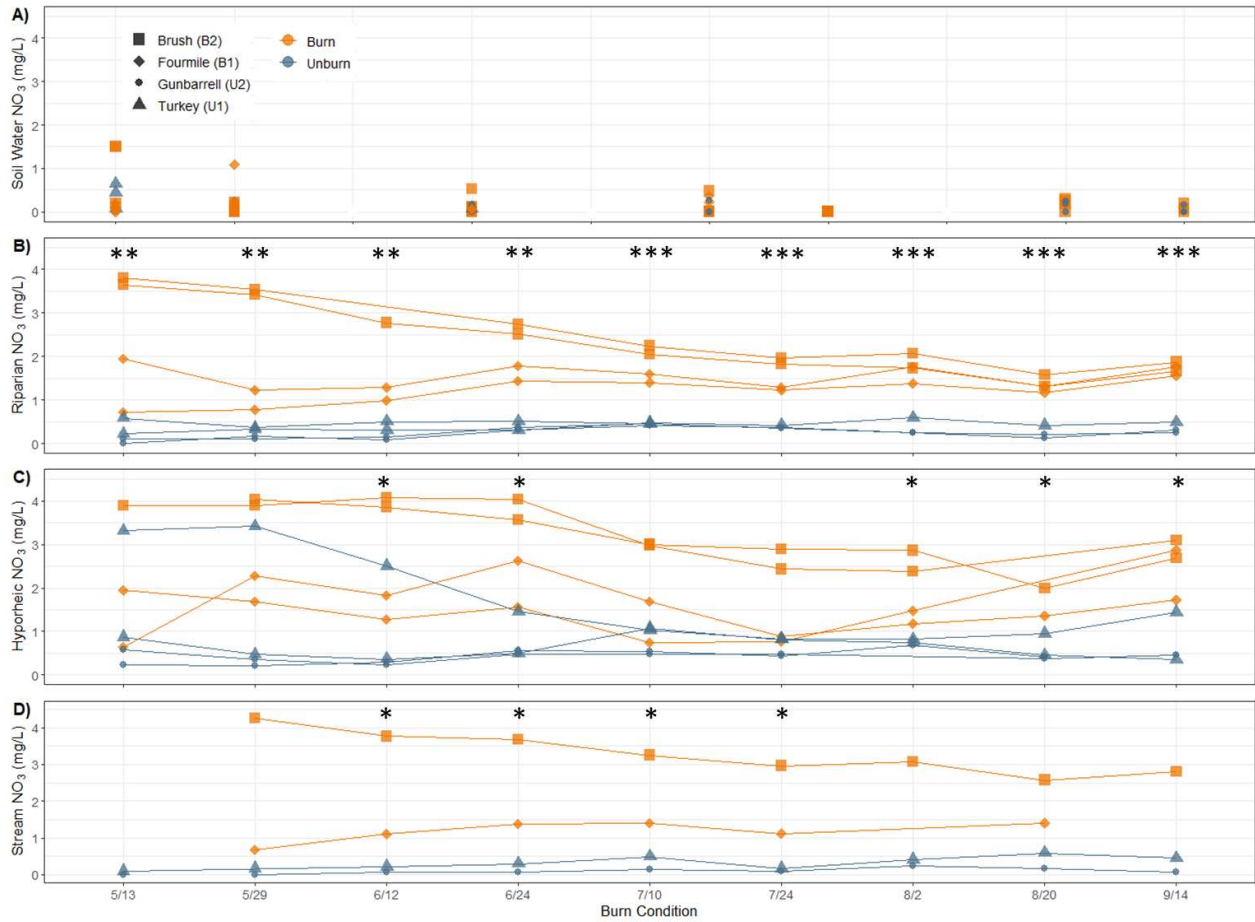


Figure 3.7: Time series of NO_3 concentrations from A) soil water from tension lysimeters (30 cm) B) riparian groundwater from wells (1 m), C) hyporheic water (40 and 80 cm) from nested piezometers, and D) stream water. Point color varies with burn condition and point symbols varies by watershed. Burn condition significance is denoted by * $p < 0.05$, ** $p < 0.01$, *** $p < 0.001$.

3.4 Discussion

Most ecosystems have substantial capacity to store added N in soils and vegetation so N losses are an indicator of ecosystem disturbance (Chapin et al., 2011). There is evidence that severe wildfire reduces the capacity of forested watersheds to retain atmospheric N inputs. It was

estimated that 97% of pre-fire N inputs to forested headwater catchments were retained within vegetation and soils, but that value declined to <50% after severe wildfire (Rhoades, Chow, et al., 2019). I investigated whether this post-fire loss of N retention capacity was the product of elevated soil N pools and net N transformation rates (Kurth et al., 2014) or lower plant demand (Rhoades, Chow, et al., 2019) in order to improve our understanding of long-term ecosystem resilience when extreme fire behavior and climatic conditions inhibit vegetation recovery.

3.4.1 Post-fire soil N supply

Ecosystem C and N stocks control terrestrial productivity (Chapin et al., 2011) and can be substantially reduced by high severity fire (Bormann et al., 2008). There was evidence of large C and N losses from O horizon combustion (~1,500 g/m² and 50 g/m² of C and N respectively) and erosion (7-225 g/m² and 0.3-11 g/m² of C and N over 4 post-fire years) (Pierson et al., 2019) after the Hayman fire. However, the C and N stocks were similar in burned and unburned mineral soils (Table 3.1) potentially because mineral soils have a higher heat capacity than O horizons, making them less susceptible to combustion losses (Neary et al., 1999). Mineral soil C stocks were only reduced by 6%, on average, which is similar to the 11% reductions reported in a meta-analysis of 57 fires (Nave et al., 2011). Conversely, I saw a 5% increase in mineral soil N stocks post-fire. While this finding differs from previously reported 12% reductions (Nave et al., 2011), it is not entirely surprising. Combustion losses of N from severe fire are generally small relative to total pre-fire stocks (Page-Dumroese & Jurgensen, 2006) and soil N retention can increase after fire due to the incorporation of N into microbial biomass (Xu et al., 2022). C:N ratios were also similar in burned (19:1) and unburned (23:1) mineral soils. In the absence of underlying differences in substrate quality, net N mineralization rates did not differ between burned and unburned mineral soils (Figure 3.6).

Observed nitrification rates, and consequently soil NO_3^- concentrations, were also similar in burned and unburned soils (Figures 3.4 and 3.6). While fire can stimulate nitrification (DeLuca & Sala, 2006; Kurth et al., 2014) through increased NH_4^+ (Hanan et al., 2016), favorable abiotic conditions (i.e., soil temperature and moisture) (Bauhus et al., 1993; Hanan et al., 2016), and the presence of alkaline char and ash (Bauhus et al., 1993; DeLuca & Sala, 2006), these effects are generally short-term (Covington & Sackett, 1992; Grogan et al., 2000; Raison, 1979; Wan et al., 2001a). Observed soil NH_4^+ concentrations (0.23-3.4 mg/kg) were much lower than other values reported immediately post-fire (<33 mg/kg, Turner et al., 2007) and were similar in burned and unburned mineral soils (Figure 3.4). Likewise, soil pH was similar in burned and unburned soils and therefore did not have a distinctive impact on nitrification. However, N transformation rates have been shown to decrease with time since fire in mineral soils, but increase with time in O horizons (Yermakov & Rothstein, 2006). While there may be unmeasured post-fire increases in O horizon nitrification, mean O horizon depths were only 0.5 cm in burned plots compared to 12 cm in unburned plots suggesting that these potential increases would be relatively small when scaled by area.

Overall, I found similar total C and N stocks, inorganic N concentrations, and N transformations rates (i.e., N mineralization and nitrification) in burned and unburned mineral soils (Figures 3.4-3.6). Together, these results demonstrate that there are no lasting changes to soil inorganic N supply 17 years after severe wildfire, corroborating numerous other studies that demonstrate only short-term soil N responses (Covington & Sackett, 1992; Grogan et al., 2000; Raison, 1979; Wan et al., 2001a).

3.4.2 Evidence of persistent plant-mediated NO_3^- losses

Following fire, mineral N that is not taken up by plants or microbes is either eroded and deposited downslope as N-rich soil or ash (Grogan et al., 2000; Lane et al., 2008; Pierson et al., 2019) or leached through soils to hillslope groundwater in the mobile, dissolved form, NO_3^- (Gresswell, 1999; Turner et al., 2007). While particle-associated fractions dominate N exports immediately post-fire (Lane et al., 2008), these contributions decline sharply within 2 years post-fire due to reduced sediment delivery (Pierson et al., 2019). However dissolved NO_3^- tends to have a slower recovery, likely due to elevated nitrification or persistent leaching (Lane et al., 2008, Rhoades et al., 2019). Indeed, stream NO_3^- concentrations were 10-times higher in burned compared to unburned watersheds 17 years post-fire (Figure B3). This pattern has been consistent throughout 15 years of post-fire monitoring and across flow states (Rhoades et al., 2011a; Rhoades, Chow, et al., 2019). However, N supply did not differ between burned and unburned mineral soils (Figures 3.4-3.6).

In the absence of differences in soil N supply, I explored the links between plant uptake and N losses. I characterized the relationship between NO_3^- concentration and streamflow over time in order to better understand watershed-scale patterns of N production and transport (Arora et al., 2020; Creed et al., 2015; Godsey et al., 2009). In the unburned watersheds, stream NO_3^- concentration decreased linearly with increased stream stage (Figure 3.8). This source-limitation is associated with depletion of a finite resource (i.e., NO_3^-) or mixing with dilute waters (Basu et al., 2011; Godsey et al., 2009). This pattern is typical of N-limited watersheds with high vegetation or microbial uptake that limits inorganic N export (Shogren et al., 2021). Most undisturbed forests are N-limited (Schlesinger & Bernhardt, 2013) and high vegetation N demands (Figure 3.3b) limit NO_3^- export. In contrast, stream NO_3^- varied little with increasing stream stage in the burned

watersheds (Figure 3.8), demonstrating a chemostatic behavior that is associated with the storage and slow release of legacy solutes after limited biogeochemical processing (Basu et al., 2011). I use the term legacy with specific reference to hydrologic legacy where dissolved solute transport is delayed in its transition to the stream due to slow groundwater transport pathways (Van Meter & Basu, 2015). I propose that the shift I observed from source-limitation in unburned watersheds to chemostatic behavior is driven by N storage in the shallow groundwater of burned watersheds. Groundwater NO_3^- concentrations were four-time higher in burned watersheds (Figure B3) and were inversely related to NPP (Figure 3.9) and by extension, plant demand. Based on NPP at the time of this study, plant N demand in burned areas was roughly 30% of that in unburned forest vegetation (Figure 3.3b). This NPP estimate is consistent with earlier remotely-sensed surveys of post-fire vegetation greenness for the Hayman fire that indicated burned areas had recovered to within 25% of the pre-fire NDVI (Rhoades, Chow, et al., 2019) and further supports the link between reduced plant nutrient demand and high NO_3^- export in burned watersheds.

Elevated stream NO_3^- will likely persist until the legacy stores of groundwater NO_3^- are substantially depleted (Basu et al., 2010). Within the context of this study, post-fire groundwater NO_3^- appears to be driven by reduced vegetation demand so regeneration would have to occur at the landscape-scale in order to mitigate NO_3^- losses to groundwater. However, post-fire regeneration is slow, particularly in dry conifer forests (Chambers et al., 2016; Rother & Veblen, 2016; Stevens-Rumann et al., 2018). This is driven in part by increasing climate water deficits that have created unfavorable post-fire growing conditions and limited seedling recruitment in the 21st century (Coop et al., 2020; Stevens-Rumann et al., 2018). Furthermore, large, severe wildfires can limit post-fire recruitment by extending the distance to seed sources (i.e., >50 m) (Chambers et al., 2016; Rother & Veblen, 2016). As a result, large high severity patches have little to no ponderosa

pine regeneration, even 10 years post-fire (Chambers et al., 2016; Rother & Veblen, 2016) and this trend of poor regeneration is expected to worsen as the occurrence of high severity fire increases across the Western US (Parks & Abatzoglou, 2020).

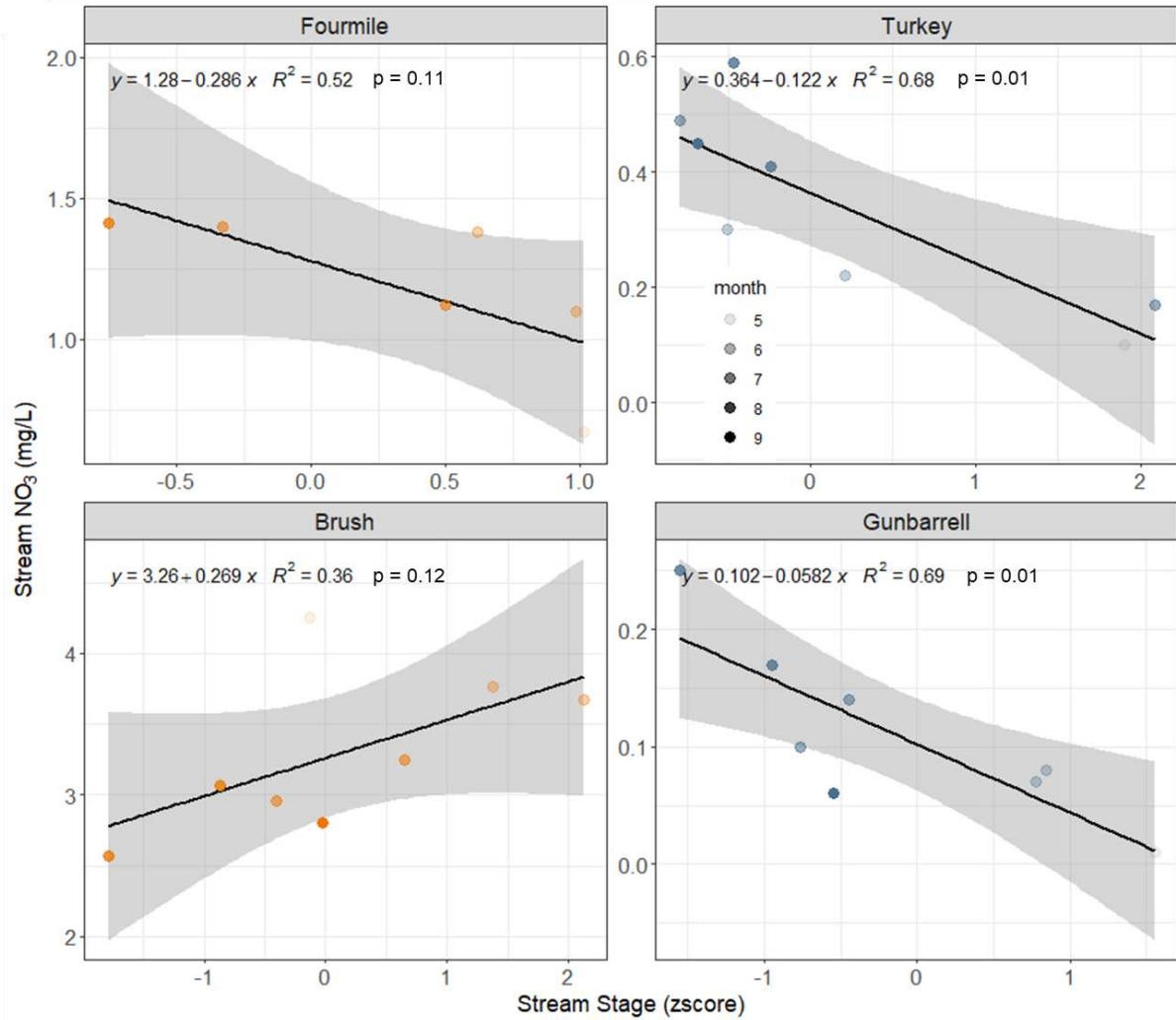


Figure 3.8: Relations between stream NO₃⁻ concentrations and stream stage throughout the summer of 2019. Burned watersheds include Fourmile (B1) and Brush (B2) whereas unburned watersheds include Turkey (U1) and Gunbarrel (U2).

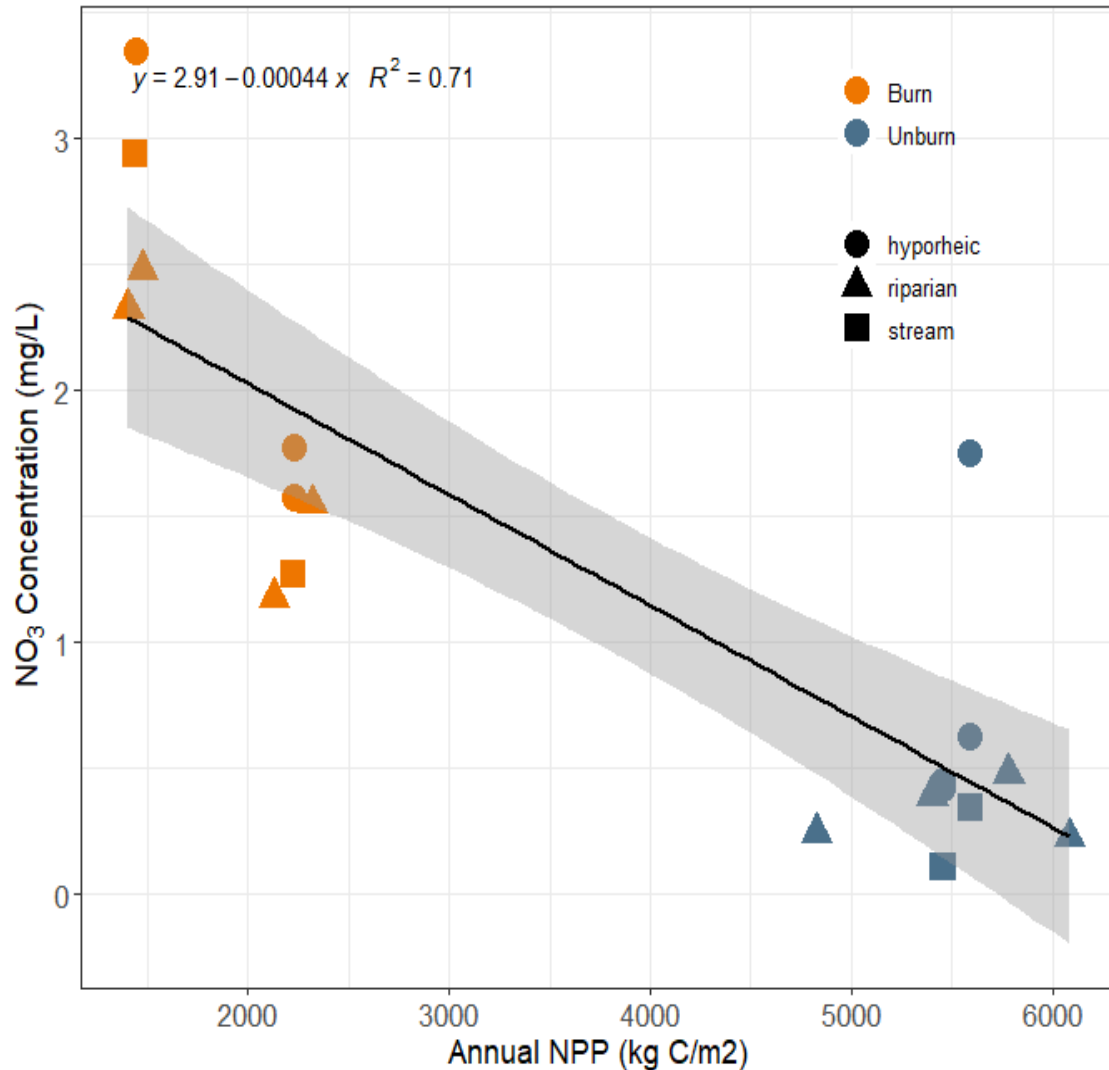


Figure 3.9: Relationship between annual NPP and mean summer NO₃ concentration for shallow groundwater (triangles and circles) and streams (squares).

While landscape-scale vegetation recovery may be hard to achieve after large, high severity fires, riparian restoration offers an opportunity for targeted NO₃⁻ mitigation. After insect infestation killed 50-60% of the trees in a forested watershed, significant NO₃⁻ losses accumulated in soil water and hillslope groundwater (Biederman et al., 2016). However, N removal in riparian zones and streams significantly reduced exports such that only 13-16% of hillslope losses were measured in streams (Biederman et al., 2016). Previous work at the Hayman fire demonstrated elevated in-stream N demand in burned watersheds 15 years post-fire, but terrestrial N supply

greatly exceeded in-stream demand (Rhea et al., 2021). This demonstrates the limited capacity for stream retention and highlights riparian zones as strategic locations to target for post-fire restoration. This concurs with previous work that called for targeted tree planting in exposed headwater riparian zones (Rhoades, Chow, et al., 2019) and I also suggest prioritizing restoration that enhances hydrologic connection, variable redox conditions, and slow residence times to maximize NO_3^- reductions (Fennessy & Cronk, 1997; Gift et al., 2010; McClain et al., 2003; Vidon & Hill, 2004). Width is a dominant factor controlling riparian buffer effectiveness (Fernández et al., 2012; Phillips, 1989) and the extent of wide valley bottoms will likely be limited in steep, confined headwaters. While nitrate removal is generally the greatest in the first 10-15 m of the riparian zone, larger buffer widths are required to efficiently remove nitrate in watersheds with steep slopes and high nitrate loading (Fennessy & Cronk, 1997; Fischer & Fischenich, 2000; Sabater et al., 2003; Vidon & Hill, 2004) such as the watersheds included in this study. For riparian restoration projects aimed at water quality protection (i.e., nitrate removal), the suggested minimum riparian buffer width varies from 20 – 40 m (Fennessy & Cronk, 1997; Fischer & Fischenich, 2000; Hansen et al., 2010) so using a conservative threshold of 40 m, I found that 15-88% of the stream networks in this study were wider than than 40 m indicating they could be suitable for riparian restoration (Figure B4). Furthermore, restoration should target long, continuous riparian buffers in headwater positions (Figure B5) to maximize buffering potential (Fischer & Fischenich, 2000). As large, severe disturbances become more common, this targeted restoration will be a critical tool to increase watershed N retention capacity.

3.5 Conclusions

Stream N has remained elevated after the Hayman fire (Rhoades, Chow, et al., 2019) and other fires in the western US (Rust et al., 2018; Smith et al., 2011) for years to decades indicating

consistent changes in ecosystem N cycling. This study aimed to determine if post-fire stream NO_3^- exports were driven primarily by higher soil N supply or decreased plant demand. I found no evidence that soil N supply was higher along burned hillslopes 17 years after the Hayman Fire. Conversely, I found elevated NO_3^- concentrations in shallow groundwater along burned hillslopes which is consistent with their low forest cover and plant N demand. These findings indicate that slow regeneration limits the capacity of burned watersheds to store N. While landscape-scale vegetation recovery will be required to attenuate NO_3^- losses to groundwater, riparian restoration may offer an opportunity for targeted NO_3^- mitigation.

4. Use of Geostatistical Models to Evaluate Landscape and Stream Network Controls on Post-Fire Stream Nitrate Concentrations

4.1 Introduction

Wildfires are a natural part of many forested ecosystems, but the frequency and severity of wildfires has been increasing across the Western US (Abatzoglou et al., 2017; Westerling, 2016). Elevated wildfire activity can threaten the function of critical forested watersheds that supply clean water to much of the Western US (Brown et al., 2008). Nitrogen (N) typically limits plant growth so N export often indicates ecosystem disturbance and shifts in nutrient supply and demand (Chapin et al., 2011). Short-term (<5 years) increases in stream nitrate (NO_3^-) have been documented following wildfires across the Western US (Rust et al., 2018; Smith et al., 2011) due to elevated soil N mineralization and leaching (Smithwick et al., 2009; Turner et al., 2007; Wan et al., 2001a). In some cases, stream NO_3^- can remain elevated for decades and has been shown to decrease with post-fire vegetation cover (Rhoades, Chow, et al., 2019; Rust et al., 2019) and increase with burn extent (Rhoades, Chow, et al., 2019). These results suggest that a lack of vegetation recovery is likely a dominant driver of persistent post-fire NO_3^- export, but this relationship remains poorly understood.

The interaction of vegetation cover, watershed structure, and stream network geometry regulates watershed solute export (Abbott et al., 2021; Covino et al., 2021; Creed & Beall, 2009; Likens & Bormann, 1974; Lovett et al., 2002; Shogren et al., 2021; Zarnetske et al., 2018). Watershed structure is the spatial arrangement of divergent and convergent hillslopes across the landscape (Baiaomonte & Singh, 2016; Jencso et al., 2010). Divergent hillslopes are convex and contribute little flow to the stream, whereas convergent hillslopes concentrate hydrologic flowpaths and contribute large inputs to channel networks (Detty & McGuire, 2010). In headwater

positions, water and solutes are primarily derived from shallow groundwater contributions from adjacent hillslopes (Covino et al., 2021; Gomi et al., 2002; Likens & Bormann, 1974) whereas upstream sources increasingly dominate water composition in lower network positions (Vannote et al., 1980). Therefore, headwaters are particularly sensitive to disturbance in the surrounding uplands (Lowe & Likens, 2005) and contributions to the stream in these locations have the potential to exert strong control on downstream solute concentrations (Abbott et al., 2018; Alexander et al., 2007; Wohl, 2017).

To better understand the spatial patterns in post-fire water chemistry, I consider both conservative and reactive solutes. Conservative solutes, such as sodium (Na^+), have low biological demand (Dingman, 2015; Stream Solute Workshop, 1990) and thus are primarily driven by physical transport processes (Webster & Valett, 2006) and watershed geophysical properties (Brennan et al., 2016; French et al., 2020; McGuire et al., 2014). In contrast, biologically active solutes such as NO_3^- are controlled by interactions between hydrologic transport and biological uptake (Bernhardt et al., 2003, 2005). In particular, forest cover can be a primary control on NO_3^- export at the watershed scale (Bormann & Likens, 1967; Likens et al., 1970).

Statistical models can be used to partition the spatial variance in stream Na^+ and NO_3^- among landscape (i.e., topographic, vegetation, and fire predictors) and stream network (i.e., flow-connected distance) characteristics. Multiple linear regression (MLR) modeling can be used to determine the relative influence of specific landscape characteristics on spatially distributed solute concentrations (Cho & Lee, 2018; McManus et al., 2020), but this approach assumes independence of sampling locations. Geostatistical modeling approaches, such as spatial stream network (SSN) models, are better suited to differentiate landscape from stream network attributes since they account for spatial autocorrelation of flow-connected samples and the dendritic and unidirectional

nature of stream networks (Ver Hoef et al., 2014; Isaak et al., 2014; Peterson & Ver Hoef, 2010). I paired spatially distributed water chemistry sampling with terrain analysis and vegetation and fire mapping to address the following objectives: 1) examine the degree to which topographic, vegetation, and fire variables predict stream Na^+ and NO_3^- across spatial scales and 2) evaluate the performance of MLR and SSN models in predicting stream solute concentrations. To my knowledge, this study is the first to use geostatistics to investigate the drivers of elevated post-fire stream NO_3^- .

4.2 Methods

4.2.1 Site description

In 2002, the Hayman Fire burned more than 554 km² of ponderosa pine (*Pinus ponderosa*) and Douglas-Fir (*Pseudotsuga menziesii*) forest in the Pike San Isabel National Forest (Graham, 2003) (Figure 4.1). This was one of the largest wildfires in Colorado's recorded history and 35% of the fire burned at high severity (P. Robichaud et al., 2003). The fire burned the contributing area of Cheesman Reservoir, a primary drinking water supply to the city of Denver (Graham, 2003). In combination, the 2002 Hayman and 1996 Buffalo Creek fires cost Denver's public water utility tens of millions of dollars on water quality treatment, sediment and debris removal, and reclamation (Hall, 2017). Watersheds within the Hayman Fire burn perimeter receive an annual average of 40 cm of precipitation (WRCC, 2021) and 60-75% of that comes from summer monsoonal rains (Wilson et al., 2018). Mean elevation within the fire perimeter is 2462 m which is within the intermittent snow zone that does not maintain snow cover throughout the winter (Richer et al., 2013). The parent material underlying the study area is dominated by Pike's Peak Formation granite (Ruleman et al., 2011) which weathers to form coarse, sandy loam soils (Cipra

et al., 2003). Ambient Na^+ concentrations are relatively low in granitic basins in the study area. There were no reported post-fire increases in stream Na^+ and measured post-fire increases in other geochemical ions (i.e., calcium, acid neutralizing capacity, and conductivity) recovered to pre-fire levels 2 years after the Hayman Fire (Rhoades et al., 2011b).

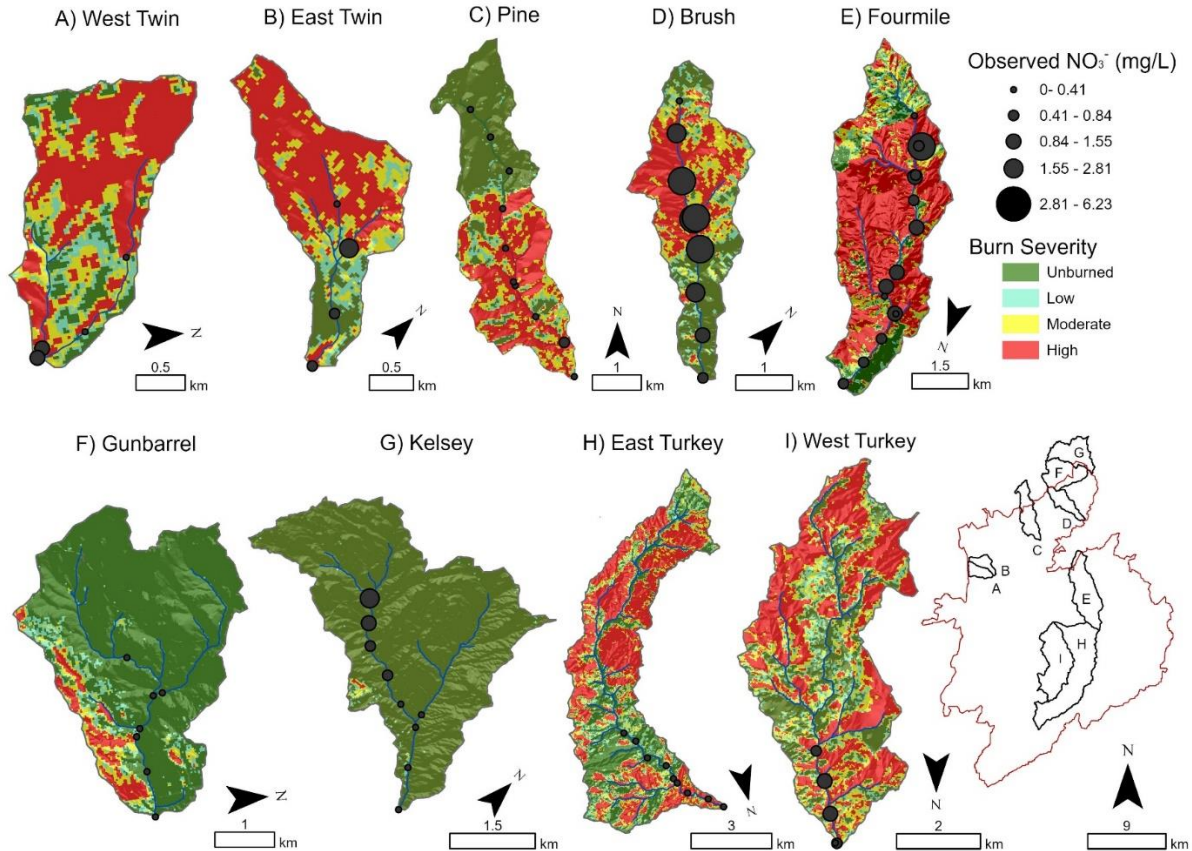


Figure 4.1: Sampling locations within the study watersheds affected by the 2002 Hayman Fire, Colorado, USA. Water chemistry samples ($n=71$) were collected in June 2018 and symbol size at each sampling point increases with stream NO_3^- concentration.

The nine study watersheds ranged in size from 3.2 to 35.4 km^2 , slope from 17-38%, and elevation from 2284-2694 m (Table 4.1). At the time of sampling, 16 years after the fire, mean normalized differenced moisture index (NDMI) was the lowest in Brush (-0.13) and highest in Gunbarrel (-0.02) where burn extents were 71 and 18% respectively (Tables 4.1-4.2). Burn extent varied from 1-90% across the watersheds, but seven of them had more than half of their

contributing area burned and 36-64% of that burned at high severity (Table 4.2). Patch density was high which is consistent with a mixture of fire severity classes. High severity patches, defined by complete canopy consumption, generally had the largest patch size and radius (Table 4.2), suggesting that post-fire pine reestablishment may be limited in high severity areas (Chambers et al., 2016).

Table 4.1: Physical characteristics and solute concentrations of each study watershed for samples collected in June 2018.

Watershed	Physical Characteristics				Solute Concentrations			
	Outlet UAA (km ²)	Mean Slope (%)	Mean Elev. (m)	Mean NDMI ()	----- NO ₃ ⁻ ----- mean (cv) (mg/L)	min-max (mg/L)	----- Na ⁺ ----- mean (cv) (mg/L)	min-max (mg/L)
Fourmile	18.8	26	2441	-0.11	1.14 (1.28)	0.17-6.23	6.38 (0.26)	4.95-10.88
East Twin	3.2	30	2640	-0.06	0.88 (1.07)	0.005-2.21	6.46 (0.08)	5.77-6.91
West Twin	3.3	38	2694	-0.05	0.55 (0.88)	0.08-0.97	7.61 (0.15)	6.13-8.8
West Turkey	22	25	2523	-0.08	0.88 (0.22)	0.71-1.07	7.73 (0.01)	7.68-7.82
East Turkey	35.4	17	2571	-0.08	0.29 (0.23)	0.19-0.38	6.78 (0.03)	6.48-7.13
Brush	6.1	28	2277	-0.13	3.06 (0.65)	0.28-5.63	6.23 (0.42)	4.71-12.96
Pine	9.3	35	2516	-0.06	0.23 (0.80)	0.005-0.63	8.40 (0.36)	3.89-13.11
Gunbarrel	12.3	27	2361	-0.02	0.16 (0.66)	0.03-0.30	7.80 (0.07)	6.74-8.18
Kelsey	12.1	22	2284	-0.04	0.56 (1.06)	0.01-1.92	8.94 (0.11)	7.56-10.86

Note: UAA is upslope accumulated area, NDMI is the average normalized differenced moisture index in June 2018, and cv is the coefficient of variation.

Table 4.2: Burn metrics by severity for each study watershed. These metrics represent immediate fire impacts by differencing one pre-fire (8/24/2001) and one post-fire (8/14/2003) Landsat image and severity is classified according to MTBS thresholds (Eidenshink et al., 2009).

Watershed	Burn Extent			Mean Patch Size / Mean Patch Radius				Patch Density (#/100 ha)
	Low (%)	Moderate (%)	High (%)	Unburned (ha / m)	Low (ha / m)	Moderate (ha / m)	High (ha / m)	
Fourmile	8	17	64	2 / 29	1 / 22	1 / 32	18 / 53	42
East Twin	10	22	57	1 / 21	1 / 23	1 / 38	13 / 63	44
West Twin	12	26	51	1 / 39	1 / 27	1 / 42	10 / 73	56
West Turkey	13	20	46	3 / 41	0 / 23	1 / 37	11 / 67	59
East Turkey	12	17	45	4 / 37	0 / 23	1 / 34	11 / 72	56
Brush	11	23	38	4 / 40	0 / 23	2 / 41	8 / 49	50
Pine	7	16	36	8 / 43	0 / 20	1 / 40	21 / 98	31
Gunbarrel	6	6	6	73 / 130	0 / 20	1 / 28	5 / 79	24
Kelsey	1	0	0	597 / 758	0 / 8	1 / 26	1 / 72	6

4.2.2 Stream sampling

To capture a gradient of disturbance and quantify the spatial variability of post-fire stream Na^+ and NO_3^- , I sampled stream water roughly every 800 meters along the mainstems of the study watersheds (Figure 4.1). This distance was selected to ensure a consistent sampling interval that maximized the number of samples collected per watershed but would allow us to complete watershed sampling within one day. Low-flow conditions were stable and there were no precipitation events during the sampling period (6/1/2018-6/7/2018). Previous research at the Hayman Fire demonstrated that patterns of elevated stream NO_3^- in severely burned watersheds persist across flow conditions (Rhoades, Chow, et al., 2019) so the June sampling date should be broadly representative. All stream samples from a given watershed were collected within a single day in pre-washed 1 L high-density polyethylene bottles moving in the upstream direction. Samples were immediately filtered with 0.45 μm polyvinyl diethylene filters (MilliporeSigma, Burlington, MA) and analyzed for concentrations of stream Na^+ and NO_3^- using ion chromatography (Dionex ICS-3000, Waltham, MA and Waters 580, Sunnyvale, CA). Detection

limits for both Na^+ and NO_3^- were 0.01 mg/L; any concentrations below that were replaced with $\frac{1}{2}$ the detection limit.

4.2.3 Geospatial analysis

I conducted a terrain analysis to characterize the underlying watershed structure. First, flow direction was derived from a 10-m digital elevation model (DEM) (U.S. Geological Survey, 2018) using the multiple triangular flow direction algorithm (Seibert & McGlynn, 2007). Watershed contributing areas were delineated and upslope accumulated area (UAA) was calculated for all sampling points (0.32 – 35.4 km²) using the openSTARS package (Peterson & Ver Hoef, 2014) in R Studio. I summarized topographic, vegetation, and fire variables as means and proportional extents within the contributing areas for each sampling location (Table 4.3).

Topographic metrics included watershed area, mean slope, mean elevation, riparian extent, and mean topographic wetness index (TWI) (Table 4.3). Slope, elevation, and TWI were derived from the 10-m DEM using Whitebox tools (Lindsay, 2020; Wu, 2021) and summarized as watershed means. I used a physical definition of the riparian corridor that included pixels <2 m above the stream surface elevation (*sensu* Jencso et al., 2010) and calculated riparian extent as the total riparian corridor area divided by UAA of each sampling point. This approach differs from an earlier estimate of the extent of riparian vegetation in these watersheds (Rhoades, Chow, et al., 2019).

I characterized vegetation condition using normalized differenced vegetation index (NDVI), normalized differenced moisture index (NDMI), and enhanced vegetation index (EVI). I obtained mean June 2018 vegetation indices from Landsat using Climate Engine (Huntington et al., 2017) to match the vegetation characterization with the timing of stream sampling. I also

included 2018 fractional land cover estimates derived from satellite imagery that was extensively calibrated across the Western US and estimated the proportion of each Landsat pixel covered by trees, shrubs, and bare ground (Allred et al., 2021).

Table 4.3: Watershed predictor variables that were summarized for the contributing area to each sampling point. Pearson correlation coefficients were calculated between each predictor variable and Na⁺ or NO₃⁻. Vegetation metrics represent current conditions (i.e., June 2018) whereas fire metrics represent immediate post-fire condition (i.e., August 2003). Variables marked with a * were removed prior to linear mixed model selection due to strong correlation (>0.90) with another predictor variable. Coefficients depicted in grey identify variables removed during linear mixed model selection; those in black were retained for subsequent modeling.

Variable	Summary Statistic	Data Source	Correlation Coefficient		
			Na ⁺	NO ₃ ⁻	
Topographic	Watershed area	value at sampling point	Whitebox flow accumulation tool	0.12	-0.03
	Slope	watershed mean	Whitebox slope tool	0.27	-0.32
	Elevation	watershed mean	10-m digital elevation model	-0.23	-0.27
	Riparian extent	% of watershed area	Whitebox elevation above stream tool	0.24	-0.01
	TWI	watershed mean	Whitebox twi tool	-0.33	0.14
Vegetation	Tree cover	watershed mean	Rangeland Analysis Platform	0.15	-0.5
	Shrub cover	watershed mean	Rangeland Analysis Platform	-0.24	0.15
	Bare *	watershed mean	Rangeland Analysis Platform	-0.12	0.44
	NDMI	watershed mean	Climate Engine	0.09	-0.67
	NDVI *	watershed mean	Climate Engine	0.05	-0.64
	EVI *	watershed mean	Climate Engine	-0.02	-0.62
Fire	Burn extent	% of watershed area	MTBS	-0.24	0.43
	dNBR *	watershed mean	MTBS	-0.26	0.37

Note: TWI: topographic wetness index, Bare is bare ground cover; NDMI: normalized differenced moisture index, NDVI: normalized differenced vegetation index, EVI: enhanced vegetation index, dNBR: differenced normalized burn ratio, and MTBS: monitoring trends in burn severity database.

Mean differenced normalized burn ratio (dNBR, a measure of burn severity) and burn extent were calculated for the area contributing to each sampling point. These fire metrics represent immediate post-fire impacts by differencing one pre-fire (8/24/2001) and one post-fire (8/14/2003) Landsat image. dNBR was then classified into categorical burn severity as follows: -150-140 unburned; 140-211 low severity; 211-350 moderate severity, 350-953 high severity (Eidenshink

et al., 2009). Low severity fire tends to leave tree canopies largely unaltered whereas high severity fire typically causes complete consumption of surface organic matter and canopy foliage (Parsons et al., 2010). Wildfire severity varies spatially across topographic, vegetation (i.e., fuel composition, arrangement, condition), and weather gradients (Taylor et al., 2021) which creates mosaics of post-fire vegetation structure and composition that vary at scales finer than mapped severity patches (Lentile et al., 2007). To characterize the spatial burn patterning of each watershed, I calculated burn extent, patch size, patch radius, and patch density by severity (Table 4.2). Burn extent reflects the proportion of watershed area that was burned by each severity class. All patch metrics were calculated with the landscape metrics package (Hesselbarth et al., 2019) in R Studio which defines contiguous cells belonging to the same burn severity class. For each watershed, I determined patch area and calculated patch radius as the mean distance from each cell in a patch to its centroid, and patch density as the number of patches divided by watershed UAA.

4.2.4 Statistical modeling

I used statistical models to evaluate the degree to which topographic, vegetation, and fire variables and flow-connected distance control post-fire stream water chemistry – specifically, concentrations of Na^+ and NO_3^- . Concentration data were log-transformed to improve normality and a correlation analysis removed redundant predictor variables with a correlation >0.90 (Figure 4.2, Table 4.3). To identify the top-performing Na^+ and NO_3^- models, I went through a two-step model selection process (sensu McManus et al., 2020; Rodríguez-González et al., 2019). First, I identified which landscape characteristics best predicted stream Na^+ and NO_3^- using linear mixed model selection (Table C1). The Na^+ and NO_3^- models with the lowest maximum likelihood estimate of Akaike's Information Criteria (AIC) then progressed to the second phase of model selection where I compared spatial autocorrelation approaches. I initially ran multiple linear

regression (MLR) models which use landscape characteristics to predict observed water chemistry at each sampling location. The predictor variables are spatially explicit given that they characterize the area contributing to a specific sampling point, but MLR models assume independence between stream water samples. I then compared MLR models to spatial stream network (SSN) models that jointly consider landscape and stream network characteristics. This approach captures spatial effects beyond those directly attributable to predictor variables by accounting for flow-connection (Isaak et al., 2014). MLR and SSN model performance was compared through iterative leave-one-out cross-validation. Observations at sampling points were removed one at a time and the model was used to predict each of the removed values along with the prediction standard error (Ver Hoef & Peterson, 2020). The model with the lowest AIC and root mean square prediction error (RMSPE) was selected for subsequent analyses.

To build SSN models, stream sampling locations were incorporated into a landscape network (LSN) to characterize network geometry (Peterson & Ver Hoef, 2014) using the openSTARS package (Kattwinkel & Szöcs, 2020). The additive function quantified the proportional influence of each stream segment (Ver Hoef & Peterson, 2020) and calculated distance matrices between all sampling points. I used a tail-up autocovariance structure to restrict the modeling to flow-connected distance, which is only measured between points with an upstream-to-downstream connection (Isaak et al., 2014; Peterson & Ver Hoef, 2010). This distance metric is better suited for stream network studies than straight-line Euclidean distance because it characterizes downstream transport and longitudinal connectivity of dissolved solutes (Peterson & Ver Hoef, 2010). I then modeled an empirical semivariogram and derived 3 associated parameters – the nugget, sill, and range. Empirical semivariograms quantify the variation between samples (i.e., stream Na^+ or NO_3^- concentrations) as a function of distance between sampling points (Ganio

et al., 2005). Positive autocorrelation occurs when semivariance is smaller (i.e., measurements are more similar) near the origin and increases at greater lag distances. In some cases, the semivariogram will reach an inflection point at a given lag distance ('range') where semivariance begins to flatten out ('sill'). Samples are considered uncorrelated at distances greater than the range and the sill represents the dissimilarity of the uncorrelated data (Isaak et al., 2014). The nugget describes spatial variation at scales smaller than the minimum sampling interval (i.e., ≤ 52 m in this study).

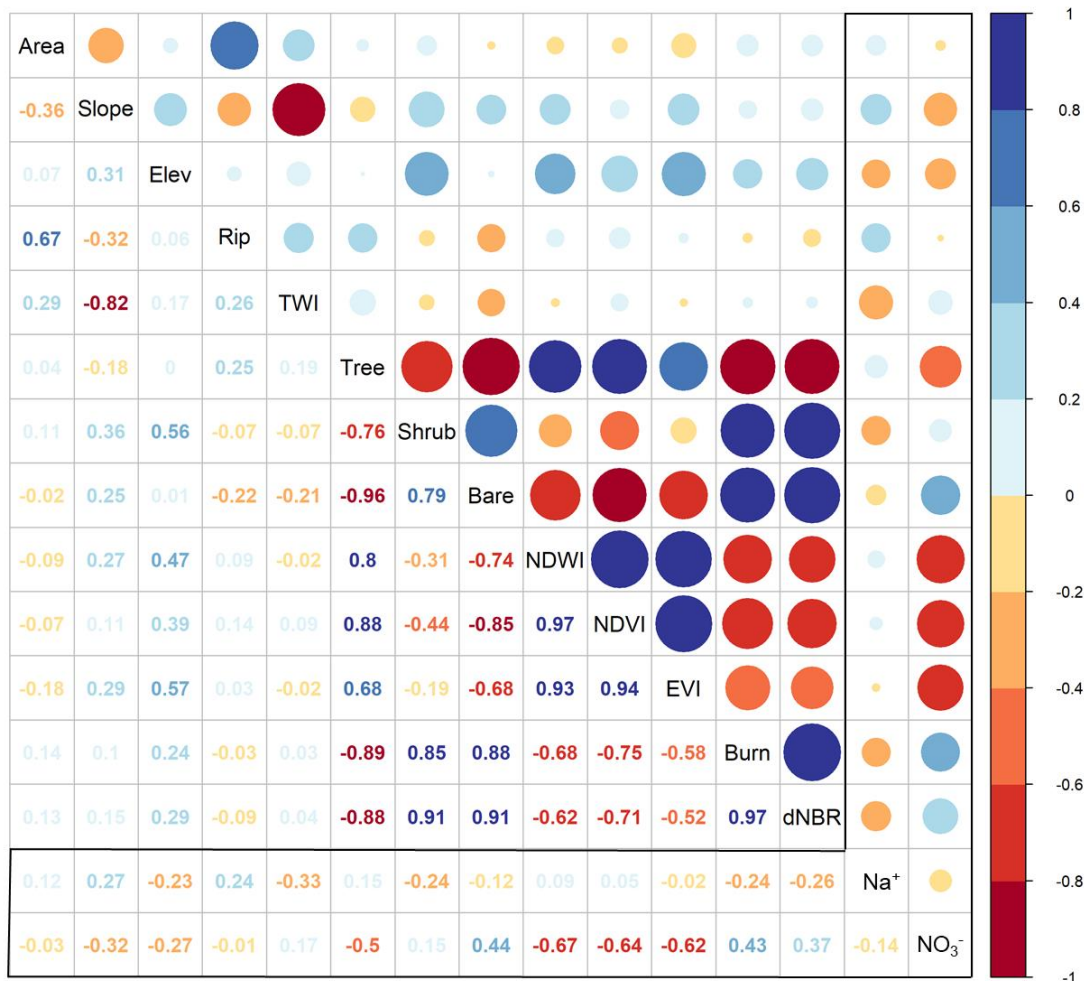


Figure 4.2: Pearson correlation matrix between all potential predictor and response variables. The black box highlights correlations between the predictor variables and stream Na^+ and NO_3^- , both of which were log-transformed. Everything beyond the black box represents correlations among predictor variables.

Note: Area is watershed area, Slope is mean watershed slope, Elev is mean watershed elevation; Rip is riparian extent, TWI is mean topographic wetness index, Tree is mean tree cover (%), Shrub is mean shrub cover (%), Bare is mean bare ground cover (%), NDWI is mean normalized differenced water index, NDVI is mean normalized vegetation index, EVI is mean enhanced vegetation index, Burn is burn extent (%), dNBR is mean differenced normalized burn ratio, and both stream NO_3^- and stream Na^+ concentrations are log-transformed (mg/L).

4.2.5 Longitudinal patterns across two watersheds with inverse burn patterns

Finally, I used kriging to interpolate stream NO_3^- concentrations along the mainstems of two paired watersheds and compared spatial NO_3^- patterns to continuous measures (i.e., every 10 m) of hydrologic inputs and the vegetation condition of those inputs. These two watersheds had similar contributing areas (6.1 and 9.3 km^2 , Table 4.1) and were extensively burned (i.e., >50% of UAA burned). For both watersheds, patch density was high and fire severity was mixed equally among burn severity classes (Table 4.2). However, the headwaters were severely burned in Brush Creek and unburned in Pine Creek (Figure 4.1). I distributed 3,000 equally spaced prediction points along the geomorphic channel networks of each watershed, delineated the contributing area of each prediction point, and calculated topographic, vegetation, and fire predictor variables (see section 2.3). I also calculated the flow-connected distance between all observed and prediction locations. The NO_3^- SSN model then predicted NO_3^- concentration and standard error at each location based on both landscape characteristics (i.e., watershed area, riparian extent, mean TWI, and mean NDMI) and flow-connected distance. I then calculated the relative lateral input (LI) as the incremental downstream increase in contributing area relative to the total contributing area (i.e., $\text{Relative LI} = (UAA_{\text{cell}(n)} - UAA_{\text{cell}(n-1)})/UAA_{\text{cell}(n)}$). Because stream discharge scales with contributing area (Bergstrom et al., 2016), this metric reflects the contribution of hillslope water relative to mainstem flow. Finally, mean NDMI was calculated for the discrete lateral input (LI) contributing to each 10-m stream cell using the same June 2018 NDMI image described in

section 2.3. I also resampled the paired watersheds in June of 2019 at a 300 m resolution to assess the accuracy of the NO_3^- SSN predictions with observed values.

4.3. Results

4.3.1 Stream Na^+ and NO_3^- concentrations

Observed stream Na^+ concentrations ranged from 3.9-13.1 mg/L (Figure C1), with an average concentration of 7.3 mg/L which is similar to the pre-fire average of 6.1 mg/L reported in these granitic basins (Rhoades et al., 2011b). Kelsey had the highest and Brush had the lowest mean stream Na^+ concentration whereas Brush had the highest and West Turkey had the lowest coefficient of variation (Table 4.1). Observed stream NO_3^- concentrations varied by three orders of magnitude (0.005 – 6.2 mg/L) and average stream NO_3^- concentration was 0.91 mg/L which is five times greater than pre-fire concentrations (0.18 mg/L) (Rhoades, Chow, et al., 2019). Brush watershed had the highest (3.06 mg/L) and Gunbarrel the lowest (0.16 mg/L) mean NO_3^- concentration whereas Fourmile had the greatest and West Turkey the lowest coefficient of variation (Table 4.1). The coefficient of variation was consistently higher for stream NO_3^- (Table 4.1) indicating greater within-watershed variability in stream NO_3^- compared to Na^+ .

4.3.2 Landscape controls on Na^+ and NO_3^-

Topographic, vegetation, and fire predictor variables were weakly correlated (≤ 0.33) with $\log[\text{Na}^+]$ (Table 4.3). Linear mixed model selection identified watershed area, slope, riparian extent, TWI, and tree and shrub cover as the best predictors of $\log[\text{Na}^+]$ (Table C1). Stream Na^+ was related positively to watershed area, slope, riparian extent, and tree cover, and negatively to TWI, and shrub cover (Figure 4.2). All watershed predictors were significant in the Na^+ MLR model and together explained 54.4% of the variance in $\log[\text{Na}^+]$ (Table 4.4). Predictor variables

explained 45% of the variance in $\log[\text{Na}^+]$ in the Na^+ SSN model and all predictors except watershed area were significant (Table 4.4).

Table 4.4: Summary of spatial stream network (SSN) and multiple linear regression (MLR) models that predict log-transformed stream Na^+ and NO_3^- concentrations. Parameter estimates represent the regression coefficient, which is the change in the response variable based on a 1-unit change in the predictor variable while holding all other variables constant. Statistical significance of predictor variables is denoted with symbols *=0.05, **=0.01, ***=0.001. Variance decomposition assigns variance in Na^+ or NO_3^- to watershed predictor variables, flow-connected autocorrelation, and unexplained variance. MLR models do not account for flow-connected autocovariance. Model performance metrics come from iterative leave-on-out cross-validation.

		Na⁺ Models		NO₃⁻ Models	
		SSN	MLR	SSN	MLR
Parameter Estimates	Watershed Area	0.008	0.012 **	-0.03	-0.04 *
	Slope	0.090 ***	0.104 ***	-	-
	Elevation	-	-	-	-
	Riparian Extent	0.100 **	0.106 ***	0.32	0.29
	TWI	0.651 *	0.813 ***	1.33 *	0.91 *
	Tree cover	-0.02 ***	-0.018 ***	-	-
	Shrub cover	-0.115 ***	-0.111 ***	-	-
	NDMI	-	-	-17.64 ***	-17.37 ***
	Burn extent	-	-	-	-
Variance Components (%)	Predictor variables	45.0	54.4	36.0	51.4
	Flow-connected distance	53.1	-	41.5	-
	Total explained	98.1	54.4	77.5	51.4
	Unexplained	1.9	45.6	22.5	48.6
Model Performance	AIC	-55.35	-34.29	210	212
	RMSPE	0.165	0.205	1.00	1.07

Note: TWI is topographic wetness index, NDMI is normalized difference moisture index, AIC is Akaike's information criteria, and RMSPE is root mean square prediction error.

Fire and vegetation variables generally had stronger correlations (0.15-0.67) with $\log[\text{NO}_3^-]$ than topographic variables (0.03 – 0.32) (Table 4.3). Linear mixed model selection identified watershed area, riparian extent, TWI, and NDMI as the best predictors of $\log[\text{NO}_3^-]$ (Table C1). Stream NO_3^- was positively related to riparian extent and TWI, but negatively related to watershed area and NDMI (Figure 4.2). Mean NDMI had the strongest correlation with $\log[\text{NO}_3^-]$ (Figure 4.2). In the NO_3^- MLR model, the selected predictor variables, with the exception of riparian

extent, were significant and accounted for 51.4% of the variance in $\log[\text{NO}_3^-]$ (Table 4.4). In the NO_3^- SSN model, TWI and NDMI were the only significant predictor variables and the predictors explained 36% of variation in $\log[\text{NO}_3^-]$ (Table 4.4).

Topographic variables had weak correlations (<0.32) with both stream Na^+ and NO_3^- (Table 4.3). Vegetation predictors generally had much stronger correlations with NO_3^- compared to Na^+ , with the exception of shrub cover (Table 4.3). Burn variables had slightly higher correlations with NO_3^- compared to Na^+ (Table 4.3). All predictor variables that were selected through linear mixed model selection were weakly correlated with water chemistry (<0.33) (Figure C2). The one exception was a strong inverse relationship between mean NDMI and stream NO_3^- which had a correlation coefficient of -0.67 (Figure C2).

4.3.3 Stream network controls on Na^+ and NO_3^-

In the Na^+ SSN model, a majority of variation (53.1%) in $\log[\text{Na}^+]$ was explained by flow-connected autocorrelation (Table 4.4). Na^+ exhibited strong positive autocorrelation where semivariance was low at short lag distances, but increased with distance (Figure 4.3). When flow-connected autocovariance was modeled with a spherical fit, Na^+ had a nugget of 0.001, sill of 0.029, and range of 3700 m (Figure 4.3). The low nugget suggests that the sampling adequately captured variability at small spatial scales and that there is relatively little unexplained variation. The low sill reflects the low overall variance in streamwater Na^+ concentrations. The range indicates that samples that are > 3700 m apart are no longer correlated.

In the NO_3^- SSN model, flow-connected autocorrelation explained 41.5% of variation in $\log[\text{NO}_3^-]$ (Table 4.4). Stream NO_3^- had high semivariance across all flow-connected distances, though semivariance peaked at intermediate lag distances (1000-5000 m) (Figure 4.3). When flow-

connected autocovariance was modeled with an exponential fit, NO_3^- had a nugget of 0.385, sill of 0.708, and range of 8800 m which is equal to the maximum sampling distance (Figure 4.3). The large nugget and sill values are consistent with the substantial unexplained variance and high overall variance in stream NO_3^- concentrations. The lowest semivariance in NO_3^- is still greater than the maximum Na^+ semivariance (Figure 4.3).

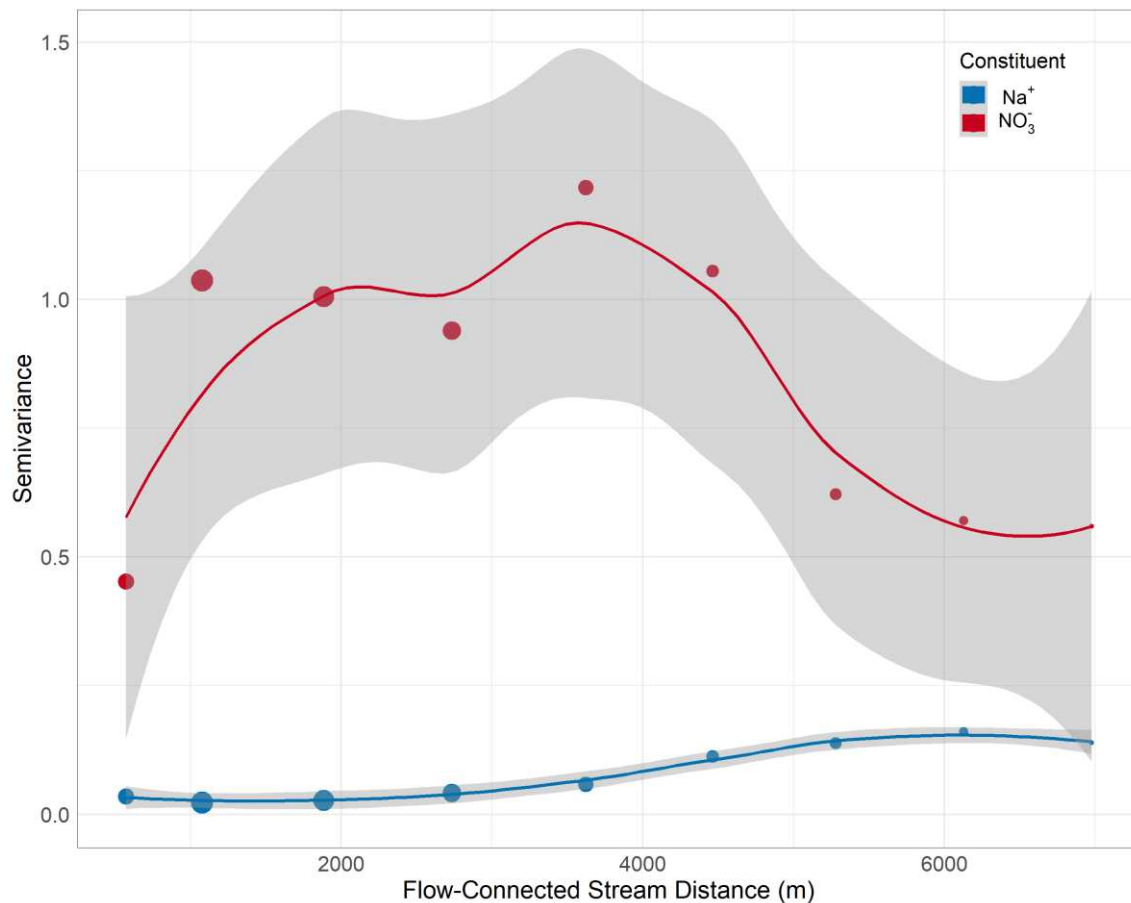


Figure 4.3: Empirical semivariograms of log-transformed stream Na^+ (blue) and NO_3^- (red) based on the flow-connected distance between sampling points. Symbol sizes are proportional to the number of data pairs included in each bin. The grey shaded region represents the 95% confidence interval from a local polynomial regression of each semivariogram. Semivariograms show evidence of strong positive autocorrelation in Na^+ (blue) and weak spatial autocorrelation in NO_3^- (red).

4.3.4 Statistical model performance

The SSN model improved Na^+ predictions relative to the MLR model, as indicated by lower AIC and RMSPE values (Table 4.4). Leave one-out-cross validation demonstrated that SSN predictions were closer to observed values (Figure 4.4A) and prediction standard errors were lower (Figure 4.4C) in the Na^+ SSN model compared to the Na^+ MLR model. In the Na^+ SSN model, predictor variables explained 45% of the variance in $\log[\text{Na}^+]$, flow-connected autocovariance explained 53.1% and only 1.9% was left unexplained (Table 4.4).

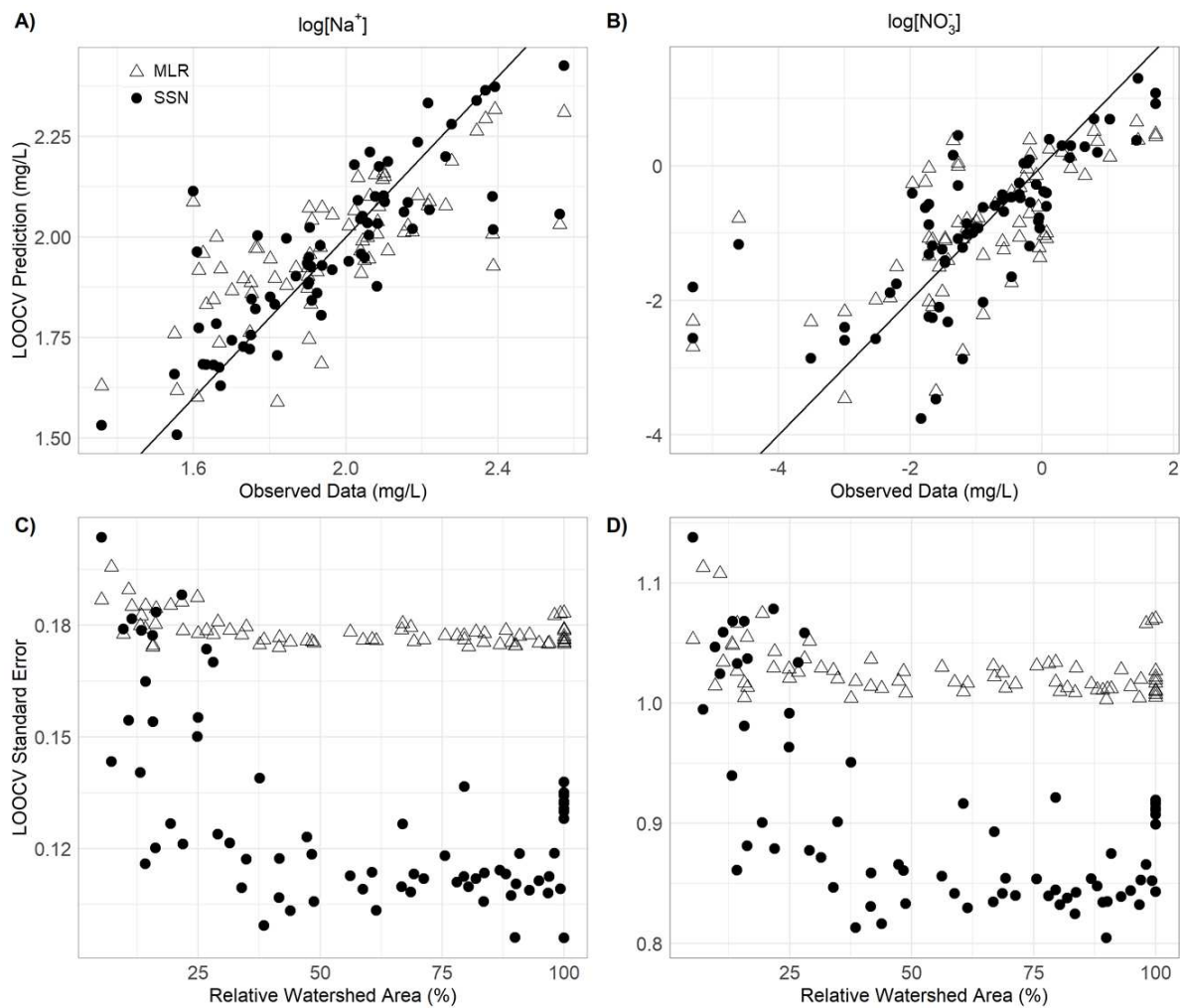


Figure 4.4: Leave-one-out cross validation to assess A, C) Na^+ and B, D) NO_3^- model performance. A-B) Model predictions are plotted against observed values for both MLR (open triangles) and SSN (black circles) models. C-D) Prediction standard error is plotted against relative watershed

area, with headwater positions on the left side of the plot and lower watershed positions on the right side.

The NO_3^- SSN model also had a lower AIC value and RMSPE relative to the NO_3^- MLR model (Table 4.4). SSN predictions were closer to the observed values (Figure 4.4B) and prediction standard error was lower (Figure 4.4D) in the NO_3^- SSN model than the MLR model. In the NO_3^- SSN model, predictor variables (36%) and flow-connected autocovariance (41.5%) explained a majority of the variation in $\log[\text{NO}_3^-]$, leaving 22.5% unexplained (Table 4.4). Based on NO_3^- SSN model, 81% of the predicted stream NO_3^- concentrations that fell within the fire perimeter exceeded the pre-fire mean concentrations of 0.18 mg/L (Rhoades et al., 2011, Figure C3).

4.3.5 Longitudinal patterns across two watersheds with inverse burn patterns

The two paired watersheds with inverse burn patterns exhibited distinct patterns in stream NO_3^- concentration. 72% of Brush watershed was burned and most of the burn occurred in the upper half of the watershed (Figure 4.5A). Mean NDMI was generally low throughout Brush, but was inversely related to burn extent (Figure 4.5C). Stream NO_3^- concentrations spanned a 4.6 mg/L range throughout Brush Creek. The minimum concentration (0.4 mg/L) occurred at the upper most sampling location and the highest observed concentration (5.0 mg/L) occurred nearby within the upper watershed (Figure 4.5E). Nitrate generally declined in the lower half of the watershed and reached 0.9 mg/L at the lowest sampling location. Conversely, the majority of the burned area in Pine Creek occurred in the lower watershed (Figure 4.5B). Burn extent was again inversely related to mean catchment NDMI, but NDMI remained relatively high throughout (Figure 4.5D). Pine stream NO_3^- concentration increased gradually downstream from below detection levels in the headwaters to 0.3 mg/L at the outlet (Figure 4.5F). Maximum and mean stream

NO_3^- concentrations was 14- and 17-times higher in Brush than Pine. The NO_3^- SSN model predictions agreed with measured stream NO_3^- concentrations during the 2019 sampling (Figure C4).

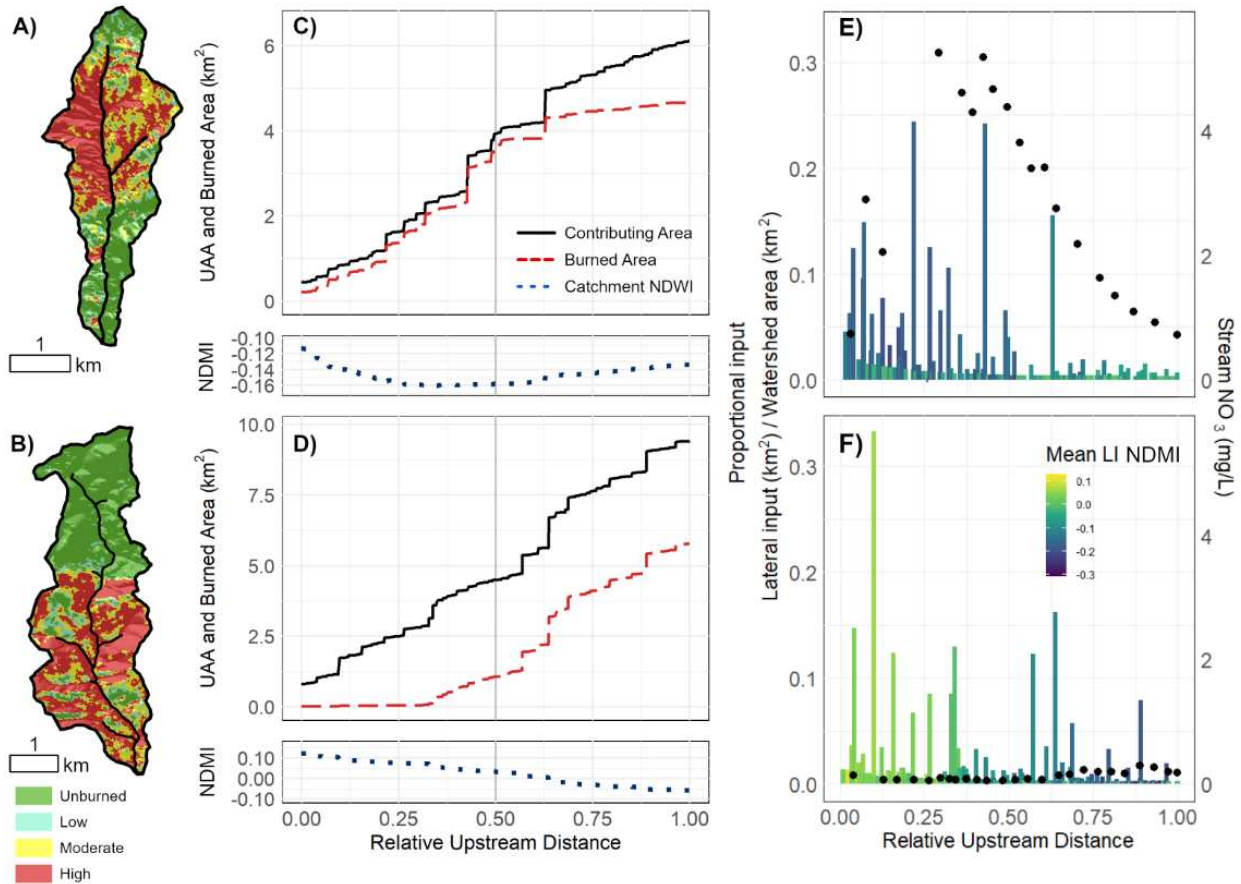


Figure 4.5: Spatial arrangement of burn severity in A) Brush Creek which was 71% burned with most high severity fire occurring in the upper watershed and B) Pine Creek which was 59% burned with most high severity fire occurring in the lower watershed. Distribution of cumulative upslope accumulated area (black solid lines), cumulative burned area (red dashed lines), and mean catchment normalized differenced moisture index (NDMI, blue dotted lines) for C) Brush and D) Pine. Upstream distance was relativized between 0 and 1 in all plots, with headwaters on the left and outlet on the right, to allow for comparisons between watersheds. The vertical grey line denotes the mid-point of the watershed. Distribution of relative lateral inputs with upstream distance for E) Brush and F) Pine where bars are colored according the mean NDMI of each discrete lateral input. Stream NO_3^- concentrations predicted from the NO_3^- SSN model (black circles) are compared for both E) Brush and F) Pine.

4.4 Discussion

4.4.1 Modeling streamwater chemistry in burned watersheds

Multiple lines of evidence indicated that stream NO_3^- concentrations had greater spatial variability and weaker spatial structuring relative to Na^+ . First, semivariance was greater for stream NO_3^- than Na^+ across all flow-connected distances (Figure 4.3) which suggests higher variability in stream NO_3^- concentrations across all measured scales (Isaak et al., 2014). Secondly, the nugget effect was orders of magnitude greater for stream NO_3^- than Na^+ (0.385 and 0.001 respectively) which indicates unmeasured fine-scale variability in stream NO_3^- concentrations (Cooper et al., 1997). Finally, Na^+ semivariance increased with lag distance and stabilized around 3,700 m (Figure 4.3). This strong positive autocorrelation indicates that downstream hydrologic transport was the primary driver of spatially distributed Na^+ concentrations. In contrast, the empirical semivariogram for NO_3^- exhibited irregular trends in semivariance that did not stabilize across the measured range in spatial scales (Figure 4.3).

SSN model improvements varied with the solute of concern and network position. For Na^+ , the SSN model reduced the AIC by 61%, RMSPE by 20%, and unexplained variance by 96% compared to the MLR model (Table 4.4). In contrast, the NO_3^- SSN model only reduced the AIC by <1%, the RMSPE by 7%, and the unexplained variance by 54% (Table 4.4). SSN model improvements tend to be smaller where spatial autocorrelation is lower (Isaak et al., 2014) such as with NO_3^- at these sites. Additionally, SSN models improved predictions more in downstream positions whereas MLR prediction error was relatively consistent across network positions (Figure 4.4C-D). Moving downstream, SSN models are informed by an increasing number of upstream

data points. Conversely, SSN predictions in headwater locations rely more on watershed attributes than upstream data, much like MLR models.

4.4.2 Post-fire vegetation is a dominant driver of stream NO_3^- patterns

Large high severity fire has the potential to shift ecosystems from forest to grass and shrubland which can have implications for watershed N cycling. Even decades after the Hayman and nearby fires, 75% of high severity plots had no conifer regeneration and it is possible that forest density will never return to pre-fire levels in these areas (Chambers et al., 2016). Beyond these field sites, there is broad evidence of declining post-fire tree regeneration due to increasing climate aridity and fire activity which can shift previously forested systems into alternative stable states dominated by grassland and weedy, herbaceous vegetation types (Coop et al., 2020; Stevens-Rumann et al., 2018; Tepley et al., 2017; Walker et al., 2018). Forest cover is often a primary mechanism for terrestrial N retention (Dunnette et al., 2014; Vitousek et al., 1979) and changes from forest to grass and shrub cover can impact ecosystem N retention (Lovett et al., 2002). For example, conifers will more strongly regulate N cycling than grasses and forbs given their underlying nutrient use efficiencies (Chapman et al., 2006). Therefore, post-fire watersheds with little tree regeneration will likely be leakier with respect to N cycling.

Spectral vegetation indices were the strongest predictors of stream NO_3^- in this and other studies. For example, reduced post-fire plant cover, measured as NDVI, explained the persistence of elevated post-fire stream N (Rust et al., 2019). In this study though, the strongest predictor of stream NO_3^- concentration was mean NDMI (Table 4.3), a vegetation index that considers both canopy cover and the water stress of that vegetation. NDMI is more sensitive to burn severity, forest type, and forest loss and recovery than NDVI which is broadly sensitive to the amount of

photosynthetically active vegetation (Morresi et al., 2019). The strong inverse relationship between NDMI and stream NO_3^- demonstrates that vegetation cover was a primary control on watershed N retention across spatial scales and the loss of forest cover lead to elevated stream NO_3^- . This is consistent with earlier work demonstrating that stream NO_3^- concentrations were inversely related to riparian vegetation exposure (Rhoades, Chow, et al., 2019).

Rapid in-stream uptake and processing contribute to variability in stream NO_3^- concentrations (Bernhardt et al., 2003). Nitrate uptake lengths in nearby Wyoming streams ranged from hundreds to thousands of meters (Hall et al., 2009), so uptake is likely to influence NO_3^- patterns across the range of scales in this study (<9,000 m). However, headwater streams with elevated ambient inorganic N concentrations have a limited ability to moderate downstream transport of inorganic N (Covino et al., 2021b) because nutrient delivery to streams is often orders of magnitude greater than in-stream production or removal (Brookshire et al., 2009). Previous work at the Hayman Fire demonstrated that in-stream biotic N demand increased after the fire, but N supply from burned uplands exceeded the increase in stream N demand (Rhea et al., 2021). While in-stream uptake likely contributed to spatial variability in stream NO_3^- , this work demonstrates strong post-fire vegetation controls on the spatial patterns of stream NO_3^- concentrations.

4.4.3 Burned headwaters are susceptible to elevated stream NO_3^-

Patterns of vegetation cover interact with watershed structure to drive spatial distributions of stream NO_3^- concentrations. Terrestrial inputs of water and dissolved solutes comprise a large portion of streamwater composition in headwater positions, making these areas particularly sensitive to disturbance in the surrounding uplands (Gomi et al., 2002; Likens & Bormann, 1974;

Lowe & Likens, 2005). Thus, the vegetation cover of large convergent hillslopes should have stronger proportional influence on stream NO_3^- concentration in headwater positions relative to locations lower in the network. I found that convergent hillslopes in the headwaters of Brush Creek were associated with low NDMI (Figure 4.5E) and aligned with locations of high stream NO_3^- (Figure 4.5E). Proportional inflows declined downstream and were associated with higher NDMI. Stream NO_3^- also declined downstream in Brush Creek, likely due to a combination of reduced proportional influence of hillslope inputs, streamflow dilution, and in-stream N uptake. In the unburned headwaters of Pine Creek, convergent hillslopes were associated with high NDMI (Figure 4.5F) and likely high terrestrial N demand. Stream NO_3^- concentrations remained low throughout the headwaters with only slight downstream increases where hillslopes were sparsely vegetated (Figure 4.5F).

This investigation demonstrates that convergent hillslopes in headwater positions are particularly sensitive to wildfire-induced vegetation mortality and can impact both local and downstream water quality. Headwater attributes have been shown to predict downstream water chemistry (i.e., NO_3^- , PO_4^{3-} , Ca^{2+} , and Sr^{2+}) at distances > 500 km (French et al., 2020). The sampled stream networks were only 5,520 - 8,289 m, so headwater attributes could feasibly influence downstream chemistry throughout the entire stream networks. Indeed, the watershed with burned headwaters (i.e., Brush), sustained higher stream NO_3^- concentrations throughout its stream network compared to the watershed with unburned headwaters (i.e., Pine, Figure 4.5E-F). These findings may help prioritize post-fire watershed rehabilitation efforts aimed at increasing plant cover and nutrient demand to reduce stream NO_3^- concentrations. More specifically, these findings highlight the potential value for post-fire regeneration in convergent headwater locations to enhance N retention and reduce downstream NO_3^- export.

4.5 Conclusions

This study utilized spatially distributed stream solute sampling to identify the controls on stream Na^+ and NO_3^- concentrations across a gradient of burn patterns. Statistical modeling was used to partition the variance in stream Na^+ and NO_3^- among landscape (i.e., topographic, vegetation, and fire predictors) and stream network (i.e., flow-connected distance) characteristics. Topographic, vegetation, and fire variables were poor predictors of stream Na^+ whereas mean NDMI was the strongest predictor of stream NO_3^- . Strong positive spatial autocorrelation indicated that downstream hydrologic transport was the primary driver of spatially distributed Na^+ concentrations. Conversely, stream NO_3^- exhibited high spatial variability and weak spatial structure across all spatial scales. These results suggest that complex wildfire patterns that create a mosaic of unburned forest interspersed with patches of shrubs and grasses can result in high variability in stream NO_3^- concentrations. I also found that sparse forest cover in severely burned convergent hillslopes in headwater positions had a disproportionate impact on stream NO_3^- concentrations, suggesting that targeted reforestation in these locations may help limit stream NO_3^- concentrations and downstream export.

5. Conclusions

5.1 Key findings

In chapter 2, I investigated the stream biotic response to wildfire and evaluated the potential for stream uptake to attenuate NO_3^- losses. I found significant changes in-stream nutrient limitation, benthic biomass, and stream metabolism 5 and 15 years after severe wildfire. The streams draining burned watersheds had 23-times higher stream NO_3^- concentrations which led to reduced N-limitation of benthic autotrophs. Burned streams also had 2.5-times greater more autotrophic biomass and 20-times higher gross primary productivity than unburned streams. While stream N demand was elevated in burned streams, it was not enough to substantially attenuate terrestrial N losses. This finding suggests that terrestrial to aquatic nutrient supply must be reduced in order to minimize watershed NO_3^- export.

In chapter 3, I characterized terrestrial N sources by measuring inorganic N in soils, soil water, and shallow groundwater along burned and unburned topographic gradients. The goal of this research was to determine if post-fire stream NO_3^- exports were driven by soil inorganic N pools and net transformation rates or post-fire vegetation recovery. My data demonstrate that total C and N, inorganic N concentrations, and net N transformation rates were similar in burned and unburned mineral soils indicating that there was no long-term increase in post-fire soil N supply across any sampled topographic positions. Sustained elevations in N concentration seem to be a product of low vegetative demand associated with slow post-fire regeneration.

In chapter 4, I utilized statistical modeling to partition the variance in stream Na^+ and NO_3^- among landscape (i.e., topographic, vegetation, and fire predictors) and stream network (i.e., flow-connected distance) characteristics across a gradient of burn patterns. Stream Na^+ was not strongly related to any landscape variables, but rather was regulated by downstream hydrologic transport,

as indicated by strong positive spatial autocorrelation. In contrast, stream NO_3^- exhibited weak spatial structuring due to high variability across spatial scales. Mean NDWI was the best predictor of stream NO_3^- so complex post-fire mosaics of unburned forest interspersed with patches of shrubs and grasses likely contribute to spatially variable NO_3^- concentrations. For example, the highest stream NO_3^- concentrations were associated with sparse forest cover in severely burned headwaters and convergent hillslopes. These results demonstrate that there are discrete landscape features that strongly regulate the spatial distribution of post-fire stream NO_3^- .

5.2 Opportunities for future research

This work demonstrates that elevated post-fire NO_3^- can persist for decades and is linked to slow vegetation recovery. Tree regeneration may take decades to centuries in severely burned ponderosa-pine and Douglas-fir forests that do not have nearby surviving trees (Chambers et al., 2016). If a return to a forested state is desirable in these areas, active management activities, like planting, may be required (Chambers et al., 2016). Planting in post-fire landscapes is complex and there are a multitude of ecological and social tradeoffs that must be considered (Stevens et al., 2021) including clustered spacing (North et al., 2019), forest type, aspect, elevation, slope, soils, and moisture (Stevens-Rumann & Morgan, 2019). However, my findings identify specific landscape features, such as severely burned riparian zones and convergent hillslopes in headwater positions, that are likely to strongly regulate stream NO_3^- patterns. This is a first step towards understanding what post-fire planting strategies are most effective at mitigating lingering post-fire NO_3^- concerns (Rhoades, Nunes, et al., 2019). However, I recommend experimental work that explicitly monitors the effects of targeted plantings on post-fire NO_3^- .

The degree to which fires modify ecosystem N storage depends on the complex interactions between fire severity and landscape location (Smithwick et al., 2009). I began unpacking this

relationship in Chapter 4 where I found the position of severe fire within a watershed had unique implications for local and downstream NO_3^- concentrations. However, statistical modeling required singular summary metrics (i.e., watershed mean, extent, etc) for a given sub-watershed, limiting the ability to capture the complex spatial distributions of topography and fire within these watersheds. One way around this limitation would be the integration of mechanistic, process-based modeling. For example, stream NO_3^- export could be modeled using spatially-distributed measures of watershed structure (i.e., hillslope loading), stream-groundwater exchange, and transport velocities (i.e., in-stream uptake) (Bergstrom et al., 2016; Covino et al., 2011; Mallard et al., 2014).

There is also a need for studies that link post-fire nutrient responses across lentic and lotic ecosystems within freshwater networks. Previous research (French et al., 2020) and my spatially-distributed sampling have demonstrated that elevated dissolved solute concentrations can persist longitudinally throughout headwater stream networks. However, it is unclear how these stream signals propagate longitudinally into downstream storage reservoirs. Relatively few studies have focused on post-fire N responses in lakes and reservoirs (McCullough et al., 2019; Smith et al., 2011) which is surprising considering storage reservoirs are a critical component of the water supply system in the Western US. There is some evidence of elevated lake N post-fire and it is generally assumed that lakes will have similar, or more severe, algal responses to wildfire than streams (McCullough et al., 2019) because of long residence times and the accumulation of nutrient-rich mineral soil and ash in lake sediments (Bladon et al., 2014; Santos et al., 2015). Ultimately, downstream propagation will likely depend on the interaction between wildfire size and severity, pre-fire chemical condition, and lake volume and residence time (McCullough et al., 2019). Given the projected increase in wildfire-impacts on reservoirs of the Western US (Sankey et al., 2017), we must better understand potential impacts on municipal water quality.

REFERENCES

- Abatzoglou, J. T., & Williams, A. P. (2016). Impact of anthropogenic climate change on wildfire across western US forests. <https://doi.org/10.1073/pnas.1607171113>
- Abatzoglou, J. T., Kolden, C. A., Williams, A. P., Lutz, J. A., & Smith, A. M. S. (2017). Climatic influences on interannual variability in regional burn severity across western US forests. *International Journal of Wildland Fire*, 26(4), 269–275. <https://doi.org/10.1071/WF16165>
- Abbott, B. W., Gruau, G., Zarnetske, J. P., Moatar, F., Barbe, L., Thomas, Z., et al. (2018). Unexpected spatial stability of water chemistry in headwater stream networks. *Ecology Letters*, 21(2), 296–308. <https://doi.org/10.1111/ele.12897>
- Abbott, B. W., Rocha, A. V., Shogren, A., Zarnetske, J. P., Iannucci, F., Bowden, W. B., et al. (2021). Tundra wildfire triggers sustained lateral nutrient loss in Alaskan Arctic. *Global Change Biology*, 27(7), 1408–1430. <https://doi.org/10.1111/gcb.15507>
- Alexander, R. B., Boyer, E. W., Smith, R. A., Schwarz, G. E., & Moore, R. B. (2007). The role of headwater streams in downstream water quality. *Journal of the American Water Resources Association*, 43(1), 41–59. <https://doi.org/10.1111/j.1752-1688.2007.00005.x>
- Allred, B. W., Bestelmeyer, B. T., Boyd, C. S., Brown, C., Davies, K. W., Duniway, M. C., et al. (2021). Improving Landsat predictions of rangeland fractional cover with multitask learning and uncertainty. *Methods in Ecology and Evolution*, 2021(January), 1–9. <https://doi.org/10.1111/2041-210x.13564>
- APHA. (1995). *Standard methods for the examination of water and wastewater* (19th ed.). Washington, D.C.
- Arar, E. J., & Collins, G. B. (1997). *Method 445.0 In Vitro determination of Chlorophyll a and Pheophytin a in marine and freshwater algae by fluorescence*. Washington, DC.
- Arora, B., Burrus, M., Newcomer, M., Steefel, C. I., Carroll, R. W. H., Dwivedi, D., et al. (2020). Differential C-Q Analysis: A New Approach to Inferring Lateral Transport and Hydrologic Transients Within Multiple Reaches of a Mountainous Headwater Catchment. *Frontiers in Water*, 2(August), 1–20. <https://doi.org/10.3389/frwa.2020.00024>
- Baiamonte, G., & Singh, V. P. (2016). Overland Flow Times of Concentration for Hillslopes of Complex Topography. *Journal of Irrigation and Drainage Engineering*, 142(3), 04015059. [https://doi.org/10.1061/\(asce\)ir.1943-4774.0000984](https://doi.org/10.1061/(asce)ir.1943-4774.0000984)
- Basu, N. B., Destouni, G., Jawitz, J. W., Thompson, S. E., Loukinova, N. V., Darracq, A., et al. (2010). Nutrient loads exported from managed catchments reveal emergent biogeochemical stationarity. *Geophysical Research Letters*, 37(23), 1–5. <https://doi.org/10.1029/2010GL045168>
- Basu, N. B., Thompson, S. E., & Rao, P. S. C. (2011). Hydrologic and biogeochemical functioning of intensively managed catchments: A synthesis of top-down analyses. *Water Resources Research*, 47(10), 1–12. <https://doi.org/10.1029/2011WR010800>
- Battin, T. J., Kaplan, L. A., Findlay, S., Hopkinson, C. S., Marti, E., Packman, A. I., et al.

- (2008). Biophysical controls on organic carbon fluxes in fluvial networks. *Nature Geoscience*, 2(8), 95–100. <https://doi.org/10.1038/ngeo602>
- Bauhus, J., Khanna, P. K., & Raison, R. J. (1993). The effect of fire on carbon and nitrogen mineralization and nitrification in an Australian forest soil. *Australian Journal of Soil Research*, 31(5), 621–639. <https://doi.org/10.1071/SR9930621>
- Bechtold, H. A., Marcarelli, A. M., Baxter, C. V., & Inouye, R. S. (2012). Effects of N, P, and organic carbon on stream biofilm nutrient limitation and uptake in a semi-arid watershed. *Limnology and Oceanography*, 57(5), 1544–1554. <https://doi.org/10.4319/lo.2012.57.5.1544>
- Bergstrom, A., McGlynn, B., Mallard, J., & Covino, T. (2016). Watershed structural influences on the distributions of stream network water and solute travel times under baseflow conditions. *Hydrological Processes*, 30(15), 2671–2685. <https://doi.org/10.1002/hyp.10792>
- Bernhardt, E. S., Likens, G. E., Buso, D. C., & Driscoll, C. T. (2003). In-stream uptake dampens effects of major forest disturbance on watershed nitrogen export. *Proceedings of the National Academy of Sciences of the United States of America*, 100(18), 10304–10308. <https://doi.org/10.1073/pnas.1233676100>
- Bernhardt, E. S., Likens, G. E., Hall, R. O., Buso, D. C., Fisher, S. G., Burton, T. M., et al. (2005). Can't See the Forest for the Stream? In-stream Processing and Terrestrial Nitrogen Exports. *BioScience*, 55(3), 219–230. [https://doi.org/10.1641/0006-3568\(2005\)055\[0219:acstff\]2.0.co;2](https://doi.org/10.1641/0006-3568(2005)055[0219:acstff]2.0.co;2)
- Bernot, M. J., Sobota, D. J., Hall, R. O., Mulholland, P. J., Dodds, W. K., Webster, J. R., et al. (2010). Inter-regional comparison of land-use effects on stream metabolism. *Freshwater Biology*, 55(9), 1874–1890. <https://doi.org/10.1111/j.1365-2427.2010.02422.x>
- Betts, E. F., & Jones, J. B. (2009). Impact of Wildfire on Stream Nutrient Chemistry and Ecosystem Metabolism in Boreal Forest Catchments of Interior Alaska. *Arctic, Antarctic, and Alpine Research*, 41(4), 407–417. <https://doi.org/10.1657/1938-4246-41.4.407>
- Biederman, J. A., Meixner, T., Harpold, A. A., Reed, D. E., Gutmann, E. D., Gaun, J. A., & Brooks, P. D. (2016). Riparian zones attenuate nitrogen loss following bark beetle-induced lodgepole pine mortality. *Journal of Geophysical Research G: Biogeosciences*, 121(3), 933–948. <https://doi.org/10.1002/2015JG003284>
- Binkley, D., & Fisher, R. F. (2013). *Ecology and Management of Forest Soils* (4th ed.). John Wiley & Sons, Ltd.
- Binkley, Dan, & Hart, S. C. (1989). The Components of Nitrogen Availability Assessments in Forest Soils. In B. A. Stewart (Ed.), *Advances in Soil Science* (10th ed.). Springer-Verlag.
- Binkley, Dan, & Matson, P. (1983). Ion Exchange Resin Bag Method for Assessing Forest Soil Nitrogen Availability. *Soil Science Society of America Journal*, 47(5), 1050–1052. <https://doi.org/10.2136/sssaj1983.03615995004700050045x>
- Bladon, K. D., Emelko, M. B., Silins, U., & Stone, M. (2014). Wildfire and the future of water supply. *Environmental Science and Technology*, 48(16), 8936–8943. <https://doi.org/10.1021/es500130g>

- Bonnet, V. H., Schoettle, A. W., & Shepperd, W. D. (2005). Postfire environmental conditions influence the spatial pattern of regeneration for *Pinus ponderosa*. *Canadian Journal of Forest Research*, 35(1), 37–47. <https://doi.org/10.1139/x04-157>
- Bormann, B. T., Homann, P. S., Darbyshire, R. L., & Morrisette, B. A. (2008). Intense forest wildfire sharply reduces mineral soil C and N: The first direct evidence. *Canadian Journal of Forest Research*, 38(11), 2771–2783. <https://doi.org/10.1139/X08-136>
- Brennan, S. R., Torgersen, C. E., Hollenbeck, J. P., Fernandez, D. P., Jensen, C. K., & Schindler, D. E. (2016). Dendritic network models: Improving isoscapes and quantifying influence of landscape and in-stream processes on strontium isotopes in rivers. *Geophysical Research Letters*, 43(10), 5043–5051. <https://doi.org/10.1002/2016GL068904>
- Brookshire, E. N. J., Valett, H. M., & Gerber, S. (2009). Maintenance of terrestrial nutrient loss signatures during in-stream transport. *Ecology*, 90(2), 293–299.
- Brown, T. C., Hobbins, M. T., & Ramirez, J. A. (2008). Spatial distribution of water supply in the coterminous United States. *Journal of the American Water Resources Association*, 44(6), 1474–1487. <https://doi.org/10.1111/j.1752-1688.2008.00252.x>
- Certini, G. (2005). Effects of fire on properties of forest soils: A review. *Oecologia*, 143(1), 1–10. <https://doi.org/10.1007/s00442-004-1788-8>
- Chambers, M. E., Fornwalt, P. J., Malone, S. L., & Battaglia, M. A. (2016). Patterns of conifer regeneration following high severity wildfire in ponderosa pine – dominated forests of the Colorado Front Range. *Forest Ecology and Management*, 378, 57–67. <https://doi.org/10.1016/j.foreco.2016.07.001>
- Chapin, F. S., Mooney, H. A., & Matson, P. A. (2011). *Principles of Terrestrial Ecosystem Ecology* (2nd ed.). New York, NY: Springer.
- Chapman, S. K., Langlely, J. A., Hart, S. C., & Koch, G. W. (2006). Plants actively control nitrogen cycling: Uncorking the microbial bottleneck. *New Phytologist*, 169(1), 27–34. <https://doi.org/10.1111/j.1469-8137.2005.01571.x>
- Cho, J. H., & Lee, J. H. (2018). Multiple linear regression models for predicting nonpoint-source pollutant discharge from a highland agricultural region. *Water (Switzerland)*, 10(9). <https://doi.org/10.3390/w10091156>
- Cipra, J., Kelly, E., MacDonald, L., & Norman, J. (2003). Soil properties, erosion, and implications for rehabilitation and aquatic ecosystems. *Hayman Fire Case Study*, 204–219.
- Coop, J. D., Parks, S. A., Stevens-Rumann, C. S., Crausbay, S. D., Higuera, P. E., Hurteau, M. D., et al. (2020). Wildfire-Driven Forest Conversion in Western North American Landscapes. *BioScience*, 70(8), 659–673. <https://doi.org/10.1093/biosci/biaa061>
- Cooper, S. D., Barmuta, L., Sarnelle, O., Kratz, K., & Diehl, S. (1997). Quantifying spatial heterogeneity in streams. *Journal of the North American Benthological Society*, 16(1), 174–188. <https://doi.org/10.2307/1468250>
- Covington, W. W., & Sackett, S. S. (1992). Soil mineral nitrogen changes following prescribed burning in ponderosa pine. *Forest Ecology and Management*, 54(1–4), 175–191.

[https://doi.org/10.1016/0378-1127\(92\)90011-W](https://doi.org/10.1016/0378-1127(92)90011-W)

- Covington, W. W., DeBano, L. F., & Huntsberger, T. G. (1991). Soil nitrogen changes associated with slash pile burning in pinyon-juniper woodlands. *Forest Science*, 37(1), 347–355.
- Covino, T., McGlynn, B., & Mallard, J. (2011). Stream-groundwater exchange and hydrologic turnover at the network scale. *Water Resources Research*, 47(12), 1–11. <https://doi.org/10.1029/2011WR010942>
- Covino, T., Riveros-Iregui, D. A., & Schneider, C. L. (2021). *Geomorphology Imparts Spatial Organization on Hydrological and Biogeochemical Fluxes. Reference Module in Earth Systems and Environmental Sciences*. Elsevier Inc. <https://doi.org/10.1016/b978-0-12-818234-5.00068-7>
- Covino, T.P., Wlostowski, A. N., Gooseff, M. N., Wollheim, W. M., & Bowden, W. B. (2021). The Seasonality of In-Stream Nutrient Concentrations and Uptake in Arctic Headwater Streams in the Northern Foothills of Alaska’s Brooks Range. *Journal of Geophysical Research: Biogeosciences*, 126(4), 1–18. <https://doi.org/10.1029/2020JG005949>
- Covino, Timothy P., Bernhardt, E. S., & Heffernan, J. B. (2018). Measuring and interpreting relationships between nutrient supply, demand, and limitation. *Freshwater Science*, 37(3), 448–455. <https://doi.org/10.1086/699202>
- Creed, I. F., & Beall, F. D. (2009). Distributed topographic indicators for predicting nitrogen export from headwater catchments. *Water Resources Research*, 45(10). <https://doi.org/10.1029/2008WR007285>
- Creed, Irena F., McKnight, D. M., Pellerin, B. A., Green, M. B., Bergamaschi, B. A., Aiken, G. R., et al. (2015). The river as a chemostat: Fresh perspectives on dissolved organic matter flowing down the river continuum. *Canadian Journal of Fisheries and Aquatic Sciences*, 72(8), 1272–1285. <https://doi.org/10.1139/cjfas-2014-0400>
- DeLuca, T. H., & Sala, A. (2006). Frequent fire alters nitrogen transformations in ponderosa pine stands of the Inland Northwest. *Ecology*, 87(10), 2511–2522. [https://doi.org/10.1890/0012-9658\(2006\)87\[2511:FFANTI\]2.0.CO;2](https://doi.org/10.1890/0012-9658(2006)87[2511:FFANTI]2.0.CO;2)
- Detty, J. M., & McGuire, K. J. (2010). Topographic controls on shallow groundwater dynamics: Implications of hydrologic connectivity between hillslopes and riparian zones in a till mantled catchment. *Hydrological Processes*, 24(16), 2222–2236. <https://doi.org/10.1002/hyp.7656>
- Dingman, L. S. (2015). *Physical Hydrology* (3rd ed.). Long Grove, IL: Waveland Press, Inc.
- Dodds, W. K., & Smith, V. H. (2016). Nitrogen, phosphorus, and eutrophication in streams. *Inland Waters*, 6(2), 155–164. <https://doi.org/10.5268/IW-6.2.909>
- Dove, N. C., Safford, H. D., Bohlman, G. N., Estes, B. L., & Hart, S. C. (2020). High-severity wildfire leads to multi-decadal impacts on soil biogeochemistry in mixed-conifer forests. *Ecological Applications*, 0(0), 1–18. <https://doi.org/10.1002/eap.2072>
- Dunnette, P. V., Higuera, P. E., Mclauchlan, K. K., Derr, K. M., Briles, C. E., & Keefe, M. H.

- (2014). Biogeochemical impacts of wildfires over four millennia in a Rocky Mountain subalpine watershed. *New Phytologist*, 203(3), 900–912. <https://doi.org/10.1111/nph.12828>
- Earl, S. R., Valett, H. M., & Webster, J. R. (2006). Nitrogen saturation in stream ecosystems. *Ecology*, 87(12), 3140–3151. [https://doi.org/10.1890/0012-9658\(2006\)87\[3140:NSISE\]2.0.CO;2](https://doi.org/10.1890/0012-9658(2006)87[3140:NSISE]2.0.CO;2)
- Eidenshink, J., Schwind, B., Brewer, K., Zhu, Z.-L., Quayle, B., & Howard, S. (2009). A Project for Monitoring Trends in Burn Severity. *Fire Ecology*, 3(1), 3–21. <https://doi.org/10.4996/fireecology.0301003>
- Emelko, M. B., Silins, U., Bladon, K. D., & Stone, M. (2011). Implications of land disturbance on drinking water treatability in a changing climate: Demonstrating the need for “source water supply and protection” strategies. *Water Research*, 45(2), 461–472. <https://doi.org/10.1016/j.watres.2010.08.051>
- Emelko, M. B., Stone, M., Silins, U., Allin, D., Collins, A. L., Williams, C. H. S., et al. (2016). Sediment-phosphorus dynamics can shift aquatic ecology and cause downstream legacy effects after wildfire in large river systems. *Global Change Biology*, 22(3), 1168–1184. <https://doi.org/10.1111/gcb.13073>
- EPA. (2000). Ambient Water Quality Criteria Recommendations: Rivers and Streams in Nutrient Ecoregion III. *US Environmental Protection Agency EPA 822-B-00-016*, (December), 1–20.
- Fegel, T. S., Boot, C. M., Covino, T. P., Elder, K., Hall, E. K., Starr, B., et al. (2021). Amount and reactivity of dissolved organic matter export are affected by land cover change from old-growth to second-growth forests in headwater ecosystems. *Hydrological Processes*, 35(8), 1–10. <https://doi.org/10.1002/hyp.14343>
- Fennessy, M. S., & Cronk, J. K. (1997). The effectiveness and restoration potential of riparian ecotones for the management of nonpoint source pollution, particularly nitrate. *Critical Reviews in Environmental Science and Technology*, 27(4), 285–317. <https://doi.org/10.1080/10643389709388502>
- Fernández, D., Barquín, J., Álvarez-Cabria, M., & Peñas, F. J. (2012). Quantifying the performance of automated GIS-based geomorphological approaches for riparian zone delineation using digital elevation models. *Hydrology and Earth System Sciences*, 16(10), 3851–3862. <https://doi.org/10.5194/hess-16-3851-2012>
- Fischer, R. a, & Fischenich, J. C. (2000). Design Recommendations for Riparian Corridors and Vegetated Buffer Strips. *Development*, 1–17.
- Fornwalt, P. J., & Kaufmann, M. R. (2014). Understorey plant community dynamics following a large, mixed severity wildfire in a *Pinus ponderosa*-*Pseudotsuga menziesii* forest, Colorado, USA. *Journal of Vegetation Science*, 25(3), 805–818. <https://doi.org/10.1111/jvs.12128>
- French, D. W., Schindler, D. E., Brennan, S. R., & Whited, D. (2020). Headwater Catchments Govern Biogeochemistry in America’s Largest Free-Flowing River Network. *Journal of Geophysical Research: Biogeosciences*, 125(12), 1–20. <https://doi.org/10.1029/2020JG005851>
- Ganio, L. M., Torgersen, C. E., & Gresswell, R. E. (2005). A geostatistical approach for

- describing spatial pattern in stream networks. *Frontiers in Ecology and the Environment*, 3(3), 138–144.
- Gift, D. M., Groffman, P. M., Kaushal, S. S., & Mayer, P. M. (2010). Denitrification potential, root Biomass, and organic matter in degraded and restored urban riparian zones. *Restoration Ecology*, 18(1), 113–120. <https://doi.org/10.1111/j.1526-100X.2008.00438.x>
- Godsey, S. E., Kirchner, J. W., & Clow, D. W. (2009). Concentration–discharge relationships reflect chemostatic characteristics of US catchments. *Hydrological Processes*, 23, 1844–1864.
- Gomi, T., Sidle, R. C., & Richardson, J. S. (2002). Understanding processes and downstream linkages of headwater systems. *BioScience*, 52(10), 905–916. [https://doi.org/10.1641/0006-3568\(2002\)052\[0905:UPADLO\]2.0.CO;2](https://doi.org/10.1641/0006-3568(2002)052[0905:UPADLO]2.0.CO;2)
- Graham, R. T. (2003). *Hayman Fire Case Study. Gen. Tech. Rep. RMRS- GTR-114*. Ogden, UT. Retrieved from http://www.fs.fed.us/rm/hayman_fire/
- Gresswell, R. E. (1999). Fire and aquatic ecosystems in forested biomes of North America. *Transactions of the American Fisheries Society*, 128(2), 193–221. <https://doi.org/10.1577/1548-8659>
- Grogan, P., Bruns, T. D., & Chapin, F. S. (2000). Fire effects on ecosystem nitrogen cycling in a Californian bishop pine forest. *Oecologia*, 122(4), 537–544. <https://doi.org/10.1007/s004420050977>
- Hall, R. O. (2003). A stream’s role in watershed nutrient export. *Proceedings of the National Academy of Sciences of the United States of America*, 100(18), 10137–10138. <https://doi.org/10.1073/pnas.1934477100>
- Hall, R. O., & Hotchkiss, E. R. (2017). Stream Metabolism. *Methods in Stream Ecology, Volume 2: Ecosystem Function*, 219–233.
- Hall, R. O., & Tank, J. L. (2003). Ecosystem metabolism controls nitrogen uptake in streams in Grand Teton National Park, Wyoming. *Limnology and Oceanography*, 48(3), 1120–1128. <https://doi.org/10.4319/lo.2003.48.3.1120>
- Hall, R. O., Sobota, D. J., Dodds, W. K., Findlay, S. E. G., Grimm, N. B., Hamilton, S. K., et al. (2009). Nitrate removal in stream ecosystems measured by ¹⁵N addition experiments: Denitrification. *Limnology and Oceanography*, 54(3), 666–680. <https://doi.org/10.4319/lo.2009.54.3.0666>
- Hall, S. (2017). The Legacy of Colorado’s Largest Wildfire. *Denver Water*.
- Hambrook Berkman, J. A., & Canova, M. G. (2007). *Algal biomass indicators: U.S. Geological Survey techniques of water-resources investigations*. U.S. Geological Survey Techniques of Water-Resources Investigations. Retrieved from <https://doi.org/10.3133/twri09A7.4>
- Hanan, E. J., Schimel, J. P., Dowdy, K., & D’Antonio, C. M. (2016). Effects of substrate supply, pH, and char on net nitrogen mineralization and nitrification along a wildfire-structured age gradient in chaparral. *Soil Biology and Biochemistry*, 95, 87–99. <https://doi.org/10.1016/j.soilbio.2015.12.017>

- Hansen, B., Reich, P., Lake, P. S., & Cavagnaro, T. (2010). *Minimum width requirements for riparian zones to protect flowing waters and to conserve biodiversity: a review and recommendations. Report to the Office of Water, Victorian Department of Sustainability and Environment*. Retrieved from http://www.ccmaknowledgebase.vic.gov.au/resources/RiparianBuffers_Report_Hansenetal2010.pdf
- Hart, S. C., Nason, G. E., Myrold, D. D., & Perry, D. A. (1994). Dynamics of gross nitrogen transformations in an old-growth forest: The carbon connection. *Ecology*, *75*(4), 880–891. <https://doi.org/10.2307/1939413>
- Hesselbarth, M., Sciaini, M., With, K., Wiegand, K., & Nowosad, J. (2019). landscapemetrics: an open-source R tool to calculate landscape metrics. *Ecography*, *42*, 1648–1657.
- Higuera, P. E., & Abatzoglou, J. T. (2021). Record-setting climate enabled the extraordinary 2020 fire season in the western United States. *Global Change Biology*, *27*(1), 1–2. <https://doi.org/10.1111/gcb.15388>
- Hinckley, E. L. S., Ebel, B. A., Barnes, R. T., Murphy, S. F., & Anderson, S. P. (2017). Critical zone properties control the fate of nitrogen during experimental rainfall in montane forests of the Colorado Front Range. *Biogeochemistry*, *132*(1–2), 213–231. <https://doi.org/10.1007/s10533-017-0299-8>
- Ver Hoef, J. M., Peterson, E. E., Cliord, D., & Shah, R. (2014). Ssn: An R package for spatial statistical modeling on stream networks. *Journal of Statistical Software*, *56*(3), 1–45. <https://doi.org/10.18637/jss.v056.i03>
- Ver Hoef, J., & Peterson, E. (2020). SSN. R package version 1.1.15. Retrieved from <https://cran.r-project.org/web/packages/SSN/SSN.pdf>
- Holyman, Z. H., Jencso, K. G., Hu, J., Martin, J. T., Holden, Z. A., Seielstad, C. A., & Rowell, E. M. (2018). Hillslope Topography Mediates Spatial Patterns of Ecosystem Sensitivity to Climate. *Journal of Geophysical Research : Biogeosciences*, *123*, 353–371.
- Huntington, J. L., Hegewisch, K. C., Daudert, B., Morton, C. G., Abatzoglou, J. T., McEvoy, D. J., & Erickson, T. (2017). Climate engine: Cloud computing and visualization of climate and remote sensing data for advanced natural resource monitoring and process understanding. *Bulletin of the American Meteorological Society*, *98*(11), 2397–2409. <https://doi.org/10.1175/BAMS-D-15-00324.1>
- Isaak, D. J., Peterson, E. E., Ver Hoef, J. M., Wenger, S. J., Falke, J. A., Torgersen, C. E., et al. (2014). Applications of spatial statistical network models to stream data. *Wiley Interdisciplinary Reviews: Water*, *1*(3), 277–294. <https://doi.org/10.1002/wat2.1023>
- Jencso, K. G., McGlynn, B. L., Gooseff, M. N., Bencala, K. E., & Wondzell, S. M. (2010). Hillslope hydrologic connectivity controls riparian groundwater turnover: Implications of catchment structure for riparian buffering and stream water sources. *Water Resources Research*, *46*(10), 1–18. <https://doi.org/10.1029/2009WR008818>
- Johnson, D. W., Murphy, J. F., Susfalk, R. B., Caldwell, T. G., Miller, W. W., Walker, R. F., & Powers, R. F. (2005). The effects of wildfire, salvage logging, and post-fire N-fixation on

- the nutrient budgets of a Sierran forest. *Forest Ecology and Management*, 220(1–3), 155–165. <https://doi.org/10.1016/j.foreco.2005.08.011>
- Johnson, L. T., Tank, J. L., & Dodds, W. K. (2009). The influence of land use on stream biofilm nutrient limitation across eight North American ecoregions. *Canadian Journal of Fisheries and Aquatic Sciences*, 66(7), 1081–1094. <https://doi.org/10.1139/F09-065>
- Kattwinkel, M., & Szöcs, E. (2020). openSTARS: An Open Source Implementation of the “ArcGIS” Toolbox “STARS”. R package version 1.2.2. Retrieved from <https://cran.r-project.org/package=openSTARS>
- Kaye, J. P., & Hart, S. C. (1997). Competition for nitrogen between plants and soil microorganisms. *Trends in Ecology & Evolution*, 12(4), 139–143. <https://doi.org/10.1126/science.158.3807.1426>
- Keeley, J. E. (2009). Fire intensity, fire severity and burn severity: A brief review and suggested usage. *International Journal of Wildland Fire*, 18(1), 116–126. <https://doi.org/10.1071/WF07049>
- King, S. A., Heffernan, J. B., & Cohen, M. J. (2014). Nutrient flux, uptake, and autotrophic limitation in streams and rivers. *Freshwater Science*, 33(1), 85–98. <https://doi.org/10.1086/674383>
- Klose, K., Cooper, S. D., & Bennett, D. M. (2015). Effects of wildfire on stream algal abundance, community structure, and nutrient limitation. *Freshwater Science*, 34(4), 1494–1509. <https://doi.org/10.1086/683431>
- Kurth, V. J., Hart, S. C., Ross, C. S., Kaye, J. P., & Fulé, P. Z. (2014). Stand-replacing wildfires increase nitrification for decades in southwestern ponderosa pine forests. *Oecologia*, 175(1), 395–407. <https://doi.org/10.1007/s00442-014-2906-x>
- Lane, E. W. (1955). The importance of fluvial morphology in hydraulic engineering. *Proceedings of the American Society of Civil Engineers*, 81 (art.74).
- Lane, P. N. J., Sheridan, G. J., Noske, P. J., & Sherwin, C. B. (2008). Phosphorus and nitrogen exports from SE Australian forests following wildfire. *Journal of Hydrology*, 361(1–2), 186–198. <https://doi.org/10.1016/j.jhydrol.2008.07.041>
- Larimer County, Colorado Department of Transportation, Natural Resources Conservation Science, & U.S. Forest Service. (2012). *High Park Fire Burned Area Emergency Response Report*. Retrieved from https://www.larimer.org/sites/default/files/uploads/2017/bear_report_0.pdf
- Lentile, L. B., Morgan, P., Hudak, A. T., Bobbitt, M. ., Lewis, S. A., Smith, A. M. S., & Robichaud, P. R. (2007). Post-fire burn severity and vegetation response following eight large wildfires across the Western United States. *Fire Ecology*, 3(1), 91–108. <https://doi.org/10.1227/01.NEU.0000089482.80879.9A>
- Likens, G. E., & Bormann, F. H. (1974). Linkages between Terrestrial and Aquatic Ecosystems. *BioScience*, 24(8), 447–456. <https://doi.org/10.2307/1296852>
- Likens, G. E., Bormann, F. H., Johnson, N. M., Fisher, D. W., & Pierce, R. S. (1970). Effects of

Forest Cutting and Herbicide Treatment on Nutrient Budgets in the Hubbard Brook Watershed-Ecosystem. *Ecological Monographs*, 40(1), 23–47. <https://doi.org/10.2307/1942440>

Lindsay, J. B. (2020). WhiteboxTools Version 1.4.0. Guelph, Canada.

Lovett, G. M., Weathers, K. C., & Arthur, M. A. (2002). Control of nitrogen loss from forested watersheds by soil carbon:Nitrogen ratio and tree species composition. *Ecosystems*, 5(7), 712–718. <https://doi.org/10.1007/s10021-002-0153-1>

Lowe, W. H., & Likens, G. E. (2005). Moving Headwater Streams to the Head of the Class. *BioScience*, 55(3), 196–197. Retrieved from [https://doi.org/10.1641/0006-3568\(2005\)055\[0196:MHSTTH\]2.0.CO;2](https://doi.org/10.1641/0006-3568(2005)055[0196:MHSTTH]2.0.CO;2)

Mallard, J., McGlynn, B., & Covino, T. (2014). Lateral inflows, stream-groundwater exchange, and network geometry influence stream water composition. *Water Resources Research*, 50, 4603–4623. <https://doi.org/10.1002/2013WR014979>.Reply

Malone, S. L., Fornwalt, P. J., Battaglia, M. A., Chambers, M. E., Iniguez, J. M., & Sieg, C. H. (2018). Mixed-severity fire fosters heterogeneous spatial patterns of conifer regeneration in a dry conifer forest. *Forests*, 9(1). <https://doi.org/10.3390/f9010045>

Marcarelli, A. M., Bechtold, H. A., Rugenski, A. T., & Inouye, R. S. (2009). Nutrient limitation of biofilm biomass and metabolism in the Upper Snake River basin, southeast Idaho, USA. *Hydrobiologia*, 620(1), 63–76. <https://doi.org/10.1007/s10750-008-9615-6>

McClain, M. E., Boyer, E. W., Dent, C. L., Gergel, S. E., Grimm, N. B., Groffman, P. M., et al. (2003). Biogeochemical Hot Spots and Hot Moments at the Interface of Terrestrial and Aquatic Ecosystems. *Ecosystems*, 6(4), 301–312. <https://doi.org/10.1007/s10021-003-0161-9>

McCullough, I. M., Cheruvilil, K. S., Lapierre, J. F., Lottig, N. R., Moritz, M. A., Stachelek, J., & Soranno, P. A. (2019). Do lakes feel the burn? Ecological consequences of increasing exposure of lakes to fire in the continental United States. *Global Change Biology*, 25(9), 2841–2854. <https://doi.org/10.1111/gcb.14732>

McDowell, N. G., Allen, C. D., Anderson-teixeira, K., Aukema, B. H., Bond-lamberty, B., Chini, L., et al. (2020). Pervasive shifts in forest dynamics in a changing world. *Science*, 368. <https://doi.org/10.1126/science.aaz9463>

McGuire, K. J., Torgersen, C. E., Likens, G. E., Buso, D. C., Lowe, W. H., & Bailey, S. W. (2014). Network analysis reveals multiscale controls on streamwater chemistry. *Proceedings of the National Academy of Sciences of the United States of America*, 111(19), 7030–7035. <https://doi.org/10.1073/pnas.1404820111>

McManus, M. G., D'amico, E., Smith, E. M., Polinsky, R., Ackerman, J., & Tyler, K. (2020). Variation in stream network relationships and geospatial predictions of watershed conductivity. *Freshwater Science*, 39(4), 704–721. <https://doi.org/10.1086/710340>

Van Meter, K. J., & Basu, N. B. (2015). Catchment legacies and time lags: A parsimonious watershed model to predict the effects of legacy storage on nitrogen export. *PLoS ONE*, 10(5), 1–22. <https://doi.org/10.1371/journal.pone.0125971>

- Moore, R. (1992). Soil Survey of Pike National Forest, Eastern Park, Colorado. *USDA Forest Service and Soil Conservation Service*, 1–106.
- Morresi, D., Vitali, A., Urbinati, C., & Garbarino, M. (2019). Forest spectral recovery and regeneration dynamics in stand-replacing wildfires of central Apennines derived from Landsat time series. *Remote Sensing*, *11*(3). <https://doi.org/10.3390/rs11030308>
- Murphy, J. D., Johnson, D. W., Miller, W. W., Walker, R. F., Carroll, E. F., & Blank, R. R. (2006). Wildfire Effects on Soil Nutrients and Leaching in a Tahoe Basin Watershed. *Journal of Environmental Quality*, *35*(2), 479–489. <https://doi.org/10.2134/jeq2005.0144>
- Nave, L. E., Vance, E. D., Swanston, C. W., & Curtis, P. S. (2011). Fire effects on temperate forest soil C and N storage. *Ecological Applications*, *21*(4), 1189–1201. <https://doi.org/10.1890/10-0660.1>
- Neary, D. G., Klopatek, C. C., DeBano, L. F., & Ffolliott, P. F. (1999). Fire effects on belowground sustainability: a review and synthesis. *Forest Ecology and Management*, *122*, 51–71. <https://doi.org/10.2307/3977004>
- North, M. P., Stevens, J. T., Greene, D. F., Coppoletta, M., Knapp, E. E., Latimer, A. M., et al. (2019). Tamm Review: Reforestation for resilience in dry western U.S. forests. *Forest Ecology and Management*, *432*(August 2018), 209–224. <https://doi.org/10.1016/j.foreco.2018.09.007>
- NRCS. (2021). Daily Snow Water Equivalent Glen Cove, CO (Station 1057). Retrieved from <https://wcc.sc.egov.usda.gov/nwcc/site?sitenum=1057>
- Odum, H. T. (1956). Primary Production in Flowing Waters. *Limnology and Oceanography*, *1*(2), 102–117. <https://doi.org/10.4319/lo.1956.1.2.0102>
- Page-Dumroese, D. S., & Jurgensen, M. F. (2006). Soil carbon and nitrogen pools in mid- to late-successional forest stands of the northwestern United States: Potential impact of fire. *Canadian Journal of Forest Research*, *36*(9), 2270–2284. <https://doi.org/10.1139/X06-125>
- Parks, S. A., & Abatzoglou, J. T. (2020). Warmer and Drier Fire Seasons Contribute to Increases in Area Burned at High Severity in Western US Forests From 1985 to 2017. *Geophysical Research Letters*, *47*(22), 1–10. <https://doi.org/10.1029/2020GL089858>
- Parsons, A., Robichaud, P. R., Lewis, S. A., Napper, C., & Clark, J. T. (2010). *Field guide for mapping post-fire soil burn severity*. Gen. Tech. Rep. RMRS-GTR-243. Fort Collins, CO. <https://doi.org/10.2737/RMRS-GTR-243>
- Peterson, E. E., & Ver Hoef, J. M. (2010). A mixed-model moving-average approach to geostatistical modeling in stream networks. *Ecology*, *91*(3), 644–651.
- Peterson, E. E., & Ver Hoef, J. M. (2014). STARS: An ArcGIS toolset used to calculate the spatial information needed to fit spatial statistical models to stream network data. *Journal of Statistical Software*, *56*, 1–17.
- Phillips, J. D. (1989). AN EVALUATION OF THE FACTORS DETERMINING THE EFFECTIVENESS OF WATER QUALITY BUFFER ZONES One of the most effective tools for coping with nonpoint source pollution is the maintenance of buffer zones - -

- vegetated strips of land separating runoff and pollut. *Science*, *107*, 133–145.
- Pierson, D. N., Robichaud, P. R., Rhoades, C. C., & Brown, R. E. (2019). Soil carbon and nitrogen eroded after severe wildfire and erosion mitigation treatments. *International Journal of Wildland Fire*, *28*(10), 814–821. <https://doi.org/10.1071/WF18193>
- Raison, R. J. (1979). Modification of the soil environment by vegetation fires, with particular reference to nitrogen transformations: A review. *Plant and Soil*, *51*(1), 73–108. <https://doi.org/10.1007/BF02205929>
- Rantz, S. E. (1982). Measurement of discharge by tracer dilution. *Measurement and Computation of Streamflow: Measurement of Stage and Discharge, USGS Water Supply Paper 2175*, 211–259. Retrieved from <https://pubs.usgs.gov/wsp/wsp2175/>
- Rastetter, E. B., Kling, G. W., Shaver, G. R., Crump, B. C., Gough, L., & Griffin, K. L. (2021). Ecosystem Recovery from Disturbance is Constrained by N Cycle Openness, Vegetation-Soil N Distribution, Form of N Losses, and the Balance Between Vegetation and Soil-Microbial Processes. *Ecosystems*, *24*(3), 667–685. <https://doi.org/10.1007/s10021-020-00542-3>
- Reisinger, A. J., Tank, J. L., & Dee, M. M. (2016). Regional and seasonal variation in nutrient limitation of river biofilms. *Freshwater Biology*, *35*(October 2015), 474–489. <https://doi.org/10.1086/685829>.
- Rhea, A. E., Covino, T. P., & Rhoades, C. C. (2021). Reduced N-Limitation and Increased In-Stream Productivity of Autotrophic Biofilms 5 and 15 Years After Severe Wildfire. *Journal of Geophysical Research: Biogeosciences*, *126*(9), 1–16. <https://doi.org/10.1029/2020JG006095>
- Rhoades, C. C., Entwistle, D., & Butler, D. (2011a). The influence of wildfire extent and severity on streamwater chemistry, sediment and temperature following the Hayman Fire, Colorado. *International Journal of Wildland Fire*, *20*(3), 430–442. <https://doi.org/10.1071/WF09086>
- Rhoades, C. C., Entwistle, D., & Butler, D. (2011b). The influence of wildfire extent and severity on streamwater chemistry, sediment and temperature following the Hayman Fire, Colorado. *International Journal of Wildland Fire*, *20*(3), 430–442. <https://doi.org/10.1071/WF09086>
- Rhoades, C. C., Nunes, J. P., Silins, U., & Doerr, S. H. (2019). The influence of wildfire on water quality and watershed processes: New insights and remaining challenges. *International Journal of Wildland Fire*, *28*(10), 721–725. https://doi.org/10.1071/WFv28n10_FO
- Rhoades, C. C., Chow, A. T., Covino, T. P., Feghel, T. S., Pierson, D. N., & Rhea, A. E. (2019). The Legacy of a Severe Wildfire on Stream Nitrogen and Carbon in Headwater Catchments. *Ecosystems*, *22*(3), 643–657. <https://doi.org/10.1007/s10021-018-0293-6>
- Richer, E. E., Kampf, S. K., Fassnacht, S. R., & Moore, C. C. (2013). Spatiotemporal index for analyzing controls on snow climatology: Application in the Colorado Front Range. *Physical Geography*, *34*(2), 85–107. <https://doi.org/10.1080/02723646.2013.787578>
- Riggan, P. J., Lockwood, R. N., Jacks, P. M., Colver, C. G., Weirich, F., DeBano, L. F., & Brass,

- J. A. (1994). Effects of Fire Severity on Nitrate Mobilization in Watersheds Subject to Chronic Atmospheric Deposition. *Environmental Science and Technology*, 28(3), 369–375. <https://doi.org/10.1021/es00052a005>
- Robichaud, P., MacDonald, L., Freeouf, J., Neary, D., Martin, D., & Ashmun, L. (2003). Postfire Rehabilitation of the Hayman Fire. *Hayman Fire Case Study: USDA RMRS-GTR-114*, 293–313. Retrieved from http://www.fs.fed.us/rm/pubs/rmrs_gtr114/rmrs_gtr114_293_314.pdf
- Robichaud, P. R., Wagenbrenner, J. W., Lewis, S. A., Ashmun, L. E., Brown, R. E., & Wohlgemuth, P. M. (2013). Post-fire mulching for runoff and erosion mitigation Part II: Effectiveness in reducing runoff and sediment yields from small catchments. *Catena*, 105, 93–111. <https://doi.org/10.1016/j.catena.2012.11.016>
- Robinson, N. P., Allred, B. W., Smith, W. K., Jones, M. O., Moreno, A., Erickson, T. A., et al. (2018). Terrestrial primary production for the conterminous United States derived from Landsat 30 m and MODIS 250 m. *Remote Sensing in Ecology and Conservation*, 4(3), 264–280. <https://doi.org/10.1002/rse2.74>
- Roccaforte, J. P., Fulé, P. Z., Chancellor, W. W., & Laughlin, D. C. (2012). Woody debris and tree regeneration dynamics following severe wildfires in arizona ponderosa pine forests. *Canadian Journal of Forest Research*, 42(3), 593–604. <https://doi.org/10.1139/X2012-010>
- Rodríguez-González, P. M., García, C., Albuquerque, A., Monteiro-Henriques, T., Faria, C., Guimarães, J. B., et al. (2019). A spatial stream-network approach assists in managing the remnant genetic diversity of riparian forests. *Scientific Reports*, 9(1), 1–10. <https://doi.org/10.1038/s41598-019-43132-7>
- Rother, M. T., & Veblen, T. T. (2016). Limited conifer regeneration following wildfires in dry ponderosa pine forests of the Colorado Front Range. *Ecosphere*, 7(12). <https://doi.org/10.1002/ecs2.1594>
- Ruleman, C. A., Bohannon, R. G., Bryant, Bruce, Shroba, R. R., & Premo, W. R. (2011). Geologic map of the Bailey 30' x 60' quadrangle, north-central Colorado: U.S. Geological Survey, Scientific Investigations Map SIM-3156, scale 1:100,000.
- Rust, A. J., Hogue, T. S., Saxe, S., & McCray, J. (2018). Post-fire water-quality response in the western United States. *International Journal of Wildland Fire*, 27(3), 203–216. <https://doi.org/10.1071/WF17115>
- Rust, A. J., Saxe, S., McCray, J., Rhoades, C. C., & Hogue, T. S. (2019). Evaluating the factors responsible for post-fire water quality response in forests of the western USA. *International Journal of Wildland Fire*, 28(10), 769–784. <https://doi.org/10.1071/WF18191>
- Sabater, S., Butturini, A., Clement, J. C., Burt, T., Dowrick, D., Hefting, M., et al. (2003). Nitrogen removal by riparian buffers along a European climatic gradient: Patterns and factors of variation. *Ecosystems*, 6(1), 20–30. <https://doi.org/10.1007/s10021-002-0183-8>
- Sankey, J. B., Kreitler, J., Hawbaker, T. J., McVay, J. L., Miller, M. E., Mueller, E. R., et al. (2017). Climate, wildfire, and erosion ensemble foretells more sediment in western USA watersheds. *Geophysical Research Letters*, 44(17), 8884–8892. <https://doi.org/10.1002/2017GL073979>

- Santos, R. M. B., Sanches Fernandes, L. F., Pereira, M. G., Cortes, R. M. V., & Pacheco, F. A. L. (2015). A framework model for investigating the export of phosphorus to surface waters in forested watersheds: Implications to management. *Science of the Total Environment*, 536, 295–305. <https://doi.org/10.1016/j.scitotenv.2015.07.058>
- Schlesinger, W. H., & Bernhardt, E. S. (2013). *Biogeochemistry* (3rd ed.). Elsevier Inc. <https://doi.org/https://doi.org/10.1016/C2010-0-66291-2>
- Seibert, J., & McGlynn, B. L. (2007). A new triangular multiple flow direction algorithm for computing upslope areas from gridded digital elevation models. *Water Resources Research*, 43(4), 1–8. <https://doi.org/10.1029/2006WR005128>
- Shogren, A. J., Zarnetske, J. P., Abbott, B. W., Iannucci, F., Medvedeff, A., Cairns, S., et al. (2021). Arctic concentration–discharge relationships for dissolved organic carbon and nitrate vary with landscape and season. *Limnology and Oceanography*, 66(S1), S197–S215. <https://doi.org/10.1002/lno.11682>
- Silins, U., Bladon, K. D., Kelly, E. N., Esch, E., Spence, J. R., Stone, M., et al. (2014). Five-year legacy of wildfire and salvage logging impacts on nutrient runoff and aquatic plant, invertebrate, and fish productivity. *Ecohydrology*, 7(6), 1508–1523. <https://doi.org/10.1002/eco.1474>
- Smith, H. G., Sheridan, G. J., Lane, P. N. J., Nyman, P., & Haydon, S. (2011). Wildfire effects on water quality in forest catchments: A review with implications for water supply. *Journal of Hydrology*, 396(1–2), 170–192. <https://doi.org/10.1016/j.jhydrol.2010.10.043>
- Smithwick, E. A. H., Turner, M. G., Mack, M. C., & Chapin, F. S. (2005). Postfire soil N cycling in northern conifer forests affected by severe, stand-replacing wildfires. *Ecosystems*, 8(2), 163–181. <https://doi.org/10.1007/s10021-004-0097-8>
- Smithwick, E. A. H., Kashian, D. M., Ryan, M. G., & Turner, M. G. (2009). Long-term nitrogen storage and soil nitrogen availability in post-fire lodgepole pine ecosystems. *Ecosystems*, 12(5), 792–806. <https://doi.org/10.1007/s10021-009-9257-1>
- Steinman, A. D., Lamberti, G. A., & Leavitt, P. R. (2006). Biomass and Pigments of Benthic Algae. In *Methods in Stream Ecology* (2nd ed., pp. 357–379). Academic Press Publications.
- Stephan, K., Kavanagh, K. L., & Koyama, A. (2012). Effects of spring prescribed burning and wildfires on watershed nitrogen dynamics of central Idaho headwater areas. *Forest Ecology and Management*, 263, 240–252. <https://doi.org/10.1016/j.foreco.2011.09.013>
- Stephens, S. L., Finney, M. A., & Schantz, H. (2004). Bulk density and fuel loads of ponderosa pine and white fir forest floors: Impacts of leaf morphology. *Northwest Science*, 78(2), 93–100. Retrieved from https://www.researchgate.net/publication/289973466_Bulk_density_and_fuel_loads_of_ponderosa_pine_and_white_fir_forest_floors_Impacts_of_leaf_morphology
- Stevens-Rumann, C. S., & Morgan, P. (2019). Tree regeneration following wildfires in the western US: a review. *Fire Ecology*, 15(1), 1–17. <https://doi.org/10.1186/s42408-019-0032-1>
- Stevens-Rumann, C. S., Kemp, K. B., Higuera, P. E., Harvey, B. J., Rother, M. T., Donato, D.

- C., et al. (2018). Evidence for declining forest resilience to wildfires under climate change. *Ecology Letters*, 21(2), 243–252. <https://doi.org/10.1111/ele.12889>
- Stevens, J. T., Haffey, C. M., Coop, J. D., Fornwalt, P. J., Yocom, L., Allen, C. D., et al. (2021). Tamm Review: Postfire landscape management in frequent-fire conifer forests of the southwestern United States. *Forest Ecology and Management*, 502(June), 119678. <https://doi.org/10.1016/j.foreco.2021.119678>
- Stream Solute Workshop. (1990). Concepts and Methods for Assessing Solute Dynamics in Stream Ecosystems. *Journal of the North American Benthological Society*, 9(2), 95–119. <https://doi.org/10.2307/1467445>
- Tank, J., & Dodds, W. (2003). Nutrient limitation of epilithic and epixylic biofilms in ten North American streams. *Freshwater Biology*, 48, 1031–1049.
- Taylor, A. H., Poulos, H. M., Kluber, J., Issacs, R., Pawlikowski, N., & Barton, A. M. (2021). Controls on spatial patterns of wildfire severity and early post-fire vegetation development in an Arizona Sky Island, USA. *Landscape Ecology*, 36(9), 2637–2656. <https://doi.org/10.1007/s10980-021-01260-4>
- Tepley, A. J., Thompson, J. R., Epstein, H. E., & Anderson-Teixeira, K. J. (2017). Vulnerability to forest loss through altered postfire recovery dynamics in a warming climate in the Klamath Mountains. *Global Change Biology*, 23(10), 4117–4132. <https://doi.org/10.1111/gcb.13704>
- Turner, M. G., Smithwick, E. A. H., Metzger, K. L., Tinker, D. B., & Romme, W. H. (2007). Inorganic nitrogen availability after severe stand-replacing fire in the Greater Yellowstone ecosystem. *Proceedings of the National Academy of Sciences of the United States of America*, 104(12), 4782–4789. <https://doi.org/10.1073/pnas.0700180104>
- Turner, M. G., Smithwick, E. A. H., Tinker, D. B., & Romme, W. H. (2009). Variation in foliar nitrogen and aboveground net primary production in young postfire lodgepole pine. *Canadian Journal of Forest Research*, 39(5), 1024–1035. <https://doi.org/10.1139/X09-029>
- U.S. Geological Survey. (2018). 3D Elevation Program 10-Meter Resolution Digital Elevation Model. Retrieved from <https://www.usgs.gov/core-science-systems/ngp/3dep/data-tools>
- USGS. (n.d.). USGS 06700000 SOUTH PLATTE RIVER ABOVE CHEESMAN LAKE, CO. Retrieved from https://waterdata.usgs.gov/co/nwis/uv/?site_no=06700000&PARAMeter_cd=00065,00060
- Vannote, R., Minshall, G., Cummins, K., Sedell, J., & Cushing, C. (1980). The River Continuum Concept. *Canadian Journal of Fisheries and Aquatic Sciences*, 37, 130–137.
- Vidon, P. G. F., & Hill, A. R. (2004). Landscape controls on nitrate removal in stream riparian zones. *Water Resources Research*, 40(3), 1–14. <https://doi.org/10.1029/2003WR002473>
- Vitousek, P. M., & Melillo, J. M. (1979). Nitrate Losses From Disturbed Forests: Patterns and Mechanisms. *Forest Science*, 25(4), 605–619.
- Vitousek, P. M., & Reiners, W. A. (1975). Ecosystem Succession and Nutrient Retention: A Hypothesis. *BioScience*, 25(6), 376–381. <https://doi.org/10.2307/1297148>

- Vitousek, P. M., Gosz, J. R., Grier, C. C., Melillo, J. M., William, A., & Todd, R. L. (1979). Nitrate Losses from Disturbed Ecosystems. *Science*, 204(4392), 469–474.
- Walker, R. B., Coop, J. D., Parks, S. A., & Trader, L. (2018). Fire regimes approaching historic norms reduce wildfire-facilitated conversion from forest to non-forest. *Ecosphere*, 9(4). <https://doi.org/10.1002/ecs2.2182>
- Wan, S., Hui, D., & Luo, Y. (2001a). Fire effects on nitrogen pools and dynamics in terrestrial ecosystems: A meta-analysis. *Ecological Applications*, 11(5), 1349–1365. [https://doi.org/10.1890/1051-0761\(2001\)011\[1349:FEONPA\]2.0.CO;2](https://doi.org/10.1890/1051-0761(2001)011[1349:FEONPA]2.0.CO;2)
- Wan, S., Hui, D., & Luo, Y. (2001b). Fire effects on nitrogen pools and dynamics in terrestrial ecosystems: A meta-analysis. *Ecological Applications*, 11(5), 1349–1365. [https://doi.org/10.1890/1051-0761\(2001\)011\[1349:FEONPA\]2.0.CO;2](https://doi.org/10.1890/1051-0761(2001)011[1349:FEONPA]2.0.CO;2)
- Weaver, S. A. (2019). *Resource limitations of autotrophs and heterotrophs in boreal forest headwater streams*. University of Alaska Fairbanks.
- Webster, J. R., & Valett, H. M. (2006). Solute Dynamics. In *Methods in Stream Ecology* (2nd ed., pp. 169–185). Elsevier.
- Weier, J., & Herring, D. (2000). *Measuring Vegetation (NDVI & EVI)*. Retrieved from <http://earthobservatory.nasa.gov/Features/MeasuringVegetation/>
- Westerling, A. L. R. (2016). Increasing western US forest wildfire activity: Sensitivity to changes in the timing of spring. *Philosophical Transactions of the Royal Society B: Biological Sciences*, 371(1696). <https://doi.org/10.1098/rstb.2015.0178>
- Whitlock, C., Shafer, S. L., & Marlon, J. (2003). The role of climate and vegetation change in shaping past and future fire regimes in the northwestern US and the implications for ecosystem management. *Forest Ecology and Management*, 178(1–2), 5–21. [https://doi.org/10.1016/S0378-1127\(03\)00051-3](https://doi.org/10.1016/S0378-1127(03)00051-3)
- Williams, A. P., & Abatzoglou, J. T. (2016). Recent Advances and Remaining Uncertainties in Resolving Past and Future Climate Effects on Global Fire Activity. *Current Climate Change Reports*, 2(1), 1–14. <https://doi.org/10.1007/s40641-016-0031-0>
- Williams, A. P., Abatzoglou, J. T., Gershunov, A., Guzman-Morales, J., Bishop, D. A., Balch, J. K., & Lettenmaier, D. P. (2019). Observed Impacts of Anthropogenic Climate Change on Wildfire in California. *Earth's Future*, 7(8), 892–910. <https://doi.org/10.1029/2019EF001210>
- Williams, C. A., Gu, H., MacLean, R., Masek, J. G., & Collatz, G. J. (2016). Disturbance and the carbon balance of US forests: A quantitative review of impacts from harvests, fires, insects, and droughts. *Global and Planetary Change*, 143, 66–80. <https://doi.org/10.1016/j.gloplacha.2016.06.002>
- Wilson, C., Kampf, S. K., Wagenbrenner, J. W., & MacDonald, L. H. (2018). Rainfall thresholds for post-fire runoff and sediment delivery from plot to watershed scales. *Forest Ecology and Management*, 430(August), 346–356. <https://doi.org/10.1016/j.foreco.2018.08.025>
- Wohl, E. (2017). The significance of small streams. *Frontiers of Earth Science*, 11(3), 447–456.

<https://doi.org/10.1007/s11707-017-0647-y>

- WRCC. (2021). Daily Total Precipitation Cheesman, Colorado (Station 053102). Retrieved from <https://wrcc.dri.edu/cgi-bin/rawMAIN.pl?coCCHE>
- Wu, Q. (2021). whitebox: “WhiteboxTools” R Frontend. R package version 1.4.0. Retrieved from <https://github.com/giswqs/whiteboxR>
- Xu, W., Elberling, B., & Ambus, P. L. (2022). Fire increases soil nitrogen retention and alters nitrogen uptake patterns among dominant shrub species in an Arctic dry heath tundra. *Science of the Total Environment*, 807, 150990. <https://doi.org/10.1016/j.scitotenv.2021.150990>
- Yermakov, Z., & Rothstein, D. E. (2006). Changes in soil carbon and nitrogen cycling along a 72-year wildfire chronosequence in Michigan jack pine forests. *Oecologia*, 149(4), 690–700. <https://doi.org/10.1007/s00442-006-0474-4>
- Zarnetske, J. P., Bouda, M., Abbott, B. W., Saiers, J., & Raymond, P. A. (2018). Generality of Hydrologic Transport Limitation of Watershed Organic Carbon Flux Across Ecoregions of the United States. *Geophysical Research Letters*, 45(21), 11,702-11,711. <https://doi.org/10.1029/2018GL080005>

APPENDIX A: Chapter 2 supplemental material

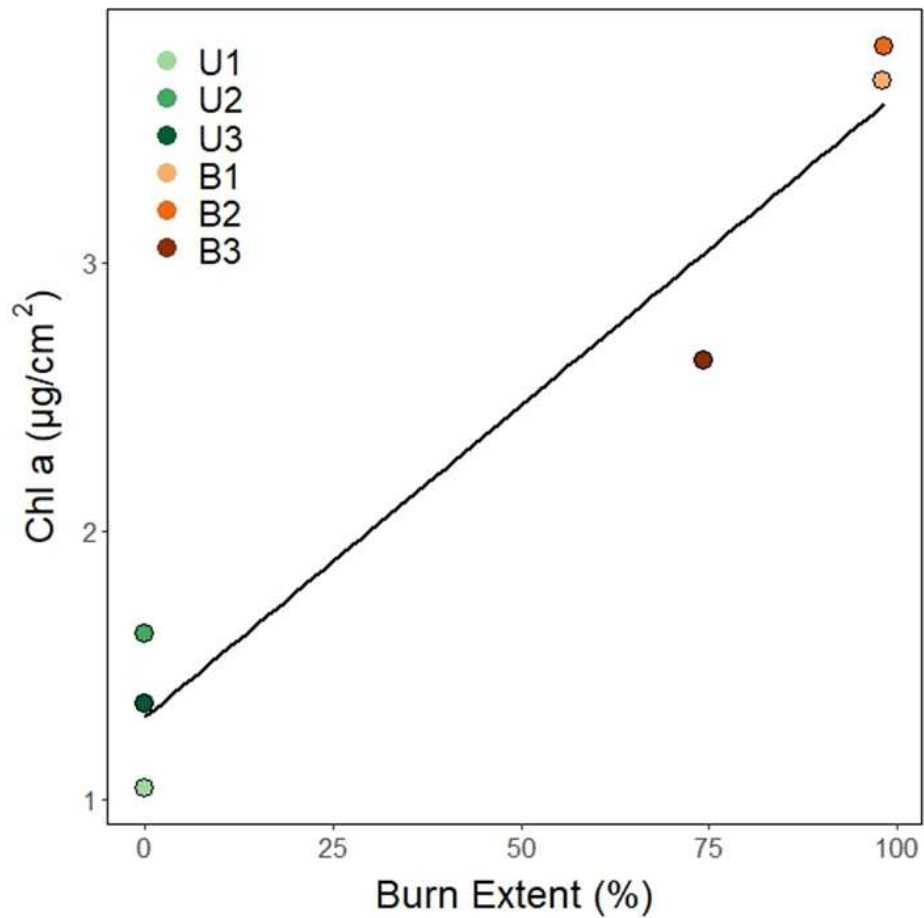


Figure A1: Linear regression between watershed burn extent and mean Chl *a* concentration ($p=0.015$, $R^2=0.80$). Each point and color is associated with a different study watershed. The green colors denote unburned watersheds whereas the orange colors denote burned watersheds.

APPENDIX B: Chapter 3 supplemental material

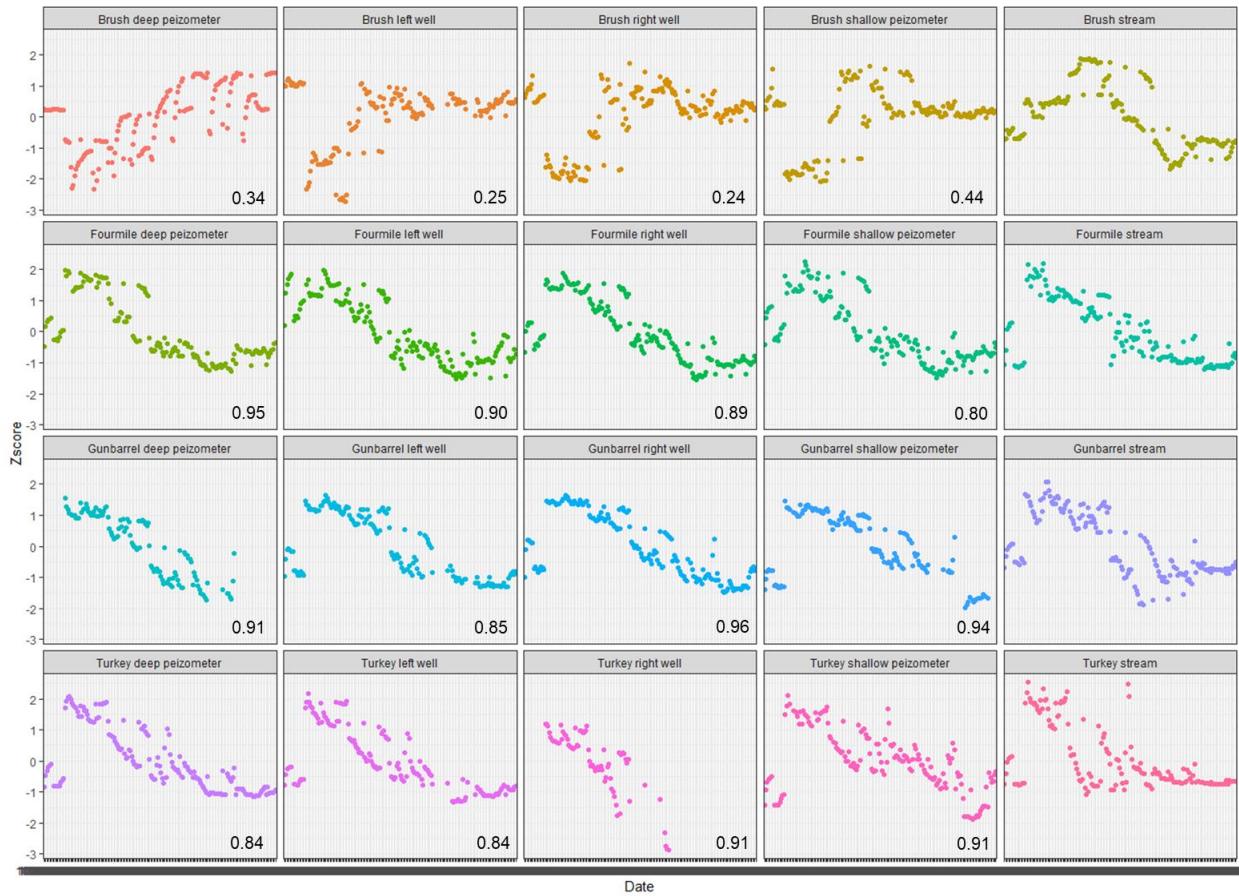


Figure B1: Continuous stage records that were summarized as daily z-scores by station for inter-site comparison. The correlation coefficient between stream stage and groundwater or hyporheic water from a given watershed is denoted in the bottom right of each panel. Brush = B2, Fourmile = B1, Gunbarrel = U2, Turkey = U1.



Figure B2: Volumetric water content (%) of the top 20 cm of mineral soil by site and burn condition. Observations were recorded monthly in 2019 (riparian-midslope, n=18 each) and in 2020 (upland, n=20). The centerline of the boxplots denote median whereas the open diamond denotes the mean, the upper and lower limits span the interquartile range, the whiskers include data within 1.5-times the interquartile range, and the dots beyond the whiskers are outliers. Burn condition significance is denoted by * $p < 0.05$, ** $p < 0.01$, *** $p < 0.001$.

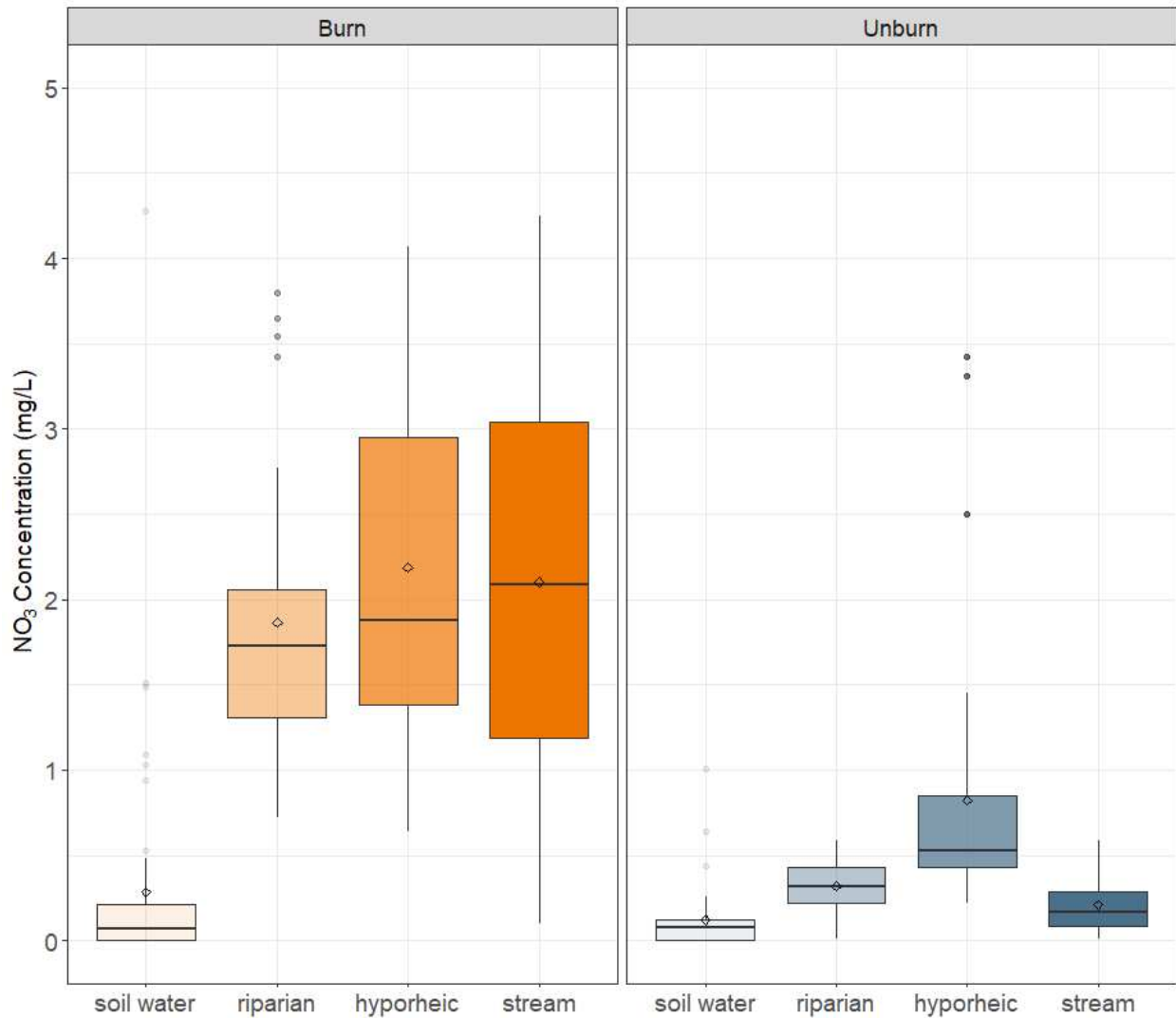


Figure B3: NO₃⁻ concentrations along a downslope flowpath from soil water through riparian groundwater and hyporheic water to streams. The centerline of the boxplots denote median values, the upper and lower limits span the interquartile range, the whiskers include data within 1.5-times the interquartile range, and the dots beyond the whiskers are outliers.

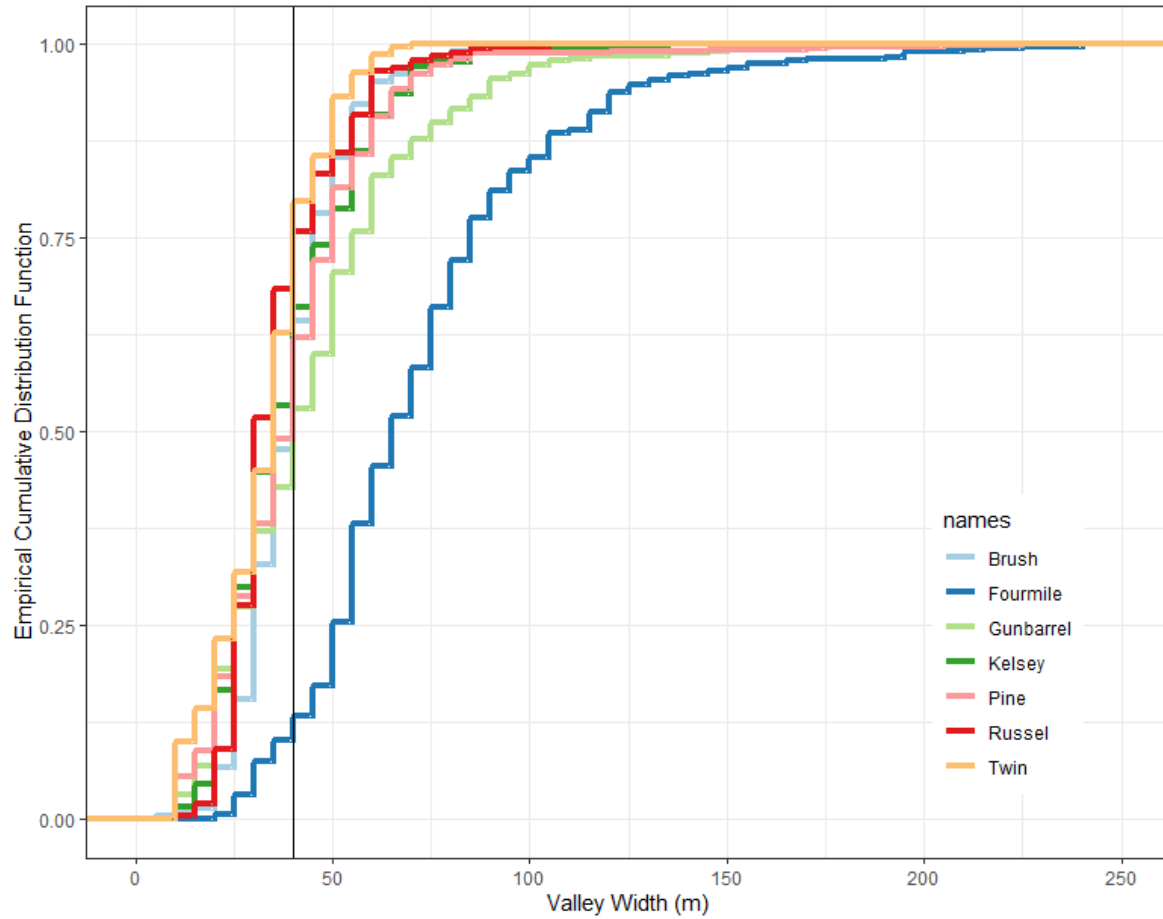


Figure B4: Cumulative distribution of valley widths, which are defined as all areas < 4m in elevation above the stream, by watershed. The vertical black line at 40 m represents a conservative estimate of the minimum width required for riparian buffering.

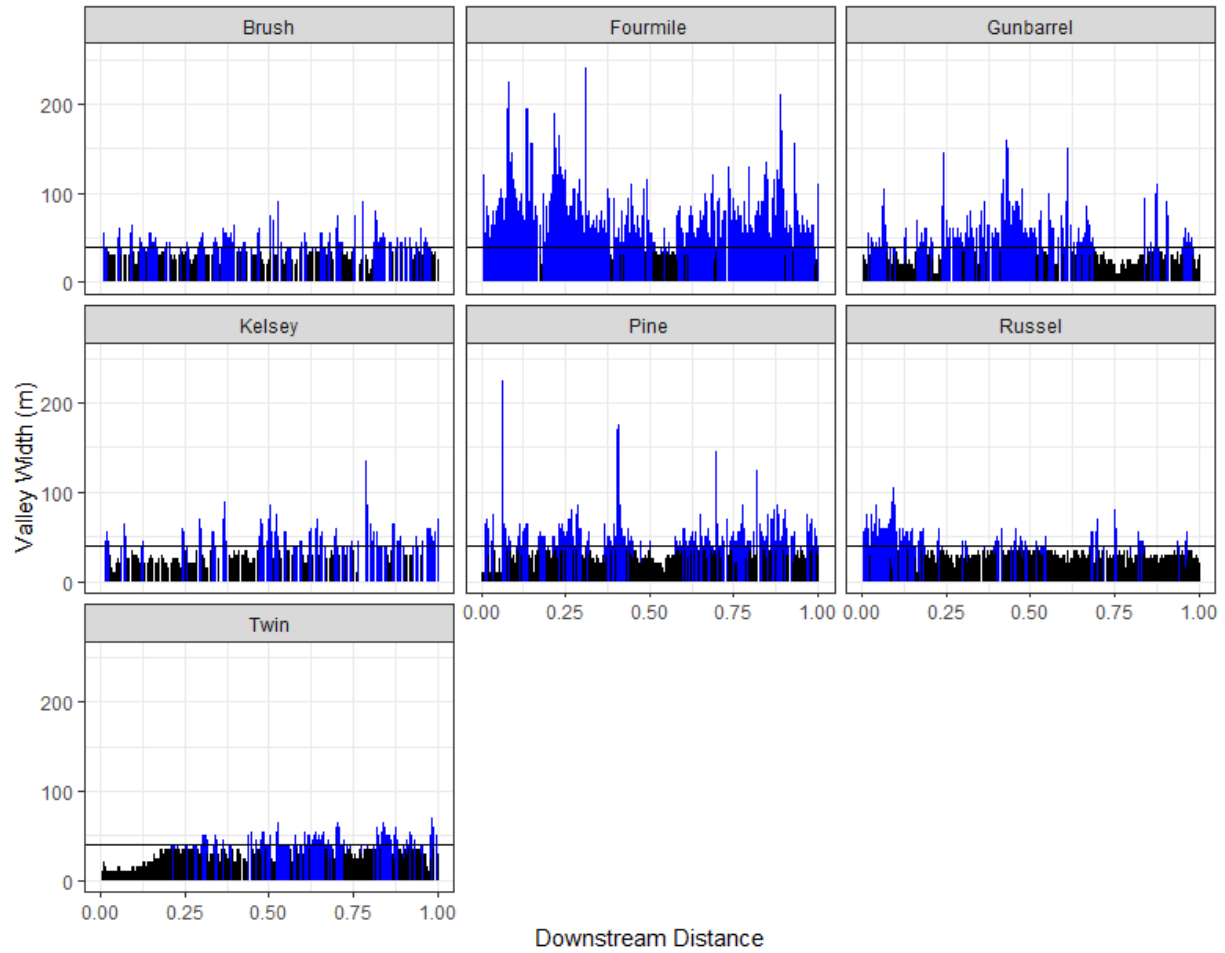


Figure B5: Continuous valley width estimates along watershed mainstems where black bars represent widths < 40 m and blue bars > 40 m. Riparian restoration would be most effective in continuous wide (>40 m) corridors in headwater positions.

APPENDIX C: Chapter 4 supplemental material

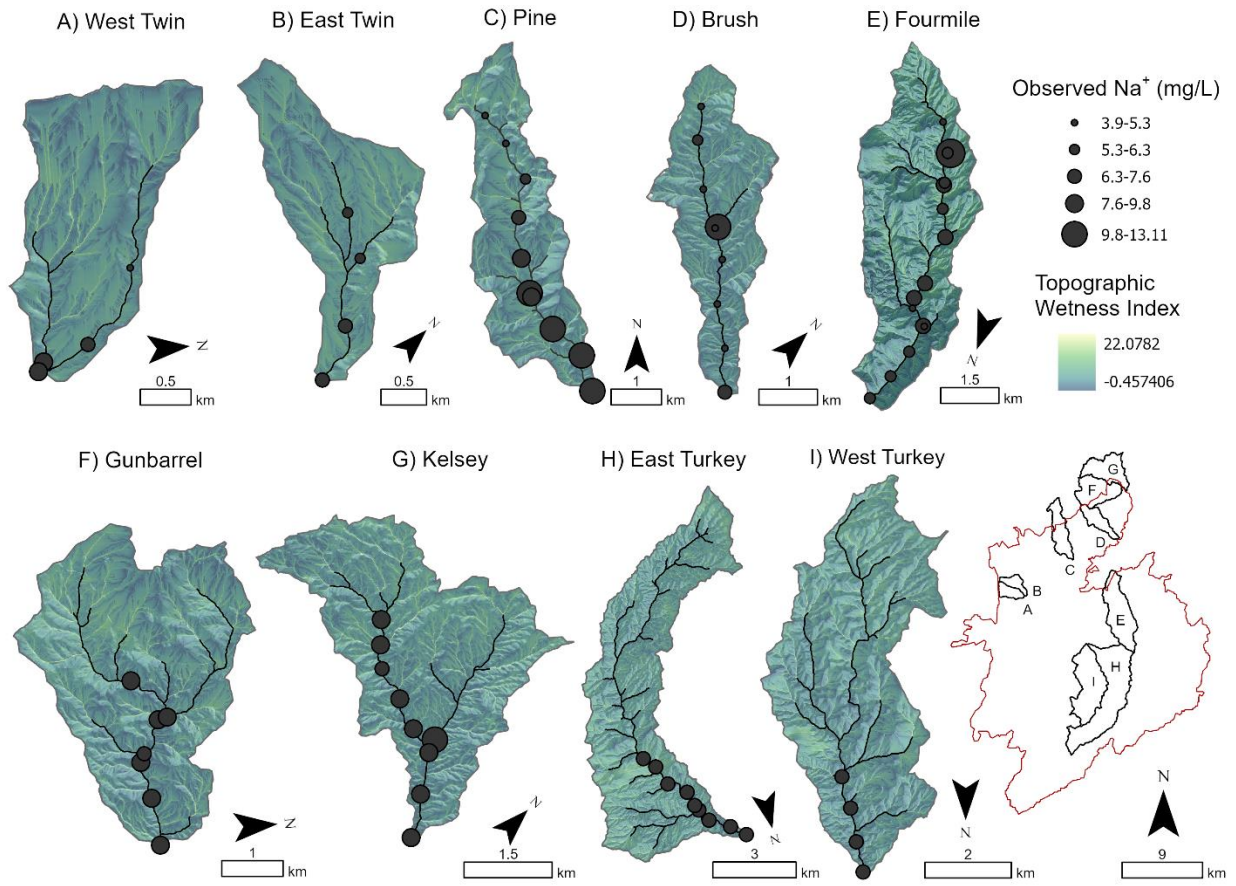


Figure C1: Water chemistry samples (n=71) were collected in June 2018 and the symbol size at each sampling point increases with stream Na⁺ concentration.

Table C1: The top 10 Na⁺ and NO₃⁻ models from linear mixed model selection. Each row represents a different model and the best model has the lowest Akaike’s information criterion (AIC) value. If a variable does not have a numeric coefficient and instead is represented by “-“, that variable was not included in the model. The best Na⁺ model included watershed area, mean slope, riparian extent, mean TWI, mean tree cover, and mean shrub cover. The best NO₃⁻ model included watershed area, riparian extent, mean TWI, and mean NDMI.

	Intercept	Watershed Area	Mean Slope	Mean Elevation	Riparian Extent	Mean TWI	Mean Tree	Mean Shrub	Mean NDMI	Burn Extent	AIC
Na ⁺ Model	-0.41	0.01	0.09	-	0.08	0.72	-0.02	-0.11	-	-	-34.7
	-0.23	0.01	0.10	-0.001	0.09	0.99	-0.02	-0.08	-	-	-34.0
	-0.40	0.01	0.09	-	0.10	0.76	-0.03	-0.11	-	-0.002	-33.2
	0.12	-	0.11	-0.001	0.12	1.08	-0.02	-0.06	-	-	-32.8
	0.23	0.01	0.08	-	0.08	0.69	-0.03	-0.12	1.4	-	-32.3
	0.69	0.01	0.10	-0.001	0.10	1.00	-0.03	-0.10	2.0	-	-31.9
	-0.28	0.01	0.10	-0.001	0.10	0.98	-0.02	-0.09	-	-0.002	-31.8
	1.11	-	0.10	-0.001	0.12	1.10	-0.03	-0.09	2.2	-	-30.9
	-0.12	-	0.08	-	0.11	0.64	-0.03	-0.10	-	-	-30.7
	0.14	-	0.10	-0.001	0.13	1.04	-0.02	-0.07	-	-0.002	-30.6
NO ₃ ⁻ Model	-8.53	-0.04	-	-	0.40	1.55	-	-	-17.9	-	213.1
	-9.50	-	-	-	0.32	1.81	-	-	-17.7	-	213.8
	-7.04	-	-	-	-	1.44	-	-	-16.5	-	214.6
	-8.97	-0.04	-	-	0.43	1.76	-0.01	-	-15.9	-	214.8
	-10.07	-0.04	-	0.001	0.40	1.50	-	-	-18.8	-	214.9
	-5.61	-0.05	-0.09	0.002	0.32	-	-	-	-18.0	-	215.0
	-9.30	-0.04	-	-	0.42	1.69	-	0.02	-17.8	-	215.0
	-9.50	-0.04	0.01	-	0.41	1.75	-	-	-18.2	-	215.1
	-8.58	-0.04	-	-	0.40	1.56	-	-	-17.8	0.0004	215.1
	-1.60	-0.04	-0.07	-	0.29	-	-	-	-16.2	-	215.2

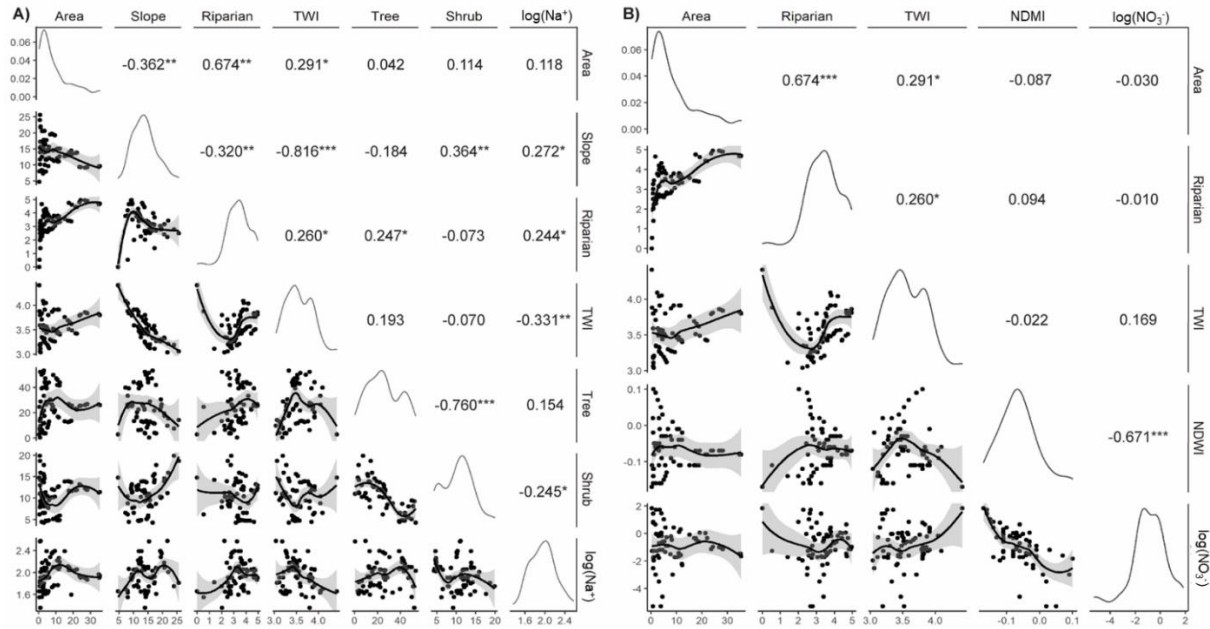


Figure C2: Pearson correlation matrices of the variables selected to predict stream A) Na⁺ and B) NO₃⁻ during linear mixed model selection. The best Na⁺ model included watershed area (Area), mean slope (Slope), riparian extent (Riparian), mean topographic wetness index (TWI), mean tree cover (Tree), and mean shrub cover (Shrub) to predict log-transformed Na⁺. The best NO₃⁻ model included watershed area (Area), riparian extent, mean topographic wetness index, and mean normalized differenced moisture index (NDMI) to predict log-transformed NO₃⁻.

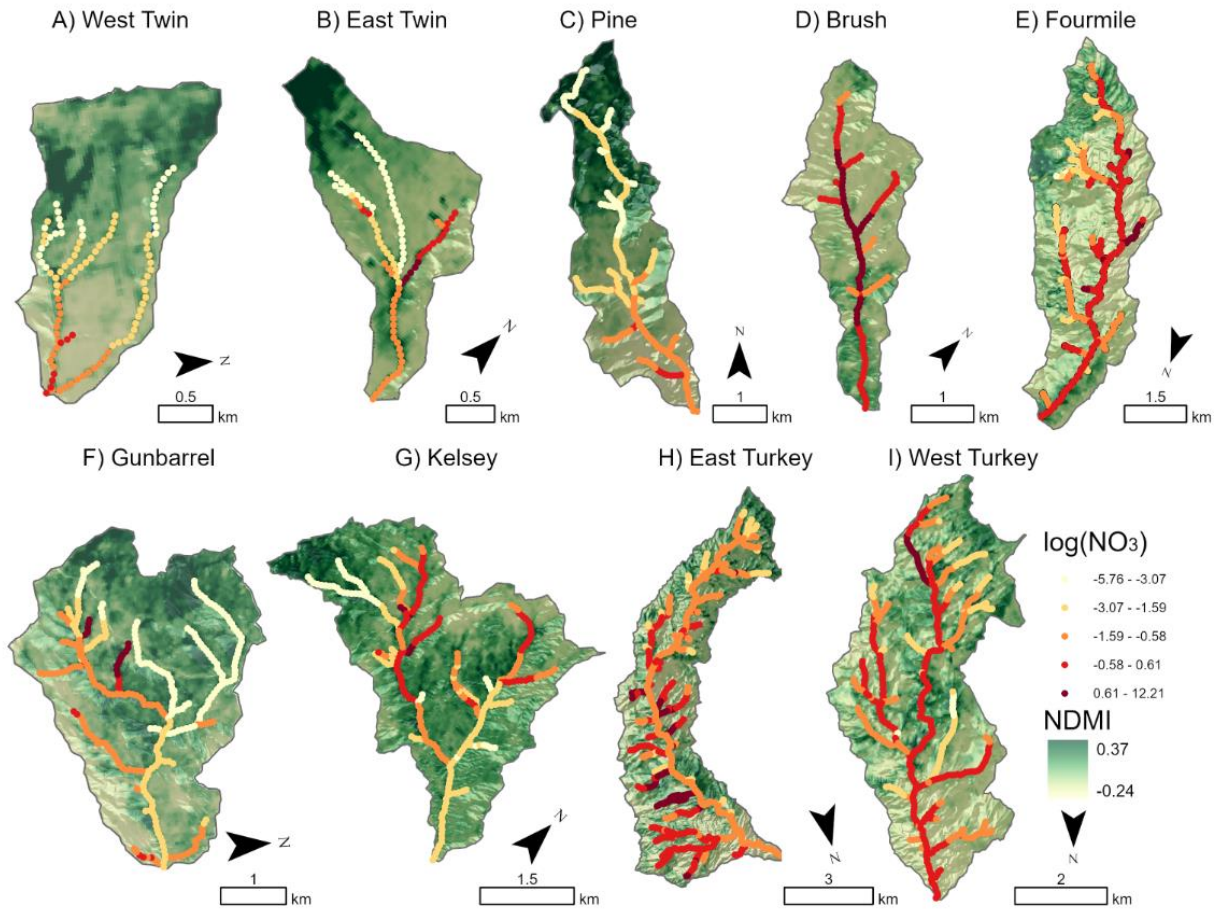


Figure C3: SSN model predictions of log-transformed stream NO_3^- overlain on normalized differenced moisture index, the top predictor of stream NO_3^- .

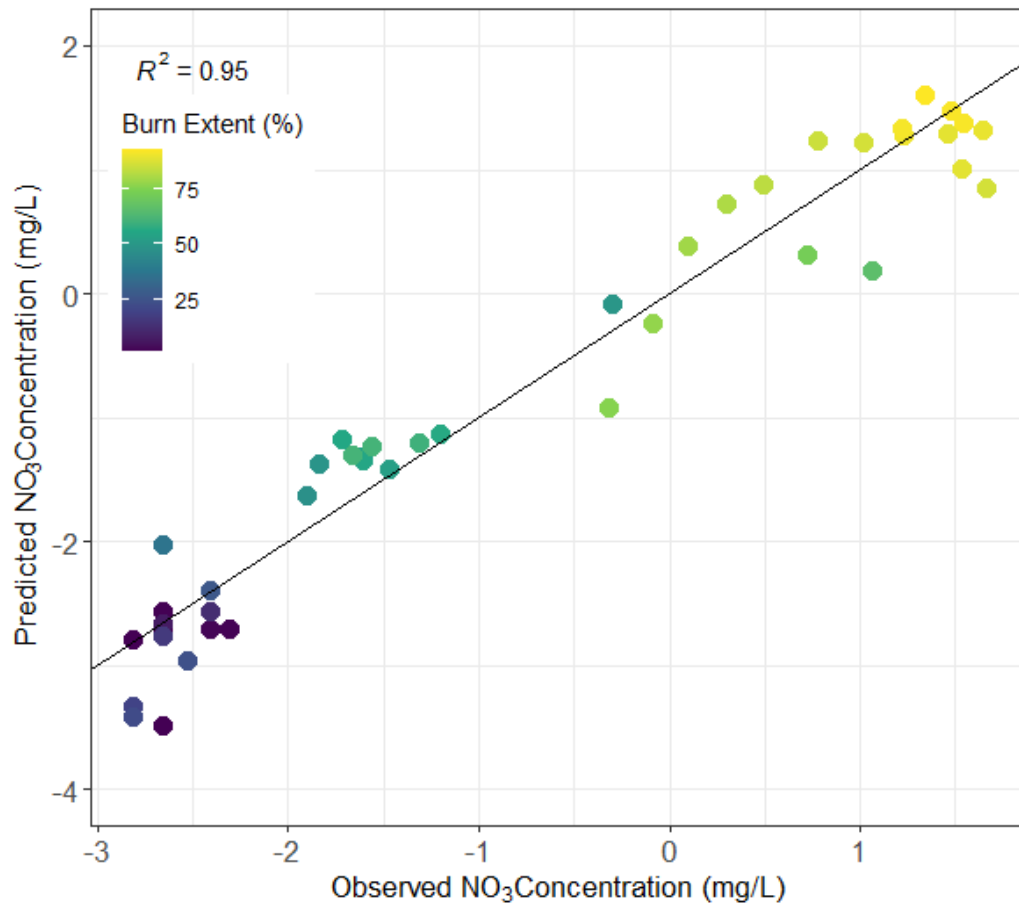


Figure C4: Comparison of observed, log-transformed stream NO₃⁻ concentrations from the Brush and Pine sampling in June of 2019 compared to predicted, log-transformed NO₃⁻ concentrations from the NO₃⁻ SSN model. Points are colored by burn extent and are plotted relative to a black 1:1 line. The R² between these two data sets was 0.95.